# Application of amyloid-secreting cellular systems in the development of preclinical models of relevance to Alzheimer's disease

A thesis submitted to the University of Manchester for the degree of

**Doctor of Philosophy (Ph.D.)**

in the Faculty of Biology, Medicine & Health

**2019**


## Bushra Ahmed Almari

**School of Health Sciences**

**Division of Pharmacy & Optometry**



المنارة للاستشارات

www.manaraa.com

ProQuest Number: 27814631

All rights reserved

INFORMATION TO ALL USERS
The quality of this reproduction is dependent on the quality of the copy submitted.

In the unlikely event that the author did not send a complete manuscript
and there are missing pages, these will be noted. Also, if material had to be removed,
a note will indicate the deletion.

ProQuest 27814631

Published by ProQuest LLC (2020). Copyright of the Dissertation is held by the Author.

All Rights Reserved.
This work is protected against unauthorized copying under Title 17, United States Code
Microform Edition © ProQuest LLC.

ProQuest LLC
789 East Eisenhower Parkway
P.O. Box 1346
Ann Arbor, MI 48106 - 1346

www.manaraa.com

# List of contents





www.manaraa.com

**Final word count: 38,513**



www.manaraa.com

# List of figures





www.manaraa.com

## List of tables





www.manaraa.com

# List of abbreviations

| | |
|---|---|
| 2D; 3D | 2-dimensional; 3-dimensional |
| 3xTg | Triple transgenic mouse line |
| 5xFAD | Transgenic mouse line expressing 5 familial mutations of Alzheimer's disease |
| ACH | Amyloid cascade hypothesis |
| AchE | Acetylcholine esterase |
| AD | Alzheimer's disease |
| AICD | Amyloid precursor protein intracellular domain |
| AP, ML, DV | Anterior to posterior; Medial to lateral; Dorsal to ventral coordinates |
| ApoE | Apolipoprotein E |
| APP | Amyloid precursor protein |
| Aβ | Amyloid-β |
| Aβo | Amyloid-β oligomer(s) |
| BACE1 | β-site APP-cleaving enzyme 1 |
| BSA | Bovine serum albumin |
| CHO | Chinese hamster ovary |
| CM | Conditioned media |
| CNS | Central nervous system |
| CSF | Cerebrospinal fluid |
| DI | Discrimination index |
| DMEM-F12 | Dulbecco's modified eagle medium and Hamm's 1:1 mix |
| DMSO | Dimethyl sulfoxide |
| EDTA | Ethylenediamine tetraacetic acid |
| ELISA | Enzyme-linked immunosorbent assay |
| FAD | Familial Alzheimer's disease |
| FBS | Foetal bovine serum |
| GABA | γ-amino butyric acid |
| HBS | HEPES-buffered saline |
| HEPES | (4-(2-hydroxyethyl)-1-piperazineethanesulfonic acid |
| HFIP | 1,1,1,3,3,3-hexafluoropropan-2-ol |
| HRP | Horseradish peroxidase |
| ICV | Intracerebroventricular |
| IHC | Intrahippocampal |
| IL-1β | Interleukin-1β |
| ITI | Inter-trial interval |
| LTP | Long-term potentiation |
| MAPT | Microtubule-associated protein tau |
| MTS | 3-(4,5-dimethylthiazol-2-yl)-5-(3-carboxymethoxyphenyl)-2-(4-sulfophenyl)-2H-tetrazolium salt |
| NFT | Neurofibrillary tangles |
| NLRP3 | Nod-like receptor protease 3 |
| NMDA | N-methyl-D-aspartate |
| NOR | Novel object recognition |
| NSAID | Non-steroidal anti-inflammatory drugs |
| ONS | Office for National Statistics |
| PBS | Phosphate-buffered saline |
| PBST | Phosphate-buffered saline-Tween® |



www.manaraa.com

| | |
|---|---|
| PET | Positron emission tomography |
| PSD-95 | Post-synaptic density-95 |
| PSEN | Presenilin |
| PV | Parvalbumin |
| SAD | Sporadic Alzheimer's disease |
| sAPP | Soluble amyloid precursor protein |
| SEM | Standard error of the mean |
| SNAP-25 | Synaptosomal nerve-associated protein-25 |
| TBST-T | Tris-buffered saline-Tween® |
| V717F | APP mutation substituting valine with phenylalanine at residue 717 |



www.manaraa.com

# Abstract


## Application of amyloid-secreting cellular systems in the development of preclinical models of relevance to Alzheimer's disease

Bushra Almari – Doctor of Philosophy (Ph.D.) – The University of Manchester

**September 2019**

Alzheimer's disease (AD) is the most common type of dementia associated with a progressive decline in cognitive function, amyloid plaque deposition and neurofibrillary tangle formation. Oligomeric forms of the amyloid-β peptide (Aβo) are considered the initiating trigger which cause synaptotoxicity leading to an impairment in memory. Although many preclinical animal models of AD exist, they often only mimic acute, short-term effects of Aβo. Their main limitation is their inadequate replication of the progressiveness of AD.

This project aims to assess the usefulness of 2-dimensional and 3-dimensional amyloid-secreting cellular systems in the development of a novel preclinical *in vivo* model for AD research. Formulation of a biocompatible delivery system allows the sustained secretion of Aβo for use in developing rodent models of chronic, sporadic AD.

Chinese hamster ovary (CHO) cells expressing the human amyloid precursor protein gene (named 7PA2 cells) and wild-type cells were cultured in standard 2D conditions and conditioned media (CM) was analysed using ELISA, dot blot and westerns. Aβo from 7PA2 cells were injected into the hippocampus of adult female rats. A novel object recognition (NOR) task and a Y-maze test were performed to assess cognitive deficits. Brains were collected and synaptic markers analysed using western analysis. 7PA2 cells consistently secreted $A\beta_{1\text{-}42}$ over time. Prefibrillar oligomeric Aβ (~48 kDa) was secreted into the CM. Rats injected with 7PA2 CM showed progressive deficits in NOR starting at Day 4, becoming significant at Day 7 and remaining persistent at Day 14. Deficits were observed in the Y-maze at Day 8. Synaptic dysregulation accompanied cognitive decline as seen in a reduction in post-synaptic marker PSD-95, increase in pre-synaptic marker SNAP-25 and a decrease in parvalbumin compared with controls.

Cell encapsulation in alginate was optimised by altering fabrication parameters (flow rate, electrostatic potential and vibration frequency). In conclusion, bioengineered 3D cellular systems encapsulating Aβo-secreting cells in an alginate microbead were found to be successful in their potential to model chronic Aβ secretion. Future engraftment of microbeads in the rat brain will allow the assessment of chronic Aβ deposition on cognition and pathology to better model aspects of sporadic AD.




www.manaraa.com

## Declaration

No portion of the work referred to in the thesis has been submitted in support of an application for another degree or qualification of this or any other university or other institute of learning.

## Copyright statement

i. The author of this thesis (including any appendices and/or schedules to this thesis) owns certain copyright or related rights in it (the "Copyright") and she has given The University of Manchester certain rights to use such Copyright, including for administrative purposes.

ii. Copies of this thesis, either in full or in extracts and whether in hard or electronic copy, may be made only in accordance with the Copyright, Designs and Patents Act 1988 (as amended) and regulations issued under it or, where appropriate, in accordance with licensing agreements which the University has from time to time. This page must form part of any such copies made.

iii. The ownership of certain Copyright, patents, designs, trademarks and other intellectual property (the "Intellectual Property") and any reproductions of copyright works in the thesis, for example graphs and tables ("Reproductions"), which may be described in this thesis, may not be owned by the author and may be owned by third parties. Such Intellectual Property and Reproductions cannot and must not be made available for use without the prior written permission of the owner(s) of the relevant Intellectual Property and/or Reproductions.

iv. Further information on the conditions under which disclosure, publication and commercialisation of this thesis, the Copyright and any Intellectual Property and/or Reproductions described in it may take place is available in the University IP Policy (see http://documents.manchester.ac.uk/DocuInfo.aspx?DocID=2442 0), in any relevant Thesis restriction declarations deposited in the University Library, The University Library's regulations (see http://www.library.manchester.ac.uk/about/regulations/) and in The University's policy on Presentation of Theses.



www.manaraa.com

# Acknowledgements

بسم الله الرحمن الرحيم

In the name of Allah, the Entirely Merciful, the Especially Merciful.

**الحمد لله**

Verily, all praise and gratitude are due to Allah, God, Lord of the worlds, creator of all its beautiful intricacies. He bestowed upon me, out of his infinite generosity and bounty, the opportunity and the means that made reaching this point possible. All the investigations in this study were only achievable because of His will. Everything I have achieved in my PhD journey I dedicate to Him, so that He may be pleased with me and grant me His mercy.

Peace and Blessings from Allah be upon His Final Messenger, Mohammed, his pure family, his noble companions, and all those who follow them with righteousness until the Day of Judgment.

To my family – my rock – I am forever indebted to you for your support, faith and prayers. Without your encouragement and help, I would not be writing this thesis today. Baba, you are my hero and my role model. Mama, your strength of character and your prayers keep me smiling. Sumaia, Fayez, Arwa and Lina – thanks for everything, especially putting up with me in the final weeks. Izzeddin, Omamah and Ibrahim, your kindness and reassurance has been so valuable to me. Omar, Reem, Maryam, Ahmad, Bilal and Zayd – thanks for keeping me entertained when I come back to see you on the weekends. Every one of you played your part in making this piece of work achievable. To my beloved Granddad, Seedo Essa, who left this world days before the submission of this thesis, may you rest in peace and may we be reunited in heaven. Thank you for your prayers and support. We are forever grateful for the generosity you have shown us and all that you have done for us.

An ocean of thanks and appreciation goes to Dr Michael Harte (Mike), my supervisor and mentor of ten years. Your support and guidance throughout this project and beyond have been invaluable in shaping the direction of this work and my research career. Many thanks also go to Dr Annalisa Tirella, my co-supervisor, for your expert insight and kind-natured help throughout this project. Your willingness to assist always leaves me filled with gratitude and appreciation.

It has been an honour and delight to share lab and office space with colleagues who supported me directly and indirectly and made my PhD years enjoyable. Kajen, with whom I worked closely and shared "deep convos" throughout your master's year; thank you. Ambreen, Amna, Anna, Chen, Dom, Enrique, Gabbie, Gio, Hager, Harry, Isabella, Iwan, Jen, Jess M, Jess T, Jonathan, Joshua, Julio, Lekha, Linzi, Lisa, Matt, Naz, Syeda, Toby, Tom, Valeria and Wia. Thank you all for keeping me sane (and driving me insane, some of you!).

I'd also like to make a special mention to team members who assisted in running experiments and data collection at some points, including Kajen Suresparan, Jonathan Wubetu, Dominik Grudzinski (encapsulation), Joshua Jackson, Matthew Burgess, Toby Aarons, Tom Metcalf, Yuhong Sun, Gabriella Portlock, Jessica Mackin (animal surgeries) and Valeria Aleksandrova (post-mortem analysis).

Finally, thanks to friends and relatives across the globe who prayed for me and encouraged me along the way. I pray your path is always success.



المنارة للاستشارات

www.manaraa.com

# Chapter 1:
## Introduction



www.manaraa.com

# 1.1. Introduction

### 1.1.1. General overview

Alzheimer's disease (AD) is the most common type of dementia, estimated to affect between 24- and 50- million individuals across the globe (Reitz and Mayeux, 2014; Prince *et al.*, 2015). In the United Kingdom, it is reported that around 850,000 people are living with dementia, the majority of which suffer from AD (Prince *et al.*, 2014). As of 2015, the Office for National Statistics (ONS) has identified dementia and AD as the leading causes of death in the UK, and they have remained so for three consecutive years, claiming one in every eight deaths (ONS, 2018). The earliest presenting symptoms that appear in patients include loss of new memories, uncertainty about places, times and dates, difficulty in articulating oneself, and changes in behaviour and mood. As the disease progresses, decision-making, communication and ordinary day-to-day tasks become affected. Behaviours worsen as patients begin to exhibit severe anxiety and a decline in cognition (Alzheimer's Association, 2016).

In 1906, Alois Alzheimer documented his observations of a 51-year-old patient experiencing some of these symptoms and the accompanying analysis of her brain pathology post-mortem. He noted that the brain had atrophied and that up to one-third of neurons were damaged and tangled. He also commented on the presence of a fibrillar material. He concluded by declaring that this illness was unlike other classifications of existing psychiatric illnesses and that it warranted its own "special" categorisation (Stelzma, Schnitzlein and Murtagh, 1995).

Alzheimer's publication in addition to more recent reports of post-mortem tissue analysis from AD patients' brains describe the classical features of the disease to be: extensively-spread dense collections of insoluble amyloid plaques deposited extracellularly around neocortical neurons and synapses; the presence of intracellular neurofibrillary tangles (NFTs) made of paired helical filaments; and neuronal loss causing brain atrophy and enlargement of the ventricles in the brain (Braak and Braak, 1995). Neurochemical changes, such as a reduction in acetylcholine transferase enzyme, noradrenaline and γ-aminobutyric acid (GABA) are also associated with AD (Rossor *et al.*, 1984).

There are two forms of AD: sporadic Alzheimer's disease (SAD) and familial Alzheimer's disease (FAD). Although FAD is far less common than the sporadic form of the disease, accounting for around 5% or less of all AD cases (Prince *et al.*, 2014), it is thought that they both share similar pathophysiological features (Bateman *et al.*, 2012). Patients with FAD are



www.manaraa.com

usually characterised by an early onset of symptoms (before the age of 65) and are associated with one or more genetic mutations which are often linked to the disease: genetic mutations in presenilin and in the amyloid precursor protein (APP) gene predispose patients to AD by altering the production and properties of the amyloid-β (Aβ) peptide, which is the product of APP processing (Bateman *et al.*, 2012; Karran and De Strooper, 2016). Therefore, FAD is not regarded as a neurodevelopmental disease but rather a result of possessing mutant genes for life (Karran and De Strooper, 2016). SAD, on the other hand, commonly appears in patients after the age of 65 and doesn't have as strong a genetic link as FAD (Guerreiro and Bras, 2015). Possessing a mutant gene, such as a mutation in some apolipoprotein E (ApoE) alleles, including possessing one or two copies of the ε4 allele, can increase the likelihood of developing SAD (Karran and De Strooper, 2016). However, the biggest risk factor for SAD remains advanced age (Guerreiro and Bras, 2015).

Due to these differences, understanding the mechanisms underpinning the onset and subsequent development of the disease requires a distinction in approach, though therapeutic tactics might overlap. Going forward in this report, the main focus of experimentation and discussion will be on the sporadic form and will simply be denoted "AD". Discussions referring to the familial branch of the disease, and where specific comparisons are made, "SAD" and "FAD" will be used as appropriate.

Over 100 years after Alzheimer's descriptive record, the underlying mechanisms leading to the pathology and symptomatology seen in AD are still debated. Innumerable studies investigating the exact causative species implicated in AD and the sequence of events leading to disease development have been conducted. The next section will explore some of the approaches taken to explain the mechanisms underlying the development and progression of the disease.

### 1.1.2. Mechanistic theories

After more than a century of research attempting to understand the pathogenesis of AD, augmented by advancements in technology and scientific methodology, scientists are still unclear about the exact causative entities responsible for triggering the disease. Looking at it generally, it is accepted that AD is the progressive loss of brain tissue over time. Important discoveries have identified several mechanisms involved in the disease process in some way, and scientists are piecing them all together. A number of theories have been proposed to attempt to explain the processes through which this progressive loss of neurons occurs, each



www.manaraa.com

theory supported by its own array of evidence. It is interesting to note that these theories admit something of an interplay between the different entities involved in the disease; one which is yet to be pinned down (Karran and De Strooper, 2016; Selkoe and Hardy, 2016).

#### 1.1.2.1. The amyloid cascade hypothesis

The leading hypothesis proposed to explain the development of AD is the amyloid cascade hypothesis (ACH) put forward by Hardy and Higgins in 1992 and supported by several others at a similar time. In this theory, it is posited that toxic Aβ peptides, resulting from the processing of the amyloid precursor protein (APP) by secretase enzymes **(Figure (1))**, triggers a series of events leaving behind downstream amyloid plaques, neurofibrillary tangles (NFTs) and neuronal loss: the classical hallmarks of the disease (Hardy and Higgins, 1992).

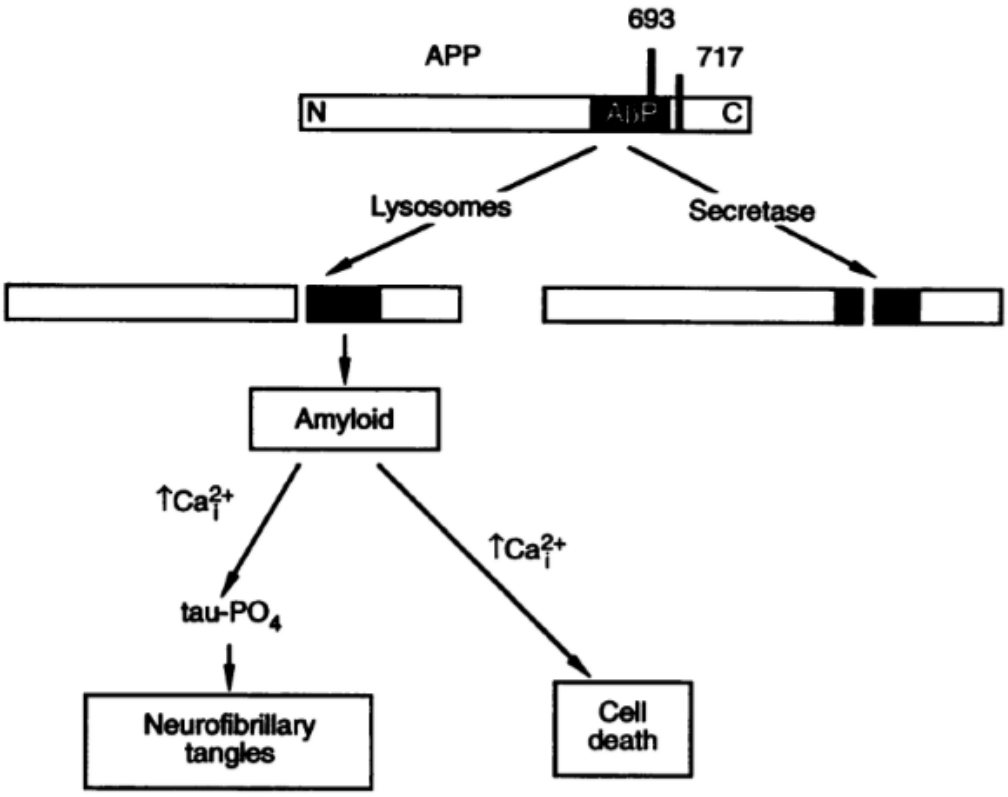


***Figure (1) A graphic representation of the amyloid cascade hypothesis reproduced from (Hardy and Higgins, 1992).***



www.manaraa.com

The mechanisms by which APP is processed have been well studied. APP is a transmembrane protein normally expressed ubiquitously but specifically expressed in high quantities in neuronal tissue. It has a long N-terminal which extends outside of the cell membrane and a short C-terminal which sits inside the cell (Chasseigneaux and Allinquant, 2012). Though its function in normal physiology remains unknown, evidence suggests it may have a role in neural stem cell development, neuronal survival, neurite outgrowth and repair of damaged neurons (Dawkins and Small, 2014). The processing of APP occurs via two opposing pathways as illustrated in **Figure (2)** below. In the first, APP is cleaved by the α-secretase enzyme to produce the non-toxic fragment soluble APP-α (sAPPα), which is believed to have neuroprotective activity, and the APP intracellular domain (AICD). In the second pathway, APP is sequentially cleaved by β-site APP-cleaving enzyme 1 (BACE1, also known as β-secretase) followed by the γ-secretase enzyme to produce soluble APP-β (sAPPβ) and the Aβ peptide, as illustrated in **Figure (2)** below (Chasseigneaux and Allinquant, 2012; Dawkins and Small, 2014). Where mutations in APP or presenilin are present, such as in FAD, an abnormal increase in APP cleavage by BACE1 produces elevated levels of the Aβ peptide (Dawkins and Small, 2014).

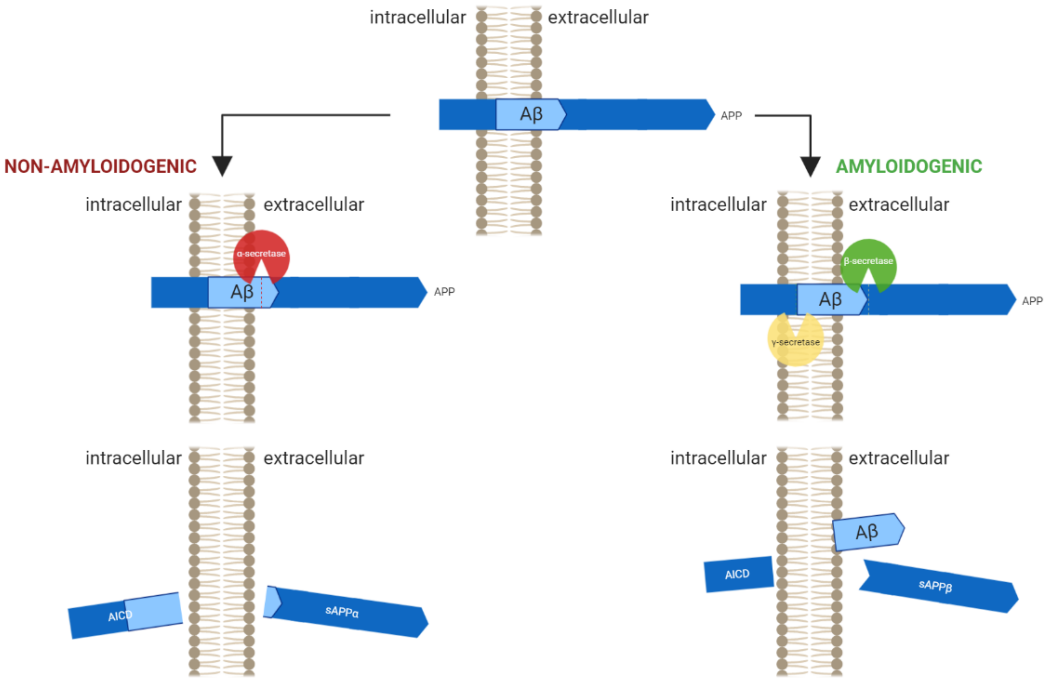


***Figure (2) APP processing.***
***The amyloid precursor protein (APP) is processed via two alternate pathways. In the non-amyloidogenic pathway, α-secretase cleaves APP generating soluble APP-α (sAPPα) and the APP intracellular domain (AICD). Alternatively, APP can be cleaved sequentially by β-secretase and γ-secretase to release the Aβ peptide, soluble APP-β (sAPPβ) and the AICD.***

***Created with Biorender.com***



www.manaraa.com

The ACH suggests that the Aβ peptide, which consists of 39 to 43 amino acids (Welander *et al.*, 2009), is the causative agent responsible for the appearance of synaptic damage, neurovascular injury, NFTs, neuronal loss and brain atrophy in patients suffering from AD (Hardy and Higgins, 1992). Countless studies before and after the proposal of this hypothesis have provided substantiation to the rationale proposed by Hardy and Higgins. The biggest body of evidence supporting this hypothesis is found in studies investigating patients with Down's syndrome. In this condition, due to an error during meiosis, chromosome 21 is abnormally present in three copies instead of two. This is known as trisomy 21. As such, three copies of the APP gene exist. Elevated expression of APP leads to a more aggressive accumulation of Aβ, and this has been used to explain why nearly all Down's syndrome patients over the age of 35 develop AD pathology and symptoms of dementia (Holland and Oliver, 1995). This suggests that increasing levels of Aβ has a direct impact on the disease pathogenesis.

Furthermore, investigations looking at deposited amyloid plaques, which are one of the classical signs of the disease, have found that they are largely composed of Aβ. Varying lengths of insoluble Aβ fibrils made up of $A\beta_{1-40}$, $A\beta_{1-42}$, and $A\beta_{1-43}$ peptides were all found in the plaques (Armstrong, 2005; Welander *et al.*, 2009). The ACH claims that the components of these plaques instigate disease pathology.

Studies exploring the toxicity of Aβ in *in vitro* systems provide further support for the ACH. The first reported study examining the cytotoxic properties of Aβ peptides was in 1990, where neuronal viability of hippocampal cell cultures from rat embryos was assessed following treatment with synthetic $A\beta_{1-40}$. This study found a marked reduction in neuronal cell viability, whilst no alteration was seen in the morphology or number of glial cells in culture (Yankner, Duffy and Kirschner, 1990). A year later, Pike and colleagues reported dose-dependent toxicity following the addition of aggregated synthetic Aβ to neuronal cultures, again providing evidence to confirm the ACH claim that Aβ causes the neuronal toxicity seen in patients with AD (Pike *et al.*, 1991). Building on this, more recent research also confirms the cytotoxic nature of Aβ, including a study looking at neuronal density within the area directly surrounding Aβ deposits in AD brains. This work showed marked cell death in the vicinity around Aβ plaques in comparison with controls (Urbanc *et al.*, 2002).

In addition, various *in vivo* experiments utilising synthetic or natural Aβ conclude that Aβ peptides impair neuronal survival, elicit a deficit in synaptic function and contribute to cognitive decline. Studies injecting synthetic Aβ in rodents report a decline in memory



www.manaraa.com

accompanied by inflammatory and synaptic changes (Forny-Germano *et al.*, 2014; Daniels *et al.*, 2016; Watremez *et al.*, 2018). Many rodent models genetically modified to overexpress APP also describe a dysfunction in memory associated with Alzheimer's-like pathology, including the presence of tangles, plaques, neuronal loss and mitochondrial changes (Sturchler-Pierrat *et al.*, 1997; Cohen *et al.*, 2013; Martins *et al.*, 2017).

A review from 2009 determines that much evidence exists suggesting that Aβ does, in fact, mediate cell toxicity, impairment in cognition and disruption in synaptic function (Yankner and Lu, 2009). All these reports indicate the strength and credibility of the ACH.

The ACH refers to the microtubule-associated protein tau (MAPT, or simply tau), which is found inside the axons of neuronal cells. The hypothesis links abnormal Aβ accumulation with a dysfunction of tau. In normal physiology, it functions as a scaffold holding together the tubules that make up nerve fibres. In the absence of tau, neurones have no tubule-forming capacity, and so dysfunction of tau would render neuronal tissue defective (Avila et al., 2012). In patients with AD, tau becomes dysfunctional as a result of abnormal hyperphosphorylation. This gives rise to paired helical filaments (Chun & Johnson, 2007) which cause tubules to destabilise. Thereafter, neuronal cells break down and die, leaving behind neurofibrillary tangles (NFTs) as dead neurones wrap around themselves (Goedert, Spillantini and Crowther, 1991). Consequently, the inability to form connections with other neurones impairs normal cognitive function. As mentioned previously, the presence of NFTs is one of the hallmarks of AD and is found in all post-mortem AD brains.

Studies looking at the toxicity of tau *in vivo* include transgenic mouse models, such as one developed by Avila et al. (2012). Avila and colleagues demonstrated the effects of overexpressing tau using transgenic and double transgenic models. They found that tau was deleterious to neurones when produced in excess.

Another study found that tau's presence in AD varied between early and late stages of the disease. Taking cerebrospinal fluid (CSF) from AD patients, Saman et al. (2011) found that tau was more abundant in vesicles in earlier stages of disease development, and in later stages, tau was found as a free protein in the CSF. Avila theorises that the presence of free tau proteins is a possible mechanism for the spreading of tau-related neurotoxicity in AD. According to the ACH, neuronal dysfunction due to hyperphosphorylated tau driven by a mishomeostasis of intracellular calcium is induced by the deposition of Aβ earlier in the cascade (Hardy and Higgins, 1992).



www.manaraa.com

Despite all the supporting evidence, the ACH has been criticised by researchers in the field. A recent systematic review (Karran and De Strooper, 2016) explains the limitations of this theory and includes the following in its critique. Firstly, and most pertinently, using the hypothesis as the basis for amyloidocentric drugs to treat AD has borne no fruit. Attempts to target aspects of this pathway have, to date, included regulating secretase enzyme activity, preventing Aβ aggregation, and inhibiting plaque formation, among other approaches. None of the drug candidates from Phase III clinical trials have met their primary endpoints. Whilst efforts to explain the lack of translatability from preclinical models to clinical use have been made (De Strooper, 2014) researchers pursuing this cascade will likely lose interest as no success is seen in targeting the cascade. Another criticism of this hypothesis is its failure to provide a detailed explanation for the link between amyloid species and tau pathology. It merely mentions briefly that an increase in intracellular calcium concentration simply promotes the phosphorylation of tau (Hardy and Higgins, 1992). Furthermore, the discussion around the absolute toxicity of amyloid species has been brought into question. The suggestion that it is elevated levels of Aβ which results in the development of AD is opposed by strong evidence suggesting that it is rather an increase in the ratio of longer to shorter lengths of Aβ proteins (Bentahir *et al.*, 2006). This is supported by data that links presenilin mutations with a shifting $A\beta_{1\text{-}40}$:$A\beta_{1\text{-}42}$ ratio (Bentahir *et al.*, 2006). Moreover, the lack of correlation between amyloid plaque burden and location with disease severity suggests there could be other factors at play in the progression of AD (Karran and De Strooper, 2016).

In response to these and other rebuttals of the ACH, Selkoe and Hardy have published a report addressing many of these points in detail. In short, they report that amyloid deposits appear earlier than other AD-associated pathological abnormalities in patients with dementia. They also state that plaques in healthy individuals are not rich in abnormal neurites, glia or Aβ. They refute the claim that tau tangles appear before amyloid deposits and cement this by adding that mutations in tau are not known to cause deposition of Aβ. Finally, they stress that the failure of clinical trials to meet endpoints was primarily down to poor trial design, including recruiting patients with far advanced disease severity, and that unpicking trial data reveals evidence of clinical benefit in patients with very mild dementia (Selkoe and Hardy, 2016).

Furthermore, after new emerging evidence looking more closely at the different toxic profiles of various Aβ species, the ACH has been updated to a more specific hypothesis known as the Aβ oligomer hypothesis (see section 1.1.2.2.3).



www.manaraa.com

#### 1.1.2.2. Other theories

Over time, and fuelled by the criticisms raised against the ACH, other theories of AD aetiology were proposed. In fact, the ACH was itself refined following more recent findings shedding light on older evidence.

##### 1.1.2.2.1. The inflammatory cascade

There is a strong base of evidence pointing towards the activation of neuroinflammatory pathways at some point during the development of AD, whether as a cause, contributing factor or a downstream effect of other mechanisms (Wyss-Coray and Rogers, 2012). Microglia and astrocytes are cellular mediators of inflammation and thus contribute to the normal defence mechanisms of the central nervous system (CNS). In healthy physiology, microglia become activated following an insult or in the presence of potential pathogens and attack foreign particles (McGeer and McGeer, 2002). In AD, it has been shown that a build-up of Aβ – whether freely soluble or confined to amyloid plaques – recruits and activates microglia in a similar fashion (Meyer-Luehmann *et al.*, 2008; Wyss-Coray and Rogers, 2012). Analysis of post-mortem brain sections of deceased AD patients established a clear association between activated microglia and amyloid plaques (McGeer and McGeer, 2002). In living AD patients, positron emission tomography (PET) imaging was used to demonstrate the communication between microglial cells and Aβ plaques in the same subjects. An increase in microglial activity was shown to correlate with a worsening cognitive function. Interestingly, however, this relationship was independent of the degree of Aβ burden (Edison *et al.*, 2008). This evidence and supporting data suggest that perhaps inflammation is linked more closely with cognitive decline in AD than are Aβ levels and cognitive decline in AD and forms the basis of the inflammatory hypothesis.

Data from animal studies investigating the effects of Aβ on inflammation give further validation to this idea. In one study, Aβ deposits elicited a reaction from microglia in a matter of days in three different transgenic mouse models, consequently initiating an inflammatory response (Meyer-Luehmann *et al.*, 2008). Another study used imaging techniques in transgenic AD mice to reveal the rapid microglial response to plaque formation. Bolmont and team noted that there was a positive correlation between plaque number and extent of microglial recruitment, reinforcing the notion that microglia interact with the classical structures associated with AD (Bolmont *et al.*, 2008).



www.manaraa.com

Molecular modulators, including the complement system, are pivotal for the body's general immunity. In the CNS, the complement system seems to be activated in neurodegenerative diseases, such as AD. In fact, the presence of amyloid plaques and NFTs have been shown to be directly associated with complement activation (McGeer and McGeer, 2002; Wyss-Coray and Rogers, 2012).

Altered concentrations of soluble signalling proteins, including cytokines, have been associated with the development of AD. In a review, Wyss-Coray & Mucke (2002) have discussed an apparent link between changes in levels of cytokines, neurodegeneration and cognitive decline, with a possible interplay with over-production of amyloid species. Drawing on data from animal experiments, the review suggests an interesting hypothesis for the mechanisms involved in Aβ-induced inflammation. Based on such studies where rats and mice injected with Aβ species have resulted in an accumulation of Aβ in the microglia, it is suggested that Aβ clearance in the brain is mediated by microglial cells via phagocytosis which then leads to further pro-inflammatory processes, eventually causing apoptosis and neurodegeneration (McGeer and McGeer, 2002; Wyss-Coray and Mucke, 2002). Recent work reported the development of a novel method of microglial depletion in transgenic mouse models of relevance to AD. Eliminating microglia was associated with the prevention of Aβ plaque formation, suggesting that microglia is essential in the appearance of plaques. This provides further evidence to support the concept of inflammation-mediated AD pathology (Spangenberg *et al.*, 2019).

Backing up the claim that AD is caused by inflammatory changes, interesting epidemiological studies have shown that using non-steroidal anti-inflammatory drugs (NSAIDs), such as indomethacin and ibuprofen, for a long time by patients with arthritis reduces the likelihood of developing AD. Though not all NSAIDs had identical protective profiles, the findings illustrate a strong correlation between NSAID use and AD risk reduction (Vlad *et al.*, 2008). In 2001, De Strooper & Konig evaluated the effects of NSAIDs on Aβ and found that NSAIDs may reduce the formation of $A\beta_{1-42}$ by regulating γ-secretase, an effect unrelated to the anti-inflammatory role they exhibit via inhibition of the cyclo-oxygenase enzymes (De Strooper and König, 2001; Vlad *et al.*, 2008).

In a more recent study, it was shown that fenamate NSAIDs, including mefenamic acid, rescued an induced memory loss in rodent models of AD, suggesting an inflammatory causation for the induced memory deficits (Daniels *et al.*, 2016). In this study, NSAIDs inhibited the nod-like receptor protease 3 (NLRP3) inflammasome. This is a complex



www.manaraa.com

consisting of multiple proteins, activation of which results in the cleavage of inactive pro-interleukin-1β (pro-IL-1β) to activated interleukin-1β (IL-1β) via the caspase-1 enzyme. Inhibiting this inflammasome using mefenamic acid in this investigation reduced microglial activation and reversed memory deficits in a transgenic mouse model for AD. These data demonstrate the presence of an important link between AD pathology and inflammatory processes (Daniels *et al.*, 2016).

The limitation of this theory is largely associated with the universal involvement of the inflammatory cascade in both health and disease. Whilst evidence suggests that targeting inflammatory markers by anti-inflammatory drugs provides better outcomes for patients with dementia, inflammation in the brain is associated with other conditions such as stroke and Parkinson's, and therefore it is difficult to attribute the cause of AD to inflammation (Karran and De Strooper, 2016; Selkoe and Hardy, 2016). Rather, it is more appropriate to think of inflammation as a downstream effect of an earlier trigger, such as Aβ deposition (Hardy and Selkoe, 2002). The hypothesis also lacks sufficient explanation of how tau phosphorylation is linked to the disease process, and so it is more likely that inflammation is a response to underlying pathology as opposed to the cause of it.

In summary, this hypothesis suggests that neurodegeneration results from neuroinflammatory activation. This is possibly a response to the build-up of Aβ, therefore ultimately playing an important role in the development of AD. At the very least, studies cited here prove a link between inflammation and AD, even if it is not causative.

#### 1.1.2.2.2. Mitochondrial cascade hypothesis

In 2004, Swerdlow and Khan proposed the mitochondrial hypothesis, suggesting that mitochondrial dysfunction leads to the development of AD. The hypothesis maintains that an individual's genetically determined baseline mitochondrial function, in addition to environmental factors, affect the rate at which age-associated mitochondrial changes develop and become visible. In individuals with poor baseline mitochondrial function and a fast rate of mitochondrial deterioration, the onset of AD is sped up, whereas a high baseline with slow deterioration delays its onset. Therefore, even though not all elderly patients go on to suffer from sporadic AD, this hypothesis posits that developing AD is an expected consequence of ageing if an individual lives long enough to allow for severe mitochondrial dysfunction (Swerdlow and Khan, 2004).



www.manaraa.com

Here, Swerdlow and Khan imply that a deficiency in normally functioning mitochondria in the brains of AD patients is thought to lead to an increase in Aβ, which in turn gives rise to AD symptomatology. Therefore, normally functioning mitochondria are thought to have a regulatory role in Aβ accumulation. Dysfunctional mitochondria are thought to exhibit their action by increasing APP expression, driving APP processing, promoting Aβ accumulation or a combination of some or all of these processes (Swerdlow and Khan, 2004; Swerdlow, Burns and Khan, 2014).

#### 1.1.2.2.3. Aβ oligomers hypothesis

Aβ oligomers (Aβo) are soluble proteins that result from the misfolding and self-aggregation of Aβ monomers (Glabe, 2008; Viola and Klein, 2015). In the Aβo hypothesis, neurotoxicity and cognitive impairment in AD patients is attributed to Aβo. Proposed by Walsh and Selkoe as an upgrade to the ACH (see section 1.1.2.1) following a decade of discovery, and supported by many other researchers, this theory identifies the trigger for synaptic dysfunction and neuronal death not only as the Aβ peptide, but assemblies of Aβ repeats known as oligomers (Haass and Selkoe, 2007; Walsh and Selkoe, 2007). It suggests that plaque formation may be a protective mechanism in response to the oligomerisation of amyloid species to avoid any resultant synaptic dysfunction by sequestering toxic oligomeric Aβ conformations (Walsh and Selkoe, 2007).

Support for this theory comes in a range of clinical, *in vitro* and *in vivo* studies. Clinically, attempts to clear plaques after aggregation have been shown to aggravate neuronal cytotoxicity, and this is probably due to the freeing of Aβo from the plaques (Kayed and Lasagna-Reeves, 2012; Karran and De Strooper, 2016). Treating *in vitro* neuronal cell cultures with Aβo has been shown to cause a reduction in cell viability (Bate and Williams, 2011; Martins *et al.*, 2017; Nolan, McHale-Owen and Bate, 2017; Williams and Bate, 2018). Using Aβo in mice and rats has been demonstrated to cause an impairment in memory function associated with synaptic damage (Haass and Selkoe, 2007; O'Hare *et al.*, 2013; Daniels *et al.*, 2016; Watremez *et al.*, 2018). A study reported that administration of Aβo into non-human primates resulted in Alzheimer's-like brain pathology. In this study, Aβo were shown to trigger cognitive dysfunction, synaptic loss, tau hyperphosphorylation, and astrocyte and microglial activation (Forny-Germano *et al.*, 2014). These studies demonstrate the validity of using Aβo-based *in vivo* models to investigate early disease mechanisms and identify novel therapeutic targets for AD.



www.manaraa.com

Ultimately, this hypothesis puts forward that the cytotoxicity and synaptic damage observed in AD is linked to the oligomeric aggregation state of Aβ species rather than the fibrillar configuration found in plaques (Walsh and Selkoe, 2007; Kayed and Lasagna-Reeves, 2012).

In conclusion, the number of intertwining theories attempting to explain the mechanisms underlying AD pathology is testament to the complexity of the disease. In order to successfully find efficacious treatments to halt the progression of the disease, it is important to understand the underlying mechanisms and attempt to replicate them in preclinical models. Although there is no consensus shared in the field that explains the cause of AD without any doubt, mounting compelling evidence indicates that amyloid-containing peptides in one conformation or another are, at least in part, responsible for its aetiology and warrant investigation.

#### 1.1.2.3. Pharmacological therapy

There are currently five drugs licensed for the treatment of AD worldwide (only four in the UK). The acetylcholine esterase (AchE) inhibitors donepezil, galantamine, rivastigmine and tacrine work by elevating levels of acetylcholine in the brain to compensate for the loss of cholinergic neurones. The N-methyl-D-aspartate (NMDA) receptor antagonist, memantine, works by interfering with glutamatergic excitotoxicity affecting neuronal cell function in the hippocampus. Establishing the clinical efficacy of these drugs was initially based on the improvement of ratings on scale-type AD tests, where AchE inhibitors and memantine were found to modestly improve cognition or dampen the decline in cognitive function (Hansen *et al.*, 2008; Blanco-Silvente *et al.*, 2017). Despite providing limited symptomatic relief, current drug treatments do not target the disease processes underlying AD and fail to halt or slow down disease progression, yet they carry the potential for many unwanted side effects (Koseoglu, 2019).

The problem AD poses with a rising worldwide prevalence, an aging population and the distressing nature of this condition is of significant magnitude. The rising estimated cost of care for people with AD is expected to create a serious public health concern in the coming decades (Gold, 2017). The lack of effective therapies presents an unmet clinical need.



www.manaraa.com

Investigations in the field attempting to find efficacious agents that target underlying disease mechanisms have been largely and disappointingly unsuccessful (Gold, 2017). As discussed above, this led to criticisms coming forth against the ACH (De Strooper, 2014; Karran and De Strooper, 2016). Despite showing promising results in the laboratory when tested *in vitro*, *in vivo* and in early stage clinical trials, drug candidates targeting different aspects of the amyloid cascade have failed to meet their primary endpoints in phase III clinical trials and have often been associated with distressing adverse drug reactions (Gold, 2017; Koseoglu, 2019).

One example is the drug bapineuzumab, a monoclonal antibody, shown in preclinical studies to bind to amyloid plaques, lower plaque burden, reduce synaptotoxicity, and improve behavioural performance in transgenic mouse models. In 2012, bapineuzumab underwent phase III clinical trials where it was hoped that clearance of excess Aβ from the brain would rescue cognitive function by preventing synaptic damage. All trials were terminated because it failed to produce clinical benefit (Salloway *et al.*, 2014; Gold, 2017).

Solanezumab, another monoclonal antibody, was tested on transgenic mice expressing human APP. The rationale for solanezumab's mechanism of action is that it targets and sequesters soluble, monomeric forms of Aβ found freely in the CSF resulting in reduced oligomerisation and avoiding synaptic toxicity and dysfunction. Preclinical results were successful, showing a reversal of memory deficits in mice without affecting plaques, as its target was Aβ monomers. Pharmacokinetic data from phase II trials suggest that while solanezumab successfully bound to plasma Aβ to some extent, levels of Aβ in CSF appeared to re-establish equilibrium, possibly as a result of plaque disintegration in the brain (Gold, 2017). Nevertheless, solanezumab went into phase III clinical trials but failed to meet its primary outcomes (Liu-Seifert *et al.*, 2015; Gold, 2017).

A few months ago, the discontinuation of another phase III trial investigating the efficacy of yet another monoclonal antibody, aducanumab, in AD was announced. Aducanumab was shown to penetrate the brain, bind with Aβ and reduce Aβ concentration in transgenic mouse models of AD. In patients with early-stage dementia, aducanumab treatment was demonstrated to reduce levels of Aβ in the brain and even showed promising data in rescuing cognitive function as assessed using clinical assessment scores in early phase studies (Sevigny *et al.*, 2016). However, the interim analysis of the drug's efficacy in the phase III trial earlier this year revealed no significant slowing of cognitive deterioration in patients (Selkoe, 2019).



www.manaraa.com

Analysing these failures, several explanations have been put forward to try and make sense of what went wrong and where to go next. One explanation is the potential fault in targeting amyloid, rendering the ACH flawed in its essence (Karran and De Strooper, 2016). Though this is plausible, the vast extent of supporting evidence demonstrating the effects of Aβ in preclinical systems and analysing patient pathology proves that amyloid must be involved in some way or another in the development of the disease. Next, the recruitment of patients to these trials may have been poorly designed. That is to say that patients were too advanced in their pathology to see significant attenuation of disease progression (De Strooper, 2014; Selkoe, 2019). However, in the case of the aducanumab trial, the designers used clinical scores and PET scanning to screen for subjects at early disease stages (Sevigny *et al.*, 2016). Perhaps attempting to reverse or slow down the damage caused by Aβ needs to start earlier still, such as implementing a primary prevention scheme in order for any benefit of these drugs to be seen (Selkoe, 2019). Another possibility is the limited reliability of the animal models on which preclinical tests were based. The validity of transgenic models has been brought under scrutiny and it is thought that they poorly mirror AD. Rather, they merely replicate specific pathological features seen in AD, and sometimes they do this in a non-physiological fashion, such as excessively concentrated Aβ levels which do not marry up with levels in patients (Drummond and Wisniewski, 2017).

To sum up, existing approved treatment options for AD have little or no impact on the underlying disease mechanisms and the progression of the disease. To address this gap, subsequent efforts attempting to target the disease in different parts of the known pathways have been to no avail. The translatability of preclinical models is vital for making headway in drug development. In order to obtain translatable models, there must be a good understanding of the underlying mechanisms and the causative factors implicated in the disease. This project aims to explore more relevant preclinical models that will allow more effective drug treatment options to be discovered.

#### 1.1.2.4. Animal models and their limitations

Thus far, several studies utilising animal models of relevance to AD have been mentioned. In this section, a selection of the most prominent preclinical animal models will be summarised, and their advantages and disadvantages discussed.

Animal models have been widely used in neuropharmacological research. Though animal models can prove extremely useful, it is important to note that attempting to approximate



www.manaraa.com

such a complex and poorly understood disease as AD in an animal promises to be a difficult task. It is also worth commenting on the lack of completeness of animal models; modelling one, or indeed a few, aspects of a disease will never provide the full clinical and social picture experienced by patients (Drummond and Wisniewski, 2017).

### 1.1.3. Transgenic models

The overwhelming majority of preclinical models used in AD research is transgenic rodents (Puzzo *et al.*, 2015; Drummond and Wisniewski, 2017). Transfecting mice and rats with single or multiple mutant human genes expressing a phenotype of interest in AD allows the investigation of behaviour *in vivo* and post-mortem pathological analysis *ex vivo*.

#### 1.1.3.1. Single transgenic mouse models

DNA incorporating a mutant human APP gene results in the overexpression of APP. Consequently, this causes animals to produce Aβ as a result of secretase enzyme activity. Games *et al.* in 1995 were among the first to generate a transgenic mouse model transfected with a mutant human APP gene (known as the Indiana mutation) that resembled AD pathology. In this model, mice expressed human APP with a FAD-associated mutation (substituting valine with phenylalanine at amino acid residue 717), which resulted in the overproduction of Aβ. Consequently, deposition of amyloid fibrils and synaptic loss were observed (Games *et al.*, 1995). Subjecting these mice to cognitive tests in a battery of behavioural tasks saw an age-related memory impairment (Puzzo *et al.*, 2015). A plethora of transgenic mouse models have been developed since then, with various genetic modifications with relevance to AD.

Impairment of memory function in transgenic mice, as measured by the Morris water maze, was seen when a single transgene expressing the Osaka mutation of APP was used. In this model, the gene encoding for human APP 695 amino acid residues in length is incorporated into the mouse DNA to result in overexpression of Aβ. Associated pathological investigations observed Aβ accumulation within neuronal cells but not extracellularly. Synaptic dysfunction was detected using *in vivo* electrophysiological examination of long-term potentiation. Aberrant tau hyperphosphorylation was also seen in sections of brain analysed using immunohistochemistry (Tomiyama *et al.*, 2010).

In addition to APP mutations, other genes of interest have been utilised in the generation of transgenic mouse models of AD. FAD has been evidently associated with mutations in presenilin genes as discussed earlier. Mutations in presenilin genes 1 and 2 (PSEN1 and



www.manaraa.com

PSEN2) result in the abnormally increased processing of APP in humans. This, in turn, results in elevated levels of Aβ (Dawkins and Small, 2014). This property of presenilins allows their application in the development of amyloidocentric transgenic animal models. Mouse models expressing mutant presenilin genes have been shown to accumulate Aβ and in some cases caused a deficit in cognition but revealed no plaques (Toda *et al.*, 2011; Cavanaugh, Pippin and Barnard, 2014). Although these types of models offer the chance to study the effects of excess amyloid production on the behaviour and pathology of the animal, and can be used to assess drug efficacy in reducing the gross levels of amyloid, they may be limited in their translatability to sporadic forms of AD since they do not exhibit other important features, such as tau pathology as an example (Cavanaugh, Pippin and Barnard, 2014; Puzzo *et al.*, 2015; Drummond and Wisniewski, 2017).

To model the involvement of tau and the resultant NFTs seen in AD, transgenic mouse models expressing human MAPT genes have been developed (Götz *et al.*, 2001). Even though mutant tau genes in rodent models are often associated with frontotemporal dementia and are therefore not considered reliable for modelling Alzheimer's type dementia (Duyckaerts, Potier and Delatour, 2008; Mullane and Williams, 2019), they do present the NFT pathology that is missing from many APP and presenilin mutations (Götz *et al.*, 2001).

#### 1.1.3.2. Multiple transgenic mouse models

In an effort to combine the various pathologies seen in AD in a single model, the use of multiple transgenes began to emerge. Mice incorporating an APP mutation as an adjunct to a presenilin mutation; i.e. double transgenic, have been shown to display a cognitive decline, neuroinflammation and the development of plaques. Presenilin was also found to accelerate the processing of APP and yield a higher concentration of Aβ in these models (Toda *et al.*, 2011; Cavanaugh, Pippin and Barnard, 2014).

A model expressing three mutant genes, known as the triple transgenic (3xTg) has been developed where mice are transfected with mutant APP, presenilin and tau (Oddo *et al.*, 2003). In Oddo's model, an observed cognitive impairment is present at four months of age, appearing ahead of any plaque or tangle formation. Amyloid plaques and NFTs in this model emerge in an age-related and progressive manner, with NFTs first appearing at 12 months (Oddo *et al.*, 2003). In another triple transgenic model with mutant APP, presenilin and tau, mice exhibited cognitive deficits tested by the Morris water maze behaviourally and revealed Aβ plaque deposition and NFTs pathologically (Grueninger *et al.*, 2010).



www.manaraa.com

Age-dependent memory deficits and motor phenotypes accompanied by amyloid plaques, neuronal loss and synaptic degeneration were seen in the 5xFAD model designed by Oakley *et al*. This model is based on mice incorporating three APP and two presenilin mutations associated with the familial class of the disease (Oakley *et al.*, 2006). In Oakley's 5xFAD model, amyloid deposition begins as early as 1.5 months followed by cognitive impairment observed in a Y-maze at 4 to 5 months. Mice transfected with these mutations exhibit a worsening pattern of neuronal dysfunction, neuronal loss and plaque deposition (Oakley *et al.*, 2006; Cavanaugh, Pippin and Barnard, 2014; Drummond and Wisniewski, 2017).

While models in which more than one transgene is used offer the advantage of modelling several pathological aspects of disease, the validity of such models is brought into question (Cavanaugh, Pippin and Barnard, 2014). Firstly, most genes used in transgenic animal models are associated with FAD, which accounts for fewer than 5% of all AD cases (Prince *et al.*, 2014; Puzzo *et al.*, 2015; Drummond and Wisniewski, 2017). And secondly, the artificially accelerated accumulation of Aβ in unrealistic concentrations bears little resemblance to progressive accumulation in sporadic AD (Selkoe, 2002; Drummond and Wisniewski, 2017; Mullane and Williams, 2019).

**Table (1)** below lists a short summary of selected single and multiple transgenic mouse models and the behavioural and pathological effects observed. The table illustrates the diversity in behavioural and pathological phenotypes exhibited by the modifications in place. These variations potentially compound the difficulty faced when attempting to search for drug candidates, as a test drug may reverse a change displayed in one model but not have the same effect in another model. For this reason, recommendations have been made to drug developers to test compounds in a battery of tests rather than in a single one, and in a number of models of the same species, then move on to another species before concluding the preclinical evaluation of a drug and moving into the clinical phases (Mullane and Williams, 2019).



www.manaraa.com

***Table (1) Transgenic mouse models of relevance to Alzheimer's disease.***

| Model | Modification | Behavioural effects | Pathological effects |
|---|---|---|---|
| APP (V717F) (Games *et al.*, 1995) | Mice expressing human APP with the Indiana mutation substituting valine with phenylalanine at residue 717. | Cognitive deficit in Morris water maze. Cognitive deficit in radial arm maze at 3 months. Age-dependent deficit in object recognition starting at 9 months. | Plaques in the cortex, corpus callosum and hippocampus from 6 months. Synaptic impairment. No neuronal loss or tau pathology observed. |
| 3xTg (Oddo *et al.*, 2003) | Mice expressing the 695 isoform of human APP with the Swedish mutation, presenilin and tau mutations. | Spatial and contextual cognitive impairment, at 4 months. Cognitive deficit in Morris water maze. Cognitive deficit in object recognition. | Intracellular Aβ deposition starting at 6 months, more extensive at 12 months. Tau pathology present starting at 12 months. Synaptic dysfunction, plaques and tangles. |
| 5xFAD (Oakley *et al.*, 2006) | Mice expressing human APP with the Swedish, Florida and London mutations, and two presenilin mutations. | Age-dependent memory deficit. Reduced motor function. | Intracellular Aβ accumulation. Extracellular plaques within 2 months. Neuronal loss in cortical layer V. Gliosis at 2 months. No tangles. |
| APP and tau (Hashimoto *et al.*, 2019) | Mice expressing human APP with the Swedish, Iberian and Arctic mutations, and tau mutation. | Cognitive deficit in the Y-maze at 12 months. | Aβ plaques at 2 months. Astrogliosis and microgliosis at 4 months. No neuronal loss observed. |

www.manaraa.com

#### 1.1.3.3. Transgenic rat models

In addition to mice, researchers have successfully introduced transgenes of relevance to AD in rats and developed useful AD transgenic rat models. Despite the preference of using mice over rats for easier technical manipulation and higher viability and success rates (Do Carmo and Cuello, 2013), rats offer some important advantages over mice when it comes to their use in modelling neurobiological conditions. Since the rat CNS is physiologically, genetically and morphologically closer to the human than the mouse (Do Carmo and Cuello, 2013), and since the rat is larger and therefore easier to facilitate multiple sampling of cerebrospinal fluid (CSF), assess *in vivo* electrophysiology, perform neurosurgical and neuroimaging procedures, and investigate extensive *ex vivo* examinations of the brain, transfecting the rat with genes of relevance to AD would be useful (Tesson *et al.*, 2005). Furthermore, a key advantage of the rat is the well characterised, more widespread behavioural spectrum it displays that includes more intricate social and motor behaviours, all of which improve the outcomes that could be achieved from their use. It is, therefore, considered that the rat may be a more suitable species to use to model AD (Leon *et al.*, 2010; Do Carmo and Cuello, 2013).

Among the genes reported in the literature to be transfected in the rat for studying AD-like pathology and behaviour are mutant forms of APP, presenilin and tau, some of which are illustrated in **Table (2)** below. Although these genes, alone and in combination, have been successful in expressing some pathological phenotypes of interest, such as neuronal and synaptic loss, few have shown consistent Aβ accumulation or NFT pathology (Cavanaugh, Pippin and Barnard, 2014). When assessing these rats in behavioural paradigms, transgenic rat models expressing APP have regularly displayed a deficit in cognition. To list a few examples of such models, **Table (2)** below summarises some of the transgenic rat models developed over the last decade.

www.manaraa.com

***Table (2) Examples of transgenic rat models of Alzheimer's disease.***

| Model & modification | Observed effects |
|---|---|
| Sprague-Dawley rats expressing the 695-isoform of human APP with the Swedish mutation, and a presenilin mutation.<br><br>(Liu *et al.*, 2008) | **Behaviour:** progressive spatial learning and memory deficits in Morris water maze, deficit in long term potentiation.<br><br>**Pathology:** accumulation of Aβ, presence of plaques in hippocampus, phosphorylation of tau but no tangles. |
| Wistar rats expressing a single APP transgene with the Swedish and Indiana mutations.<br><br>(Leon *et al.*, 2010) | **Behaviour:** cognitive deficits in Morris water maze and fear conditioning at 3 months.<br><br>**Pathology:** plaques from 6 months, marked glial activation. Neuronal and synaptic loss from 18-20 months. |
| Fischer rats expressing the human APP gene with the Swedish mutation, and a presenilin mutation.<br><br>(Cohen *et al.*, 2013) | **Behaviour:** cognitive deficits in reversal learning in the Morris water maze at 6 months.<br><br>**Pathology:** presence of plaques and tangles, microglial and astrocytic activation. Extensive neuronal loss. |
| Wistar rats expressing two human APP transgenes with the Swedish and London mutations, and a presenilin mutation.<br><br>(Audrain *et al.*, 2018) | **Behaviour:** cognitive deficits in the post-Morris water maze probe test at 9 months. No deficit in object recognition or Y-maze was seen.<br><br>**Pathology:** presence of plaques after 30 months. No clear evidence of tangles. Microglial and astrocytic activation is absent up to 30 months. |



www.manaraa.com

Providing a basis for the modelling of aspects of the disease under physiological conditions, *in vivo* transgenic models are a useful resource in AD research. Unfortunately, however, despite the large variety of different transgenic models available, such models have failed to translate to human AD when it comes to therapeutic drug testing. This may be attributed to the fact that replicating human AD in an animal model poses species-specific functional differences, and also to our inability to fully model both neuropathological signs and behavioural symptoms of the disease in the same model that can be readily translated (Cavanaugh, Pippin and Barnard, 2014).

A substantial argument against the translatability of transgenic rodent models is their artificial nature (Cavanaugh, Pippin and Barnard, 2014). Whilst some of them have successfully modelled aspects of disease pathophysiology and behavioural changes, they still use human genes associated with FAD, which accounts for under 5% of all AD cases as discussed above (Prince *et al.*, 2014). Thus, using genetic causes of AD from birth will automatically limit their effectiveness since such models will not be clearly relevant to the most common form of AD: sporadic AD (Duyckaerts, Potier and Delatour, 2008; Puzzo *et al.*, 2015; Drummond and Wisniewski, 2017). Furthermore, using a foreign gene from humans to introduce into a rodent could increase the likelihood of eliciting an immune or defensive response, thus making it difficult to attribute observed phenotypes to the direct results of the triggered AD pathophysiology instead of the defensive cellular process responding to overexpression of a foreign protein (Duyckaerts, Potier and Delatour, 2008). Finally, the focus of transgenic models on amyloid and, to a lesser extent, tau pathology limits the scope of understanding wider disease processes and risks overlooking important risk factors not captured by the incorporation of transgenes (Mullane and Williams, 2019).

To conclude this section introducing transgenic models of relevance to AD, the variability of transgenic models in presenting pathological and behavioural phenotypes pertaining to AD, along with the incomplete representation of the disease itself, illustrates the need for a robust and reliable animal model that more completely represents the disease in its pathology, behavioural impacts and its stages of progression.



www.manaraa.com

### 1.1.4. Non-transgenic models

Instead of incorporating mutant human genes into animals to mimic aspects of AD, non-transgenic approaches have been taken where administration of drugs or proteins of interest *in vivo* brings about the behavioural and pathological phenotypes related to AD. Using this method is advantageous as it enables the modelling of aspects of the disease, such as the impact of acute amyloid administration on behaviour and pathology and allows the investigation of possible mechanisms through which these effects occur (Puzzo *et al.*, 2015).

The toxic impact of Aβo and their role in AD pathogenesis has been discussed above. Aβo are known to induce synaptotoxicity and deficits in cognition (Haass and Selkoe, 2007; Kayed and Lasagna-Reeves, 2012). Their accumulation in the AD brain has been well demonstrated and linked to disease severity in clinical and post-mortem studies (Walsh *et al.*, 2000; Welzel *et al.*, 2014). There is much evidence to suggest that they appear upstream of plaque and NFT formation (Selkoe and Hardy, 2016). Hence, their utilisation in developing models of relevance to AD is logical.

Direct cranial injection of Aβo has been shown by several scientists to yield cognitive and pathological deficits *in vivo* in rodent and non-human primate models, as highlighted in **Table (3)**. Associated tau phosphorylation, synaptic dysfunction, neuronal loss and astrocyte and microglial activation have been reported to accompany Aβo-induced cognitive dysfunction. (Yamada *et al.*, 1999; Brouillette *et al.*, 2012; Forny-Germano *et al.*, 2014; Watremez *et al.*, 2018).

Intracerebroventricular (ICV) injection of synthetic Aβo in the rat in one study resulted in a long-lasting cognitive deficit in the novel object recognition (NOR) paradigm. Post-mortem analysis revealed a marked reduction in synaptic markers (Watremez et al., 2018). In another study, naturally secreted Aβo were found to inhibit *in vivo* long-term potentiation in the rat (O'Hare *et al.*, 2013). Neuronal cell death and cognitive impairment followed the intrahippocampal (IHC) administration of Aβo in the mouse in a third study (Brouillette *et al.*, 2012).

**Table (3)** overleaf summarises some of the popular established non-transgenic animal models and the behavioural and pathological effects observed in each one.



www.manaraa.com

***Table (3) Non-transgenic animal models used in Alzheimer's disease research.***

| Model | Method | Behavioural effects | Pathological effects |
|---|---|---|---|
| Wistar rats<br>(Yamada *et al.*, 1999) | Continuous ICV infusion of Aβo with mini osmotic pump at 300 pmol per day for 14 days. | Cognitive deficits in Morris water maze, Y-maze and passive avoidance impairments. | Neuroinflammation persistent 2 weeks after cessation. |
| Sprague-Dawley rats<br>(Nag, Tang and Yee, 2001) | Continuous ICV infusion of Aβo for 14 days. | Cognitive deficit in object recognition. | No information. |
| C57BL/6 mice<br>(Brouillette *et al.*, 2012) | Repeated IHC injections of Aβo daily for 6 days. | Cognitive impairment in the Y-maze. | Aβ accumulation at injection site and subsequent neuronal cell death.<br>Tau pathology present. |
| Sprague-Dawley rats<br>(O'Hare *et al.*, 2013) | ICV injection of naturally secreted Aβo. | Cognitive deficit in alternating lever cyclical test. | Deficit in long-term potentiation.<br>Reduction in synaptic markers. |
| Wistar rats & cynomolgus macaques<br>(Forny-Germano *et al.*, 2014) | Repeated ICV injections of Aβo 3 times a week for 5 weeks. | Cognitive impairment in operant task (rats). | Widespread Aβo distribution, particularly in memory- and cognition-associated regions.<br>Tau phosphorylation, tangle formation, synaptic dysfunction and astrocyte and microglial activation (macaques). |
| Lister hooded rats<br>(Watremez *et al.*, 2018) | Bolus ICV injection of synthetic Aβo. | Cognitive deficit in object recognition. | Reduction in synaptic markers. Reduction in parvalbumin interneurons. Activation of inflammatory markers. |

www.manaraa.com

A major limitation of these non-transgenic models is their short time scales. Single bolus injections are useful in assessing the short-term effects of Aβo on behaviour and pathology, can help initial identification of potential targets for drug therapies, and can provide insights into the underlying mechanisms associated with disease. Nonetheless, they are limited as they only mimic acute effects of Aβo administration and do not reproduce the gradual Aβ increase seen in humans (Jack et al., 2010; Puzzo et al., 2015).

In patients, AD is a progressive condition that increases in severity with advanced time (Braak and Braak, 1995). When screening the efficacy of novel compounds for AD treatment, preclinical testing in acute models is effectively expecting drug candidates to target pathways not fully mirrored, which sets them up to fail (Puzzo *et al.*, 2015). A key element of creating representative models for neurodegenerative diseases is time. Creation of chronic models has been attempted, such as Brouillette *et al.*, where Aβo were injected every day for 6 days, and Yamada's osmotic pump. However, repeated breach of the cranium is risky, creates room for contamination and infection, and can activate an immune response not attributable to the disease process itself. Secondly, limiting the agents used to only a single amyloid species excludes the possibility of modelling disease processes upstream of the appearance of Aβo and leaves out other toxic fragments resulting from APP processing. That could mean missing out steps in the pathway integral to the development of the disease that can only be met if the amyloid were released endogenously over time, as is the case in sporadic AD in humans (Mullane and Williams, 2019).

### 1.1.5. Aged animals

Spontaneous naturally aged wild-type animals as models of cognitive impairment, as well as senescence accelerated models have been cited in the literature in relation to AD research. Among these, researchers have investigated the use of accelerated aged mice, delayed aged mice, and naturally aged rats, rabbits, dogs and non-human primates to aid modelling natural physiological aspects of ageing (Cavanaugh, Pippin and Barnard, 2014; Mitchell *et al.*, 2015; Puzzo *et al.*, 2015; Mullane and Williams, 2019). These models are valuable in providing information on the natural processes involved in ageing. They are advantageous as they allow the examination of physiological mechanisms without the need to interfere with an animal's genome. Different species have been shown to exhibit varying degrees of Aβ accumulation (mice, macaques, rhesus monkey), tau pathology (rarely, apes), plaque formation (apes, dogs) and neuronal loss (macaques), as well as impaired cognitive function

www.manaraa.com

as a result of advanced age (dogs, macaques) (Cavanaugh, Pippin and Barnard, 2014; Puzzo *et al.*, 2015; Drummond and Wisniewski, 2017).

Whilst aged animals may provide crucial insights into naturally occurring processes related to ageing, they are not reliable enough to produce AD-like pathology consistently and unequivocally. Although advanced age is a major risk factor for AD development, AD is not a natural part of ageing and should not be modelled as such. In addition, species-specific phenotypes make it difficult to draw comparisons between aged animals and dementia patients – that is, marked differences in the location and content of Aβ plaques, the sequence of Aβ peptides and the aggregation states naturally occurring in each of these animals. Furthermore, many of these aged animals do not automatically exhibit a cognitive decline with advanced age or with AD-related pathology, casting doubt on their construct validity (Duyckaerts, Potier and Delatour, 2008; Cavanaugh, Pippin and Barnard, 2014).

#### 1.1.5.1. Preclinical models: the unmet need

To sum up the previous section discussing existing preclinical animal models used in AD research, it is obvious that a wide variety of models exist that aim to model aspects of AD. These models have been useful in establishing a number of underlying disease-related pathways and mechanisms. Although parts of the pathological and cognitive picture in AD have been successfully replicated in some *in vivo* models, there is no one model that completely and accurately encapsulates every part of the disease process (Selkoe and Hardy, 2016). Time being the most critical characteristic of neurodegenerative disease (Jack *et al.*, 2010), it appears to be missing from most of these models.

The stark failure of drug candidates to make improvements for patients in clinical trials likely indicates a weakness in the design of preclinical experiments that support the selection and optimisation of novel therapeutics. The lack of effective translatable animal models that representatively mirror disease processes forms a part of this limitation (Mullane and Williams, 2019). Hence, the rationale behind this project is to bridge the gap in the design of preclinical animal models, incorporating novel techniques to aid the expression of disease complexity. Therefore, it seems sensible for the next step along the way to be the development of a novel preclinical model of relevance to AD that mimics its chronic, sporadic nature more closely and more accurately. The development of such a model would highlight the time-dependent progressive nature of the disease as its primary focus.



www.manaraa.com

#### 1.1.5.2. Project aim

AD is a distressing progressively neurodegenerative disorder associated with an impairment in memory, deteriorating quality of life and a significant economic strain. Contributing to the economic burden is the cost of drug treatments, which are ineffective in modifying the disease (Casey, Antimisiaris and O'Brien, 2010). The staggering failure of therapeutic agents tested in clinical trials has brought the validity of preclinical animal models into question (Drummond and Wisniewski, 2017). Since over 95% of AD cases are sporadic, the use of transgenic animal models expressing familial mutations to recapitulate AD behaviour and pathology is problematic. Additionally, existing non-transgenics lack the key feature of time-associated progressive neurodegeneration and Aβ build-up (Cavanaugh, Pippin and Barnard, 2014). These limitations call for more effective preclinical model development to aid drug discovery.

The mounting evidence from human and preclinical investigations implicating Aβo in AD causation includes studies which prove Aβo-mediated cognitive dysfunction, synaptotoxicity, glial cell activation and neuronal loss (Selkoe, 2002; Walsh and Selkoe, 2007; Freir *et al.*, 2011; Selkoe and Hardy, 2016). Therefore, examining the effects of these oligomers on cognition and pathology is important in preclinical model development.

It is the aim of this project to explore the possibility of developing a more representative chronic animal model that will be of benefit in the research field, by formulating a sustained delivery system allowing the chronic secretion of Aβo. This will be a bioengineered 3D cellular system encapsulating Aβo-secreting cells in an alginate microbead for engraftment in the rat brain.

### 1.1.6. Rationale and overview

7PA2 cells are a Chinese hamster ovary (CHO) cell line that is stably transfected with human APP with the V717F Indiana mutation, and thus expresses APP (Podlisny et al., 1995). Reports examining the secretome of these cells concluded the presence of oligomeric conformations of Aβ and various fractions resulting from APP processing, similar to those found in the AD brain (Portelius *et al.*, 2013; Welzel *et al.*, 2014). Culturing these cells and obtaining the conditioned media (CM) containing Aβo has been used in acute Aβo injection models previously to yield cognitive deficits (O'Hare et al., 2013).

In the first part of the study, characterisation of 7PA2 CM using enzyme-linked immunosorbent assay (ELISA), dot blotting and western blotting will be performed to



www.manaraa.com

ascertain the type of oligomeric species obtained from 7PA2 cells (chapter 2). In the second part, a time course of the acute effects of Aβo from 7PA2 CM on cognition in the rat will be assessed using the novel object recognition (NOR) and the Y-maze tests. Post-mortem analysis of harvested brain tissue will follow investigating changes in synaptic markers in response to Aβo administration (chapter 3). Finally, fabrication of 3-dimensional (3D) hydrogel microbeads encapsulating 7PA2 cells will be optimised for future use in chronic animal model development (chapter 4).

In principle, encapsulating 7PA2 cells in 3D microbeads will immobilise them and allow naturally secreted Aβ peptides to be produced continually from the microbeads over time. In future studies, these microbeads can be embedded within the brain structures in the rat to provide a continuous source of Aβo and model the time-dependent aspect missing in many current models. The scope of this project aims to aid the development of this novel modelling system by optimising the formulation of the 3D microbeads but does not extend to the complete characterisation of the chronic model.

In this project, rats will be used in *in vivo* testing since the rat CNS shares morphological and physiological similarities with humans and enables the testing of a variety of behavioural functions (Do Carmo and Cuello, 2013).



www.manaraa.com

# Chapter 2:

## Characterisation of Aβ species secreted from a 2D cell culture system



www.manaraa.com

## Overview: Chapter 2

# Characterisation of Aβ species secreted from a 2D cell culture system

### Hypothesis: 7PA2 cells are a source of Aβ oligomers

7PA2 is a cell line expressing human APP

**CHO**
wild type

**7PA2**
CHO transfected with APP gene

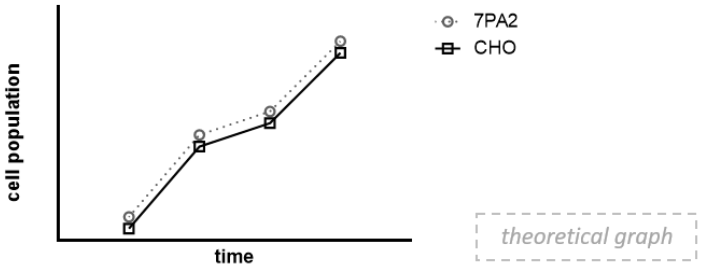


Both cell types show the same growth trend

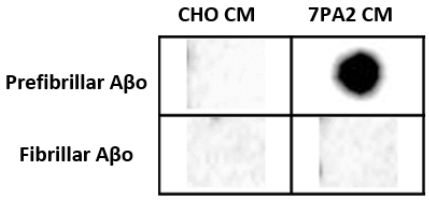


Immunoblotting 7PA2 CM confirms prefibrillar Aβo

**Why is this important?**
Prefibrillar Aβo are found in AD patients' brains and are known to be synaptotoxic.

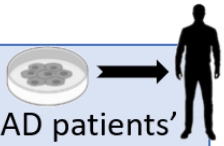



www.manaraa.com

# 2.1. Introduction

### 2.1.1. Aβo toxicity

Extensive research has established that senile plaques themselves, made of insoluble amyloid fibrils, are less liable to cause synaptic damage and neuronal death in AD. Rather, it is now widely accepted that soluble Aβo are more likely implicated in AD pathogenesis (Haass and Selkoe, 2007; Walsh and Selkoe, 2007; Kayed and Lasagna-Reeves, 2012). Various studies have explored the constituent amyloid species found in AD post-mortem brain tissue and cerebrospinal fluid (CSF), and have revealed that oligomeric forms of amyloid were found both intracellularly and extracellularly (Walsh *et al.*, 2000; Kayed and Lasagna-Reeves, 2012). These oligomers were found to be soluble, with an ability to transport across the cell membrane between intracellular and extracellular spaces, and importantly, their abundance was found to correlate with disease severity in several human studies (McLean *et al.*, 1999; Kayed and Lasagna-Reeves, 2012).

Aβ levels in brain tissue and CSF of dementia patients was assessed by many researchers with a large degree of variability in the literature. Lacking a consensus on definitive physiological levels of Aβ poses some difficulty when attempting to replicate biological environments for disease modelling. One study examined Aβ levels in five different neocortical brain regions from deceased patients and assessed their correlation with clinical dementia rating scores. A low score was associated with an overall elevated level of $A\beta_{1-40}$ and $A\beta_{1-42}$ in the brain regions studied. The $A\beta_{1-42}$ fraction was found to be particularly more prone to oligomerisation and levels were elevated more markedly. Aβ elevation was also found to precede hyperphosphorylation of tau, suggesting an earlier involvement of Aβ. Aβ levels were measured in homogenised brain tissue using enzyme-linked immunosorbent assay (ELISA) and were found to be in the scale of picomole per gram of tissue (Näslund *et al.*, 2000). Another investigation looking at levels of Aβ in the cerebral cortex reported Aβ in the order of nanomole per gram of tissue (Tamaoka *et al.*, 1998). Tapiola and colleagues in 2009 assessed patients with dementia and measured Aβ levels in the CSF. CSF was collected by lumbar puncture and levels were determined using ELISA. Levels in CSF were in the picogram per millilitre scale, most commonly detected between 200 and 1000 pg/mL (Tapiola *et al.*, 2009). The discrepancy in reported Aβ concentrations could be a result of the dynamic aggregation of Aβ fragments, transport of Aβ across membranes or variations in experimental methods.



www.manaraa.com

The toxicity of oligomeric Aβ has been demonstrated in a wide variety of *in vitro* and *in vivo* studies, some of which have been cited previously and will be discussed in more detail in the next chapter. The exact mechanisms by which Aβo induce neuronal and synaptic toxicity in patients are not yet fully understood, although proposals have been made to explain these. The diagram in **Figure (3)** below reproduced from a recent review alludes to a range of receptors identified by various researchers where Aβ has been shown to bind (Jarosz-Griffiths *et al.*, 2016). Neurotoxicity is possibly induced by activating signalling pathways as a result of receptor-binding, e.g. via the N-methyl-D-aspartate (NMDA) receptor. It is hypothesised that when Aβo bind to this receptor, they cause an increase in reactive oxygen species, lead to the dysfunction of mitochondria, and bring about a reduction in long-term potentiation – an important mechanism for memory formation. Aβo are also possibly able to disrupt cell membranes, increasing their permeability to ions, which can in turn lead to neurodegeneration as a result of an ion imbalance. Accumulation of Aβo intracellularly can possibly cause proteasome impairment and the breakdown of cellular processes (Kayed and Lasagna-Reeves, 2012). Aβ fragments are also thought to illicit inflammatory reactions by microglial activation (Jarosz-Griffiths *et al.*, 2016; Spangenberg *et al.*, 2019).

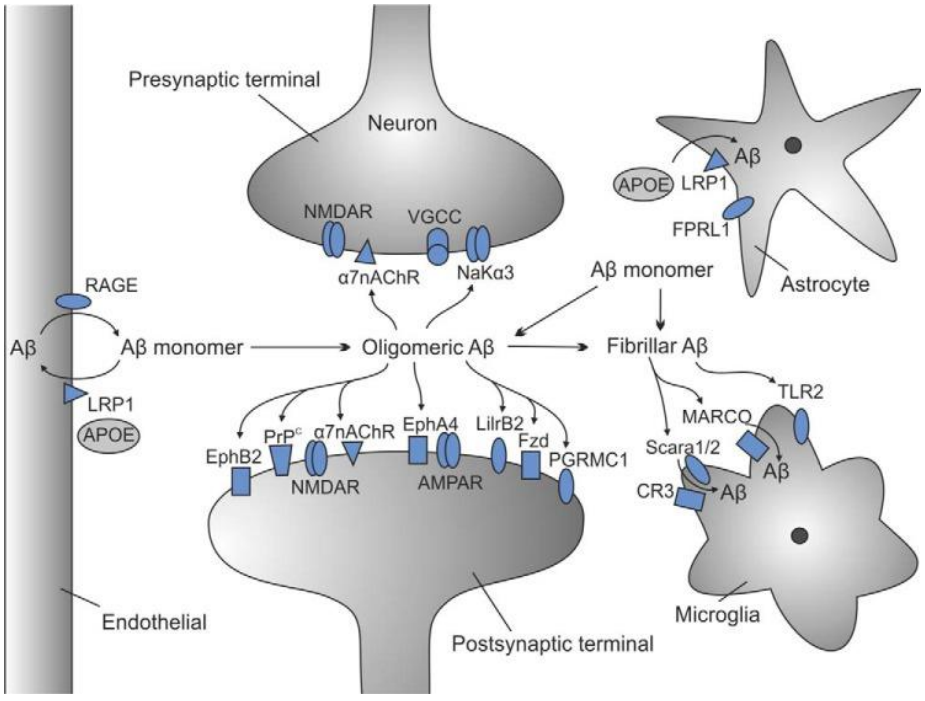


***Figure (3) Sites of Aβ toxicity.***



www.manaraa.com

***A diagrammatic representation of the possible sites of action where amyloid fragments exhibit their effect. Reproduced from (Jarosz-Griffiths et al., 2016).***

A recent review by Selkoe & Hardy summarises the extensive and compelling evidence that supports the implication of Aβo, including data from clinical trials, preclinical research and human studies. The varied mechanisms proposed for the formation and toxicity of Aβo put forward two important conclusions: firstly, modelling AD, or aspects of AD, by utilising only narrowly focused, specific proteins arising from APP (e.g. Aβ monomers only), predisposes the model to limitations in holistically mimicking the disease process; and secondly, treatments aiming to target Aβo could face a difficulty in identifying and successfully targeting the numerous conformations and sites of action of these oligomers, despite their common origin (Selkoe and Hardy, 2016). With this in mind, studies backing the Aβo hypothesis showing that Aβo are toxic, support the utilisation of Aβo (or APP as a precursor to these oligomers) in modelling the disease. It provides a rationale for their use as they are capable of inducing toxicity both *in vitro* and *in vivo*, are known to be present in the human AD brain and can be well correlated with degree of disease severity (Podlisny *et al.*, 1998; Walsh *et al.*, 2000; Haass and Selkoe, 2007; Welzel *et al.*, 2014).

### 2.1.2. Aβ species from 7PA2 cells

Cellular systems have been used to replicate biological conditions associated with AD to better understand molecular mechanisms underlying disease progression and to enable the assessment of therapeutic strategies that could be of benefit to dementia patients. Podlisny and her team successfully engineered Chinese hamster ovary (CHO) cells to stably express a mutant form of human APP known as the V717F Indiana mutation, which translates to a 751-amino acid-long APP molecule (Podlisny *et al.*, 1995). These cells have been termed “7PA2” cells.

Since 7PA2 cells express APP, analysis of the secretome of these cells is expected to reveal proteolytic products of APP, including Aβ. Immunoprecipitation of conditioned media (CM) from cultured 7PA2 cells with the R1282 polyclonal antibody sensitive to $A\beta_{1\text{-}40}$ and the 21F12 antibody sensitive to $A\beta_{31\text{-}42}$ confirmed the presence of oligomeric forms of the Aβ peptide ranging in size between 6 and 12 kDa, in addition to 3-4 kDa sized monomers. Other fragments arising from the enzymatic processing of APP, including the 17-40 or 17-42 fragment p3, were also detected (Podlisny *et al.*, 1998).

Mass spectrometry analysis investigating 7PA2 CM reported a heterogenous mixture of Aβ peptides in a range of conformations. This study found that, in addition to $A\beta_{1\text{-}40}$ and $A\beta_{1\text{-}42}$,



www.manaraa.com

there were over 90 different Aβ sequence-containing peptides naturally secreted from 7PA2 cells. Among the peptides secreted were monomers, dimers, trimers and tetramers of Aβ, as well as longer repeats. Shorter and longer fragments of the original APP molecule were also detected in the CM (Portelius *et al.*, 2013). Another study examined the CM from 7PA2 cells using gel electrophoresis and also saw that Aβ monomers, dimers and trimers were secreted into the media. Moreover, consolidating findings from other studies, it was noted that in some cases, the dimers of Aβ detected were made up of two repeats of unchanged $Aβ_{1-40}$ monomers. Purification of lower (4.5 kDa) and medium (8 kDa) molecular weight amyloid species and testing them using mass spectrometry uncovered their identity as monomer and non-covalent dimer respectively (Welzel *et al.*, 2014).

Studies mentioned here all verify the secretion of a range of amyloid species, including Aβ in monomeric and oligomeric form, from 7PA2 cells. Utilising this characteristic of this cell line can, therefore, be beneficial in studying the effects of a range of Aβ fragments in 2D and 3D *in vitro* systems and in *in vivo* systems.

### 2.1.3. Relevance of using 7PA2 cells to obtain Aβo

The volume of literature implicating Aβo in disease progression has made it clear that studying the biological effects of Aβ in cellular and animal experiments is useful in understanding mechanisms related to AD progression. Sources from which Aβ species can be obtained are varied. Aβ can be isolated from human brains, made synthetically or generated from transfected cell lines. Since Aβ species normally occurring in the human brain include Aβ monomers, oligomers and fractions of varying lengths, replicating that picture would be more useful than synthesising specific lengths and repeats of the Aβ peptide. The 7PA2 cell line expressing APP has been shown to secrete a range of amyloid-containing fractions, especially the $Aβ_{1-40}$ and $Aβ_{1-42}$ species, which are of special interest. These amyloid species, which are also found in human brain tissue and CSF as outlined above, can be considered a necessary component to be studied in AD models.

In summary, the APP-expressing 7PA2 cells are the first cell line to produce Aβ-immunoreactive species with biological activity (Welzel *et al.*, 2014). Using 7PA2 cells as a source of Aβo allows the utilisation of a full range of naturally secreted Aβ species arising from APP processing, thus attempting to replicate physiological Aβ more closely. The Aβ peptides – and specifically the oligomers – secreted from these cells are similar to those found in human AD brains and are therefore closely relevant. Because Aβo are involved in



www.manaraa.com

the underlying processes in the development of AD, 7PA2 cells are a suitable cell line to use since oligomers can be detected in the CM of these cells.

### 2.1.4. Structural classification of Aβo

The Aβ peptide can exist in various configurations following its release from APP. As illustrated in **Figure (4)** below, aggregation-prone Aβ monomers oligomerise into soluble intermediate molecules and accumulate in high-n repeats until they form insoluble Aβ fibrils (Kayed and Lasagna-Reeves, 2012). In this regard, categorising the aggregation state of amyloid species can be made based on solubility: oligomers would be defined as soluble species whereas fibrils would be defined as insoluble (Kayed *et al.*, 2007; Glabe, 2008). Another way to classify amyloid peptides is by size. Since size affects sedimentation rate, speed of elution in gel electrophoresis and fractionation in size-exclusion chromatography, larger amyloid species have been classified as protofibrils and fibrils, whereas smaller molecules have been classified as monomers, dimers, trimers and tetramers and other oligomers. Although classifying Aβ peptides by solubility and size can be useful in some practical respects, it risks overlooking the structural resolution required to make clear distinctions between the aggregation states of Aβ species (Glabe, 2008). Clarifying structural differences could help in attributing the toxic effects of amyloid to the correct moiety and therefore improve preclinical model development and better guide therapeutic approaches.

Due to the field's special interest in the oligomeric forms of Aβ for their reported toxicity, further studies have been performed that investigate the structural differences in Aβo (Kayed *et al.*, 2003, 2007). Since there is a size overlap between different types of Aβo, conformation-dependent antibodies such as A11 and OC can be used to differentiate between different types of amyloid structures and have been reported in the literature (Glabe, 2008). The specificity of these antibodies is such that the epitopes they recognise are associated with aggregation states as opposed to specific amino acid sequences. The difference in epitopes for these antibodies and their ability to exclusively and distinctly recognise fibrillar and prefibrillar amyloid aggregation states is evidence for the existence of structural differences between the various oligomers arising from APP. Charles Glabe concludes that there are two distinct classes of Aβo: prefibrillar and fibrillar. Antibodies detecting each type of oligomer are mutually exclusive due to the difference in peptide backbone alignment and not the amino acid make up nor the size of the molecule (Kayed *et al.*, 2003; Necula *et al.*, 2007; Glabe, 2008). **Figure (4)** below, adapted from Glabe (2008)



www.manaraa.com

describes the probable pathways Aβ monomers take in their aggregation into prefibrillar or fibrillar oligomers, then eventually aggregating into fibrils.

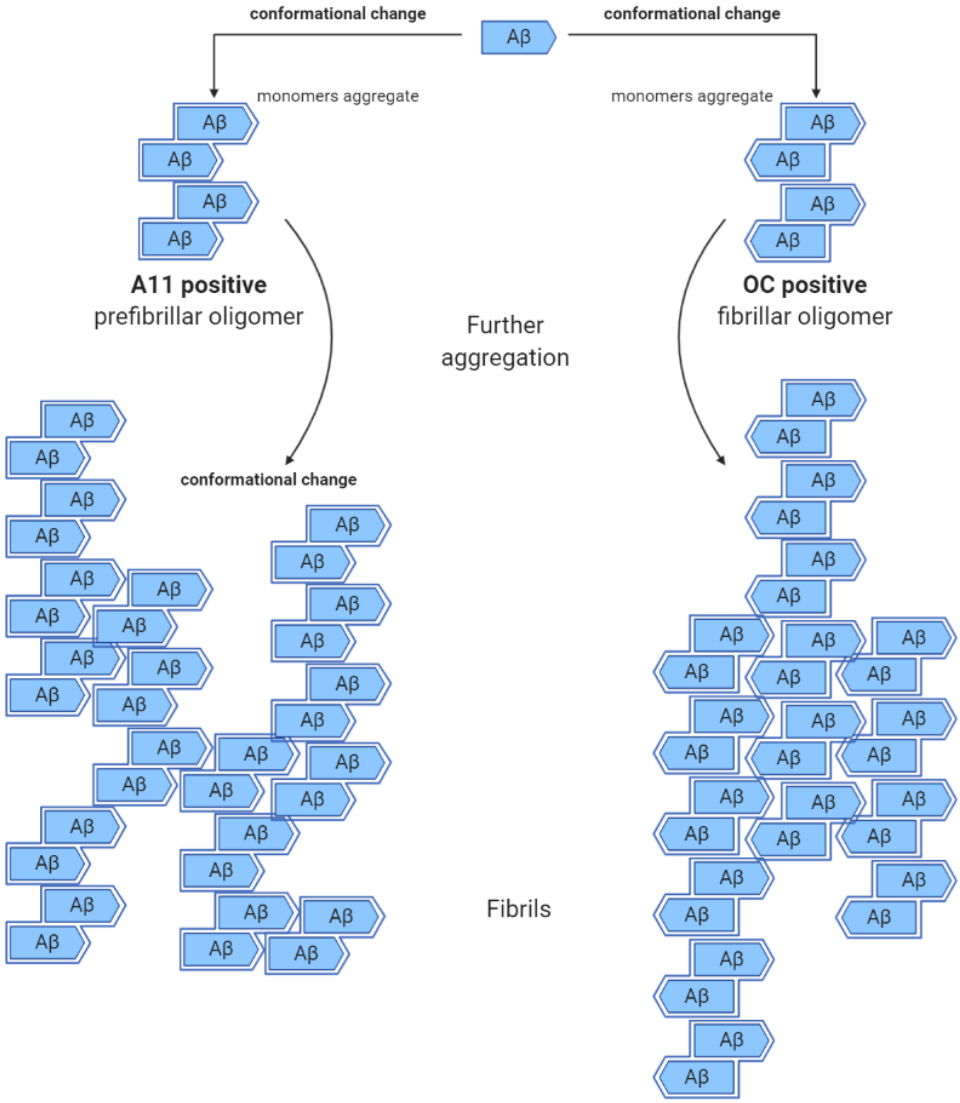


***Figure (4) Schematic representation of Aβ aggregation pathways.***
***Aβ monomers are prone to self-aggregate. Aggregation can take one of two pathways depending on which conformation the Aβ adopts. In the first, monomers aggregate to form prefibrillar oligomers which are A11 positive and OC negative (left). Prefibrillar oligomers then align to form protofibrils (not shown) and elongate by nucleation until they become insoluble fibrils. In the second, monomers aggregate to form a fibrillar oligomer lattice which is OC positive and A11 negative (right). These oligomers can recruit additional monomers at their ends and cause elongation into insoluble amyloid fibrils.***

***Created with Biorender.com***



www.manaraa.com

### 2.1.5. Aim

The investigations in the present chapter aim to characterise the structural nature of Aβo found in 7PA2 CM. Media will be assessed using ELISA, dot blot and westerns in order to identify the type of oligomers found.

The project aims to understand the nature of Aβ oligomers produced by this cell line to compare its relevance to Aβ species found in the brains of AD patients. The resulting conclusions will help identify the usefulness of this cell line in developing a preclinical animal model of use in drug discovery and drug testing.



www.manaraa.com

## 2.2. Methods

### 2.2.1. 2D cell culture

#### 2.2.1.1. Cell lines

Wild type Chinese Hamster Ovary (CHO) cells were cultured in Dulbecco's modified Eagle's medium & nutrient mixture F12 (DMEM-F12) (Gibco™, ThermoFisher) supplemented with 10% (v/v) foetal bovine serum (FBS) (Sigma) and 1% (v/v) antibiotic mixture of 10,000 units of penicillin and 10 mg/mL streptomycin (Sigma). These conditions were also used to culture CHO cells genetically modified to express APP, designated 7PA2 cells. Cells were incubated at 37 $^{o}$C in a 5% $CO_2$ environment. All cells used were handled under sterile conditions and frequently examined for contamination.

#### 2.2.1.2. Cell proliferation assay

A colorimetric assay utilising the reaction which occurs when 3-(4,5-dimethylthiazol-2-yl)-5-(3-carboxymethoxyphenyl)-2-(4-sulfophenyl)-2H-tetrazolium salt (MTS) is reduced by cells to a coloured formazan soluble in cell culture media was used to study cell proliferation (Promega).

Cells were seeded at a density of 15,000 cells $cm^{-2}$ (5000 cells per well) in triplicate in a 96-well plate and incubated in standard culture conditions. At 24-hour intervals, up to 96 hours plus at 168 hours, estimations of viable cell density were made using the MTS assay (Promega). After aspirating the medium from the wells and rinsing them, 120 µL MTS solution in cell culture media at a concentration of 1 in 6 was added to the wells and incubated for two hours in standard cell culture conditions. Absorbance was recorded at 490 nm with a Synergy2 BioTek plate reader interfaced with Gen5 software. The absorbance obtained is directly proportional to the density of living cells in the well.

#### 2.2.1.3. Cell count

Cells were washed briefly with Dulbecco's phosphate-buffered saline (Sigma) then passaged using 0.25% trypsin-EDTA solution (Sigma) for counting. Cells were counted by staining with trypan blue solution and using a haemocytometer.



www.manaraa.com

### 2.2.2. Media analysis

Conditioned media (CM) from CHO and 7PA2 cells, cultured at passages between 5 and 11, was collected at 24-hour intervals and stored at -20 °C for future analysis. Aliquots were made where multiple tests were needed to be performed on the same sample. Each sample did not exceed three freeze-thaw cycles.

#### 2.2.2.1. Sample concentration

Amicon Ultra-4 3K concentrating devices (Merck) were used to concentrate media samples by 80-fold **(Figure (5))**. 4 mL of media was loaded into the filter device and centrifuged at 4,000 x g for 40 minutes. The concentrated filtrate was collected by side-to-side pipetting motion to ensure complete recovery. Concentrated media samples were either analysed immediately or stored at -20 °C until use.

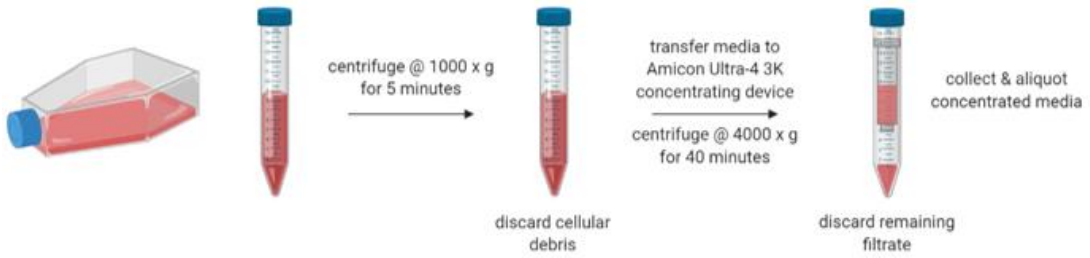


***Figure (5) Concentration of conditioned media.***
***CM was collected from CHO and 7PA2 cell cultures and centrifuged at 1,000 x g for 5 minutes to remove cellular debris. The supernatant was transferred to Amicon concentration device and was centrifuged at 4,000 x g for 40 minutes. The concentrated CM was retrieved using side-to-side pipetting motion and stored in aliquots at -20 °C until use. The remaining media was discarded.***

***Created with Biorender.com***

#### 2.2.2.2. ELISA

Concentrated and unconcentrated media was thawed in a 37 °C water bath for 10 minutes, and tubes were inverted gently to mix contents. Sandwich enzyme-linked immunosorbent assay (ELISA) sensitive to human $A\beta_{1-42}$ was used to confirm continuous secretion of Aβ from 7PA2 cells. Human $A\beta_{1-42}$-detecting immuno-plates (ThermoFisher) pre-coated with a monoclonal capture antibody were loaded with either 50 µL standards following a serial dilution, or 50 µL media samples, both in triplicate. A 50 µL volume of the rabbit detection antibody specific for the C-terminal of the 1-42 Aβ sequence was added to all standards and samples then co-incubated at room temperature for three hours with gentle agitation. After washing with wash buffer, 100 µL of horseradish peroxidase (HRP)-labelled anti-rabbit antibody was added and incubated at room temperature for 30 minutes with gentle



www.manaraa.com

agitation. The plate was washed again, followed by the addition of 100 µL of chromogen substrate to produce colour, and then incubated in the dark at room temperature for 30 minutes with gentle agitation. A stop solution was then added to end the substrate reactions and the plate was read using a BioTek plate reader interfaced with Gen5 reader software. Absorbance was measured at 450 nm. $A\beta_{1-42}$ was quantified after generation of a standard curve using the known concentrations of Aβ.

#### 2.2.2.3. Synthetic Aβ preparation

Known standards of synthetic $A\beta_{1-42}$ peptide were made up as per Hooper Lab (University of Manchester) and Chromy protocol (Chromy *et al.*, 2003). Briefly, lyophilised $A\beta_{1-42}$ (Anaspec) was dissolved in hexofluoroisopropanol (HFIP), then allowed to stand for four hours at room temperature. A film of Aβ was obtained following evaporation of HFIP with nitrogen gas or vacuum evaporation. The film was stored at -80 °C until use. $A\beta_{1-42}$ film was dissolved in DMSO to a stock concentration of 100 µM, which was snap-frozen in liquid nitrogen then stored at -80 °C until use.

#### 2.2.2.4. Dot blot

The protocol for the analysis of 7PA2 CM using dot blot was loosely based on Hooper lab and Glabe protocols (Glabe, 2008). **Table (4)** below summarises the primary and secondary antibody dilutions and the buffers used after further optimisation of the protocol.

***Table (4) Dot blot antibodies.***

***Summary of antibody and reagent concentrations used in the dot blot analysis. PBS-T = phosphate-buffered saline-Tween, TBST-T = tris-buffered saline-Tween.***

| Primary antibody | Primary dilution | Secondary antibody | Secondary dilution | Buffer |
|---|---|---|---|---|
| 6E10 | 1:5000 | Rabbit anti-mouse | 1:5000 | 0.1% PBS-T |
| A11 | 1:1000 | Goat anti-rabbit | 1:1000 | 0.001% TBS-T |
| OC | 1:1000 | Rabbit anti-mouse | 1:1000 | Tris A |

Reagents for use in dot blot analysis of 7PA2 CM were prepared. All primary and secondary antibodies were made in 3% (w/v) bovine serum albumin (BSA) (Sigma) in the relevant buffer.



www.manaraa.com

Sodium azide (Sigma) at a final concentration of 0.01% (w/v) was added to each primary antibody solution.

Phosphate-buffered saline-Tween (PBS-T) was made by adding 0.1% (v/v) Tween® 20 (Sigma) to PBS (Sigma). Tris-buffered saline-Tween (TBS-T) was made by adding 0.001% (v/v) Tween® 20 to a solution of 20 mM Tris (Sigma) and 0.8% (w/v) sodium chloride (ThermoFisher) made in ultrapure water. Tris A was made by adding 0.85% (w/v) sodium chloride (ThermoFisher) and 0.1% (v/v) Triton™ X-100 (Sigma) to a solution of 0.1 M Tris (Sigma) made in ultrapure water. All buffers were made to pH 7.4.

A 1 µL volume of each standard and sample was spotted in duplicate onto an Amersham™ nitrocellulose membrane (GE Healthcare) and left for 10 minutes to air dry. 5% (w/v) milk (Sigma) made in the appropriate buffer (PBS-T for 6E10; TBST-T for A11; Tris A for OC) was used to block the membrane for one hour at room temperature. Following this, the membrane was thoroughly washed then incubated in the primary antibody (anti-6E10 (BioLegend); anti-OC (Merck Millipore); anti-A11 (Merck Millipore)) at 4 °C overnight. The next day, the membrane was washed again using the appropriate buffer then incubated in the respective HRP-conjugated secondary antibody for one hour at room temperature. The membrane was then thoroughly washed with the appropriate buffer then was subjected to a final wash with Tween®-free buffer. Chemiluminescence was used to image antibody binding using the enhanced chemiluminescence method as per the manufacturer's protocol (BioRad).

***Table (5) Summary of anti-Aβ antibody reactivity***

| | **Monomers** | **Prefibrillar oligomers** | **Fibrillar oligomers** | **Fibrils** |
|---|---|---|---|---|
| 6E10 | ✓ | × | ✓ | ✓ |
| A11 | × | ✓ | × | × |
| OC | × | × | ✓ | ✓ |



www.manaraa.com

6E10 recognises amino acid residues 1-16 of the Aβ peptide but has no prefibrillar Aβo sensitivity. A11 is a polyclonal antibody which recognises prefibrillar oligomers only and has no fibrillar oligomer sensitivity. OC detects fibrillar oligomers and fibrils but not prefibrillar oligomers **(Table (5))** (Necula *et al.*, 2007).

#### 2.2.2.5. Capillary electrophoresis immunoblotting

Simple Western analysis was performed using the Wes platform (Harris, 2015), according to the manufacturer's protocol (ProteinSimple). In brief, Aβ standards, CHO CM and 7PA2 CM were added to a master mix containing dithiothreitol and fluorescent molecular weight marker. The samples were then heat denatured at 95 °C for 5 minutes. The samples, primary antibodies, HRP-conjugated secondary antibodies, blocking reagent, and chemiluminescent substrate were dispensed into a 384-well plate. After plate loading, the separation electrophoresis and immunodetection steps took place in the capillary system and were fully automated. The plate was pre-loaded with sample and stacking matrices (ProteinSimple). The extent of antibody binding was imaged using chemiluminescence and semi-quantitative peaks were produced by the Compass software (ProteinSimple v3.1), equating to protein levels and protein size. The data was analysed using the Compass software. Simple Western analysis was carried out at room temperature and instrument default settings were used. Antibodies used were 6E10 and A11 as reported in **Table (5)** above.

#### 2.2.2.6. Statistical analysis

Data were analysed by one-way analysis of variance (ANOVA) or a two tailed student's t-test for pairwise comparisons. All data are presented as the mean ± standard error of the mean unless stated otherwise. Statistical tests were performed in Prism (Version 8.2.1, Graphpad). Graphs were generated using Prism (Version 8.2.1, Graphpad).



www.manaraa.com

## 2.3. Results

### 2.3.1. CHO and 7PA2 cells proliferate at the same rate

The MTS assay was used to assess the rate of proliferation after seeding the two cell lines in 96-well plates at a density of 15,000 cells $cm^{-2}$ (5,000 cells per well). The transfected 7PA2 cells did not differ in proliferative behaviour in comparison with the wild type CHO cells in a standard 2D cell culture system (i.e. tissue culture treated polystyrene plates). **Figure (6A)** below is a representative graph of cell proliferation rate for CHO and 7PA2 cells at passage 9 monitored up to 7 days of culture. **Figure (6B)** shows the rate of proliferation as estimated using a live cell manual haemocytometer count after seeding cells in a T75 flask at a density of $1.3x10^4$ cells per $cm^2$.

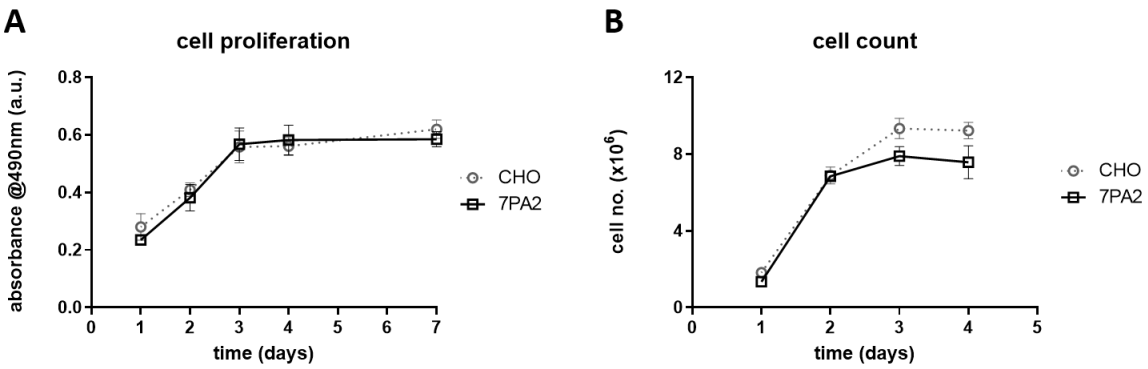


***Figure (6) Comparison of CHO and 7PA2 cell proliferation.***
***Wild type CHO and APP-transfected 7PA2 cells show a similar proliferation rate. (A) The degree of formazan absorption was used to indicate the rate of metabolic activity and proliferation in the MTS assay over a 7-day period. Cell lines show an identical trend. (B) Haemocytometer estimations of live cell number counted in a trypan blue colour exclusion method also show a similar profile of proliferative behaviour in the two cell lines. (Values plotted are averages of two independent experiments, n=3 per experiment, mean ± SEM).***

The pattern of proliferation observed was identical for cells seeded at various passages ranging between 5 and 11.

### 2.3.2. Aβ1-42 is secreted from 7PA2 cells consistently as measured using ELISA

Levels of $A\beta_{1-42}$ in unconcentrated 7PA2 CM were measured using ELISA over a series of time points 24 hours apart up to 96 hours in culture to verify the continuous production of Aβ. Cells were seeded in T75 cell culture flasks in three biological replicates per time point. Media was collected at 24-hour intervals and analysed in technical triplicates using ELISA. As



www.manaraa.com

illustrated in the graph below **(Figure (7))**, the amount of $A\beta_{1-42}$ secreted from 7PA2 cells over a 24-hour period was fairly consistent irrespective of the time point at which media was sampled. Concentrations of $A\beta_{1-42}$ in unconcentrated CM ranged between 150 and 210 pg/mL per cell. On average, the concentration of $A\beta_{1-42}$ secreted over 24 hours in the media equated to 173.9 ± 10.6 pg/mL/cell (mean ± SEM). $A\beta_{1-42}$ was absent in CM from CHO cell culture, blanks and media controls.

A one-way analysis of variance (ANOVA) showed that there were no significant differences between the amount of $A\beta_{1-42}$ detected per cell over the different time points examined ($p>0.05$).

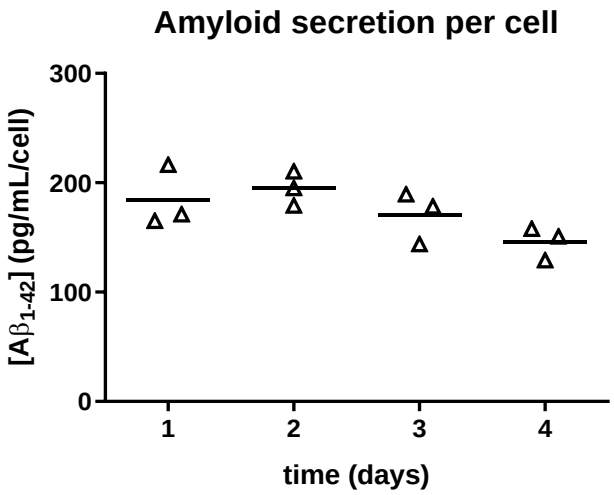


***Figure (7) Rate of Aβ$_{1-42}$ secretion from 7PA2 cells.***
***7PA2 cells secrete Aβ$_{1-42}$ at a consistent rate. On average, each cell secreted 173.9 ±10.6 pg/mL (mean ± SEM) every 24 hours. Levels of Aβ$_{1-42}$ tested between cell passages 5 and 11 retuned results in the same range.***

Concentrated 7PA2 CM was diluted and analysed using ELISA to verify the degree of concentration using the Amicon devices. CM concentrated to 80x was diluted 1 in 80 and compared with unconcentrated controls. ELISA confirmed that $A\beta_{1-42}$ levels in both unconcentrated and concentrated-diluted samples were similar (data not shown).



www.manaraa.com

### 2.3.3. 7PA2 CM contains prefibrillar oligomeric Aβ

7PA2 CM was analysed for 6E10, A11 and OC reactivity using dot blot and westerns to ascertain the configuration of amyloid species contained in the media and was compared to a known synthetic Aβ standard.

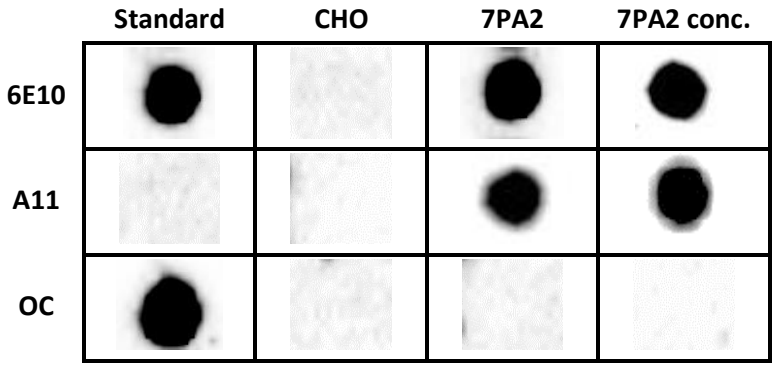


***Figure (8) Dot blot analysis of CHO and 7PA2 conditioned media.***
***Representative images of 7PA2 CM antibody reactivity. Dot blots show that 7PA2 cells secrete Aβ species with a prefibrillar (A11 positive), but not fibrillar (OC negative) oligomeric configuration.***

Analysis of 7PA2 CM using dot blot **(Figure (8))** confirms the presence of oligomeric Aβ. 6E10 reactivity implies the presence of Aβ fragments containing residues 1-16 of the Aβ peptide. 6E10 reactivity was observed in synthetic Aβ standards purchased from Anaspec and in 7PA2 CM before and after concentration using Amicon concentration columns. OC reactivity suggests the presence of fibrillar Aβo. Anaspec standards returned positive to OC, suggesting they take on a fibrillar conformation of oligomers, while 7PA2 CM did not show this, neither before nor after concentration. A11 reactivity indicates the presence of prefibrillar Aβo. Concentrated and unconcentrated 7PA2 CM were A11 positive, whereas Anaspec standards were not.

Concentrated and unconcentrated 7PA2 CM sampled at various time points in culture after 50% confluence and up to 24 hours after 100% confluence showed 6E10 and A11 reactivity in dot blot (data not shown, representative images above). 7PA2 CM incubated for 24, 48, 72 and 96 hours also showed 6E10 and A11 reactivity (data not shown, representative images above). Chemiluminescence was absent from CHO CM and DMEM-F12 control samples.

Western analysis of 7PA2 CM was carried out to confirm the oligomeric configuration of amyloid species contained in the media and to estimate the molecular weights of the Aβo.



www.manaraa.com

As illustrated in **Figure (9)** below, both 6E10 and A11 returned reactivity in the concentrated and unconcentrated CM. With 6E10, molecular weights detected ranged between 130 and 180 kDa, with most intense reactivity at 135 kDa. A11 Aβo were detected in the 39 to 55 kDa range and saw most intense detection at 48 kDa, suggesting that a range of Aβo are present in the media.

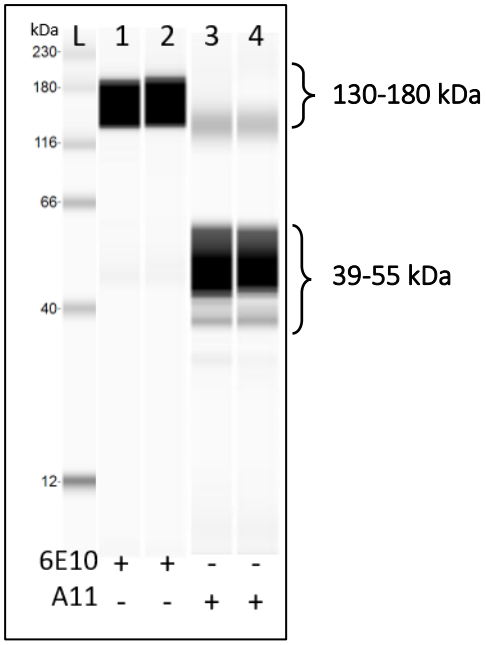


***Figure (9) Antibody reactivity.***
***Wes-generated image representing 7PA2 CM antibody reactivity. The image shows that analysed 7PA2 CM contains Aβ species reactive to 6E10 and A11. Molecular weights with a prefibrillar oligomeric configuration ranged between 39 and 55 kDa. L = ladder, 1 and 3 = unconcentrated 7PA2 CM, 2 and 4 = concentrated 7PA2 CM.***

It can be inferred from the analysis of the concentrated 7PA2 CM using dot blot and western in comparison with the unconcentrated media that the concentration process does not affect the A11 positivity and therefore does not alter the prefibrillar configuration of the Aβo seen in CM from 7PA2 cells cultured in 2D.



www.manaraa.com

## 2.4. Discussion

The present study was designed to characterise the nature of Aβ species present in 7PA2 CM. As part of this, it was of interest to assess the levels of Aβ secreted in the media using ELISA and the configuration of oligomeric Aβ found using dot blot and westerns.

The findings from this study are summarised below:

- When measured using ELISA, levels of $A\beta_{1-42}$ secreted from 7PA2 cells were consistently proportional to cell number over time and averaged 173.9 ±10.6 pg/mL/cell (mean ±SEM).
- ELISA confirmed the absence of $A\beta_{1-42}$ from CHO CM and DMEM-F12 controls.
- Dot blot analysis of Aβ species in 7PA2 CM showed immunoreactivity to 6E10 and A11 antibodies, but not OC antibody, stable over 96 hours. This means prefibrillar oligomeric Aβ is present in the media.
- Antibody reactivity in CHO CM and DMEM-F12 controls was confirmed absent in dot blot.
- Western analysis of 7PA2 CM showed Aβo of molecular weight ~48 kDa and ~135 kDa.
- Analysis of CHO CM and DMEM-F12 controls using western confirmed the lack of Aβ in the media.

Overall, the results of this section of the present study indicate that 7PA2 cells are a suitable source of Aβ fragments, including the $A\beta_{1-42}$ peptide and prefibrillar Aβo. Examining the levels of $A\beta_{1-42}$ secreted by the cells is an interesting measure as it helps confirm 7PA2 cell activity and shows that cells from different biological populations and at different time points and passages secrete comparable amounts of Aβ over a set period of time. The levels of Aβ secreted over 24 hours per cell were observed to be approximately 170 pg/mL on average. This can be used to estimate the predicted levels of amyloid secreted by a known number of cells in any 2D or 3D cell culture system. Understanding the configuration of the Aβ species present in the media was a logical next step, so immunoblotting using dot blot and western was carried out.



www.manaraa.com

The most important finding from this investigation was identifying the structure of the Aβ peptides resulting from 7PA2 cell activity. Spotting unconcentrated and concentrated 7PA2 CM onto a nitrocellulose membrane and incubating with anti-Aβ antibodies revealed reactivity to both 6E10 and A11 antibodies, but not to OC. Since A11 recognises a generic backbone epitope that is common to the oligomeric configuration of Aβ irrespective of amino acid sequence (Necula *et al.*, 2007), the positive A11-immunoreactivity of 7PA2 CM proves the presence of prefibrillar oligomeric Aβ (Kayed *et al.*, 2007; Glabe, 2008). Interestingly, examining human AD brains with the A11 antibody has also been shown to pick up prefibrillar Aβo (Kayed *et al.*, 2003). Analysis of Aβo from 7PA2 CM over time confirms the persistence of Aβ oligomers for up to 96 hours in culture. Synthetic Aβ standards (Anaspec) were OC-positive, meaning they contained fibrillar oligomers. No cross-sensitivity between fibrillar and prefibrillar oligomer detection was seen when incubated with OC and A11, which acted as an additional internal control. Absence of OC reactivity indicates there are no fibrils or fibrillar oligomers in the 7PA2 CM. All CHO CM and DMEM-F12 controls incubated with 6E10, A11 and OC returned negative, confirming no Aβ was detected from these samples.

Looking at the estimations of molecular weight using western analysis, it can be noted that 6E10 strongly detects higher molecular weight oligomers (~135 kDa) but is unable to detect the lower molecular weight prefibrillar oligomers (~48 kDa) as clearly (if at all) even though 6E10 should technically recognise amino acid residues 1-16 of the Aβ peptide. However, dot blot and ProteinSimple western analysis of Aβ using the same antibodies in a different study showed a similar finding. According to Necula's publication, it was suggested that 6E10 might have a limited capacity to detect all types of Aβ, especially different oligomeric conformations. Therefore, extending this to sandwich ELISA systems utilising 6E10, such as the one used in this investigation, suggests they might also be limited in their sensitivity to detect all types of Aβo (Necula *et al.*, 2007).

7PA2 CM sampled as early as 24 hours after seeding in culture showed 6E10 and A11 reactivity in dot blot and western examinations. Presence of prefibrillar oligomers shortly after incubation suggests that a rapid oligomerisation process follows Aβ peptide release from APP (Podlisny *et al.*, 1998). Dominic Walsh speculates that in AD, the oligomerisation process starts early and inside the neuronal cell, contrary to previously held opinions. He presents as evidence that stable oligomers of Aβ are detected from 7PA2 CM so early that they are likely to have formed intracellularly before secretion (Walsh *et al.*, 2000). Aβo reactive to A11 were previously reported to be the major species early in aggregation reactions performed *in vitro* (Necula *et al.*, 2007). Although present very early, 6E10- and



www.manaraa.com

A11-positive Aβ species persisted in the media after incubating for 96 hours. Necula's data also showed persisting A11 reactivity in synthetic $A\beta_{1-42}$ incubated over time for up to 10 hours (Necula *et al.*, 2007).

Aβo found in 7PA2 CM are similar in size and immunoreactivity to Aβo found in the CSF of human AD subjects (Walsh *et al.*, 2000; Kayed *et al.*, 2003; Glabe, 2008). Human CSF also contains Aβ fragments with residues x-15, which has been confirmed in the 7PA2 cells studied here by positive immunoreactivity with 6E10 antibody. The ELISA data showing the presence of the important $A\beta_{1-42}$ fragment was consistent with results obtained from other studies, which is of particular interest considering other transfected cell lines were reported to lack secretion of the $A\beta_{1-42}$ peptide *in vitro* (Portelius *et al.*, 2013; Welzel *et al.*, 2014). In this study, $A\beta_{1-40}$ fragment was not investigated.

The reason prefibrillar Aβo are of particular significance is their natural occurrence in human AD brain and CSF, as alluded to earlier. Additionally, toxicity studies have identified that prefibrillar Aβo are most culpable from among the variety of conformations and aggregation states in which Aβ exists. Many studies have demonstrated that prefibrillar Aβo preferentially affect neuroplasticity and cause impairment in learned behaviours in rodent experiments (Walsh *et al.*, 2002; Cleary *et al.*, 2005; Kittelberger *et al.*, 2012; O'Hare *et al.*, 2013). Furthermore, prefibrillar oligomers have been implicated in inhibiting synaptic function and impairing memory consolidation and therefore contributing to the cognitive decline seen in AD (Freir *et al.*, 2011).

The data obtained in this section of the present study conclude that 7PA2 cells are a source of prefibrillar Aβo. 7PA2 cells can be useful to model the effects of Aβo and other products of APP processing in biological environments (Portelius *et al.*, 2013). Therefore, 7PA2 CM will be used to deliver Aβo in future studies outlined in this thesis.



www.manaraa.com

## 2.5. Chapter summary and forward link

In this chapter, analysis of 7PA2 CM revealed the presence of Aβo in the prefibrillar conformation. Given the extent of supporting evidence implicating these types of oligomers in synaptic dysregulation and cognitive impairment, the potential of Aβo from 7PA2 cells in exhibiting these effects will be assessed in the next chapter.

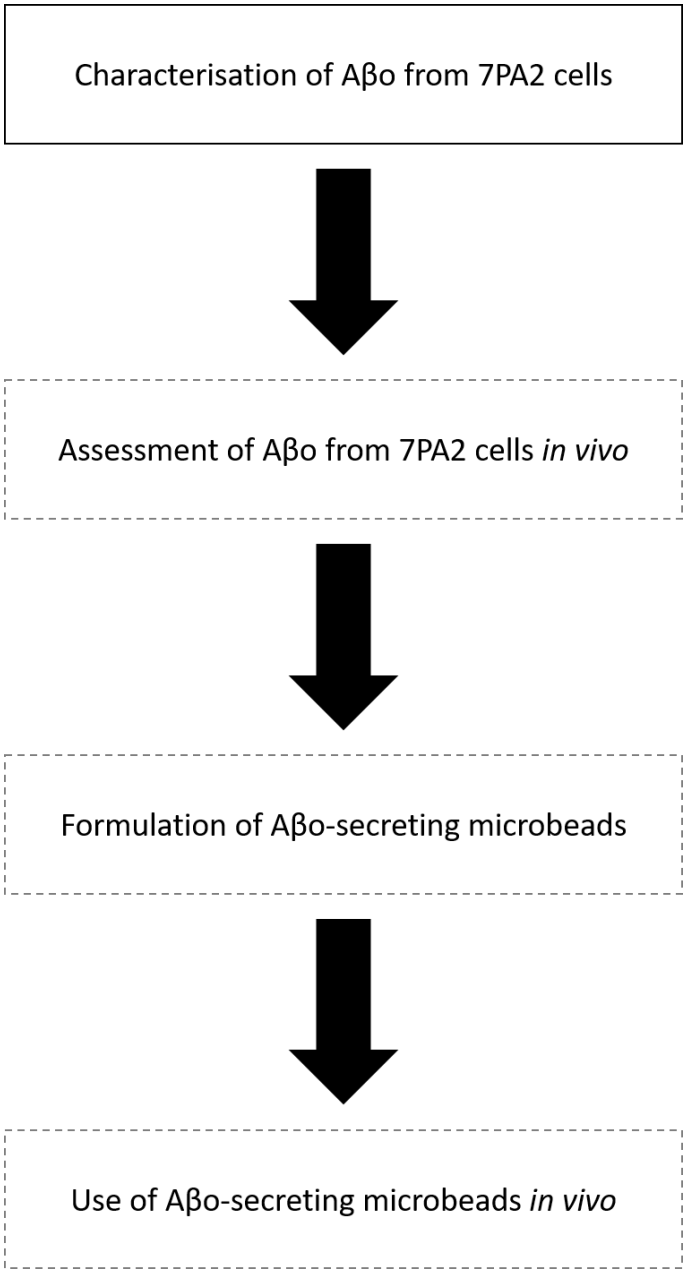




www.manaraa.com

# Chapter 3:

## Investigating the effects of acute administration of Aβo from 7PA2 cells on cognitive and pathological markers in the rodent brain.



www.manaraa.com

## Overview: Chapter 3

# Effects of Aβo from 7PA2 cells on cognitive and pathological markers in the rodent brain

### Hypothesis: Aβo from 7PA2 CM induce synaptic dysfunction leading to changes in cognition

Aβo from 7PA2 cells were injected in the hippocampus

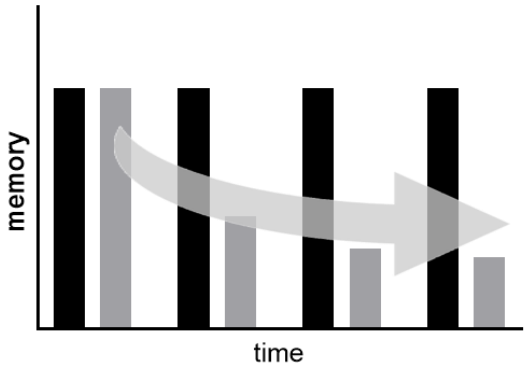


*theoretical graph*

Aβo from 7PA2 cause progressive memory loss

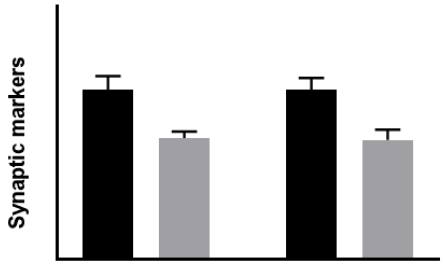


*theoretical graph*

Post-synaptic markers significantly altered in 7PA2 treated rats

**Why is this important?**

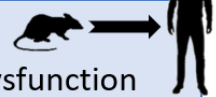

Memory loss and synaptic dysfunction in patients with AD are progressive.



www.manaraa.com

# 3.1. Introduction

### 3.1.1. Assessment of cognitive function in preclinical models of disease

Various assessment methods have been utilised to test cognitive function in preclinical models of disease. One of the most commonly used tools for assessing cognitive function in rodents is the novel object recognition (NOR) test first developed in 1988 (Ennaceur and Delacour, 1988). Recognition memory in this paradigm is examined in a two-phase trial separated by an inter-trial interval (ITI). The task is initiated by first presenting animals with two identical objects in the initial (acquisition) phase, then switching one of the familiar objects with a novel one in the subsequent (retention) phase. Untreated wild type animals are normally able to distinguish the novel object from the familiar due to retaining the memory of exploring the familiar object. Loss of this ability following treatment with compounds of interest, such as Aβ, can be used as an indicator of cognitive impairment. The NOR test is useful for testing memory in the rat as it is quick, repeatable, cost effective, relies on innate exploratory behaviour, does not require training, and has no stressful elements such as food deprivation (Grayson *et al.*, 2015).

Other behavioural tests that have been exploited for evaluating cognitive function in rodent models of AD include the Y-maze, described by Dellu, to be a test of working spatial and recognition memory. Like the NOR test, it is useful and practical because it is based on the natural drive of rats to explore new environments, does not require prior training and avoids the need to withhold food and drink from experimental animals (Dellu *et al.*, 1992). The maze consists of three arms of identical dimensions. Reported test protocols are varied in the literature in terms of duration of trial, number of trials and introduction of rewards, but the test usually assesses the animal's ability to recognise a familiar arm and enter and explore a novel arm.

Examining deficits in memory function is important when developing models of relevance to AD because memory loss is one of the earliest key features seen in dementia patients (Braak and Braak, 1995). A study linking impaired visual recognition memory in AD patients with dysfunction of the anterior subhippocampal cortex where tangles first appear, provides evidence for the relevance of using tests such as the NOR test and the Y-maze in rodents, considering they both assess recognition memory (Didic *et al.*, 2010; Grayson *et al.*, 2015).



www.manaraa.com

### 3.1.2. Assessment of pathological changes in preclinical models of disease

A deficit in cognitive function is often one of the first symptoms to appear in patients with AD. Loss of memory becomes progressively more pronounced with time and is associated with other worsening behavioural and psychological symptoms of dementia. This deterioration in behaviour reflects the gradual development of underlying damage to brain structures starting in limbic areas of the cerebral cortex, spreading to the hippocampus, across the neocortex and further to several subcortical nuclei. Mechanisms of cognitive dysfunction are underpinned by changes in molecular mechanisms of synaptic processes, signalling pathways and damaged neural networks (Braak and Braak, 1995). Assessing these changes can provide direction for therapeutic strategies, especially when attempting to target early time points in disease progression.

Synaptic damage has been shown to correlate closely with disease severity in AD patients and is believed to start upstream of neuronal degeneration (Terry *et al.*, 1991; Haass and Selkoe, 2007). Neurochemical analysis of brain tissue taken from AD patients shows depletion of cholinergic and glutamatergic synapses in early-stage studies. Deficits in neurotransmitters such as γ-aminobutyric acid (GABA) and serotonin are also noted as the disease progresses further (Selkoe, 2002). Since formation of new memories is dependent on intact synaptic performance, loss or damage of synapses could explain the loss of this ability in patients with AD, especially in the earlier stages (Small, Mok and Bornstein, 2001; Selkoe, 2002). Therefore, investigating changes in synaptic markers and how they manifest in preclinical rodent models of relevance to AD is logical.

Researchers studying preclinical animal models of relevance to AD have reported a range of pathological changes accompanying the reported deficits in behaviour. Some of the pathological markers of interest that have been studied include synaptosomal nerve-associated protein-25 (SNAP-25), post-synaptic density protein-95 (PSD-95) and parvalbumin (PV) interneurons. SNAP-25 is considered a marker of normally operational synapses as it mediates synaptic communication via aiding synaptic vesicle fusion (Hodel, 1998; Brinkmalm *et al.*, 2014). In normal physiology, PSD-95 plays a role in synaptic plasticity necessary for memory formation (Xu *et al.*, 2008; Koffie *et al.*, 2009) while PV interneurons are a subpopulation of GABAergic interneurons that are involved in regulating glutamatergic synaptic activity and cognitive function (Chen *et al.*, 2018).



www.manaraa.com

### 3.1.3. Aβo from 7PA2 cells

The toxic profile of Aβo has been of interest in the development of models of relevance to AD. Studies using cultured neurons in Bate's laboratory have reported a reduction in the levels of synaptophysin, synapsin-1 and other markers of synaptic function following treatment with Aβo from 7PA2 cells (Bate and Williams, 2011; Nolan, McHale-Owen and Bate, 2017; McHale-Owen and Bate, 2018; Williams and Bate, 2018). Co-incubation of Aβo from 7PA2 cells with organotypic slices of rat hippocampus showed spine and synapse loss (Shankar *et al.*, 2007). Acute intracerebroventricular (ICV) injection of Aβo from 7PA2 cells robustly inhibited long-term potentiation (LTP) and induced deficits in working memory in the rat in multiple studies (Poling *et al.*, 2008; O'Hare *et al.*, 2013, 2016; Welzel *et al.*, 2014). Aβo-induced impairment of synaptic remodelling was also reported in the rat after receiving 7PA2 CM, accompanied by deficits in passive avoidance and recall behavioural tests (Freir *et al.*, 2011).

Though the observed deficits in memory reported in the aforementioned studies utilising Aβo from 7PA2 cells were assessed by different behavioural paradigms, they all illustrate the capability of Aβo from 7PA2 cells to cause cognitive impairment and synaptic damage. The results seen in these models describe only acute effects and do not explore earlier changes in cognitive and pathological markers. Understanding the progression of synaptic damage and cognitive dysfunction caused by Aβo would be of utmost importance in order to target therapeutic strategies that effectively slow down or halt this progression.

### 3.1.4. Aim

The present study aims to characterise the progressive behavioural and pathological effects of Aβo from 7PA2 cells when administered intrahippocampally (IHC) in Lister hooded rats over a time course. Cognitive function will be assessed using the NOR and Y-maze tests. A related post-mortem time course analysis of pathological markers will follow the behavioural studies.

Use of the phrases "7PA2 CM" and "Aβo from 7PA2 cells" hereafter in this thesis will be interchangeable and will refer to the concentrated media containing prefibrillar Aβo as analysed in section 2.



www.manaraa.com

## 3.2. Methods

### 3.2.1. Animals

80 adult female Lister hooded rats were obtained via Charles River and housed in single sex groups of five in individually ventilated double decker GR1800 cages (Tecniplast, Italy) on a 12-hour light-dark cycle switching at 07:00 and 19:00 respectively. Environmental conditions were controlled at a temperature of 21 °C ±2 °C and humidity at 55% ±5%. Animals had continuous *ad libitum* access to food and water (Special Diet Services, UK). All surgical procedures and behavioural tests were conducted during the light hours of the cycle and complied with the UK Animals (Scientific Procedures) Act of 1986 and the University of Manchester ethical framework.

### 3.2.2. Handling

Animals were weighed weekly until the day of surgery, after which they were weighed daily. There was minimal additional handling during the cleaning of cages and restocking of food and water. Animals were also handled during induction of anaesthesia and in the behavioural tasks, but this was also limited.

### 3.2.3. Conditioned media for administration

CM from CHO and 7PA2 cell culture was collected and concentrated as described in section 2.2.2. CHO CM was used as a control and concentrated 7PA2 CM was used as a source of Aβo.

Previous work in this laboratory has determined that 100 µM is an effective dose of Aβ to yield a cognitive effect in an acute model (Watremez *et al.*, 2018). Levels of $A\beta_{1-42}$ in CM from 7PA2 cell culture were measured using ELISA (section 2). Obtained CM was concentrated to an estimated 80-fold concentration then diluted to achieve the same concentration used previously in the laboratory (100 µM).



www.manaraa.com

### 3.2.4. Experimental design

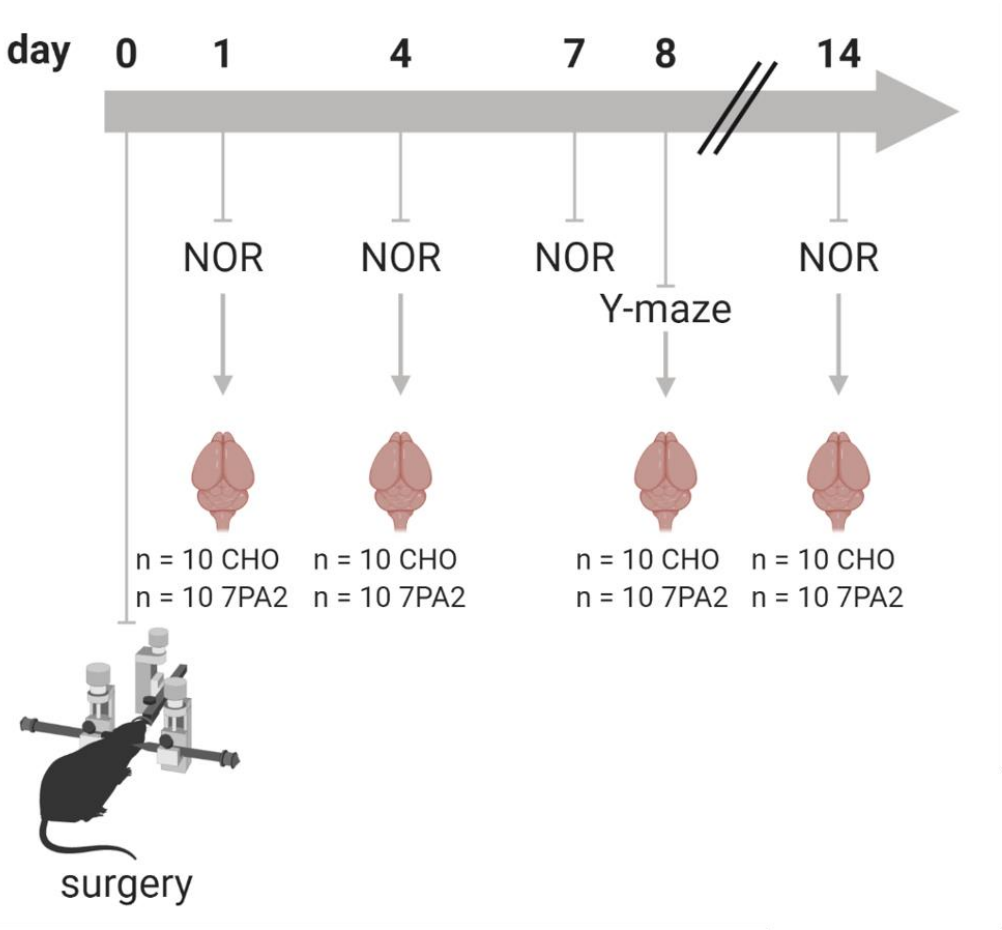


***Figure (10) Experimental design.***
***Animals were randomly assigned a treatment group and a time point, n=10 per group. Following surgery, animals underwent NOR behavioural testing 1, 4, 7 or 14 days later. The Day 7 group underwent the Y-maze test on Day 8. Animals were sacrificed and brains were collected after completion of behavioural study.***

***Created with Biorender.com***

### 3.2.5. Surgery

Rats were randomly assigned to CHO (control) and 7PA2 (Aβo) groups, n=10 per group at each of four time points. Animals undergoing surgery weighed approximately 220 ±20 g on Day 0. All experimental animals received a bolus IHC injection (co-ordinates from bregma AP -3.5, ML -2, DV -4) (Paxinos and Watson, 2007) of CHO CM or 7PA2 CM on Day 0 then were subsequently tested in one or more behavioural paradigms 1, 4, 7+8 or 14 days following surgery as illustrated in **Figure (10)** above. Upon completion of behavioural testing, animals were culled, and brains were collected for post-mortem analysis.

Surgical plane anaesthesia was induced using 4% (v/v) isoflurane (Piramal) in oxygen in an induction chamber. The rat's head was shaved using a clipper. The rat was then mounted



www.manaraa.com

onto a stereotactic frame and anaesthesia was maintained at 3% (v/v) isoflurane. The rat was placed on a sterile-draped heat blanket set to 37 °C, with the rat's temperature monitored using a thermometer probe. The head was fixed to the frame in position using blunt ear bars coated with the local anaesthetic EMLA® cream containing 2.5% (w/w) lidocaine and 2.5% (w/w) prilocaine (Aspen Pharma Trading Limited). Lacri-Lube® containing white soft paraffin, liquid paraffin and wool alcohols (Allergan Ltd) was applied to the eyes to prevent them drying out during surgery. Using a sterile swab, the antiseptic Videne® containing 10% (w/w) povidone-iodine solution scrub (Ecolab) was applied to the shaved area of the head. The rat was given a subcutaneous injection of the analgesic Vetergesic® containing 0.3 mg/mL buprenorphine (Orion Pharma) at a dose of 0.1 mg/kg. Before incision, maintenance of surgical plane anaesthesia was ensured by checking the pedal reflex.

A midline sagittal incision was then made on the scalp. The skin was pulled back to reveal the skull and, if required, was held out of the way using clamp scissors. The skull was dried using sterile swabs to reveal bregma then the coordinates on the stereotactic frame were recorded. Anaesthesia was dropped to 2% (v/v) isoflurane. Target coordinates above the CA1 area of the hippocampus were calculated in reference to bregma as follows: Anterior to Posterior -3.5, Medial to Lateral -2 (Paxinos and Watson, 2007) and marked on the skull. A handheld drill was used to carefully drill a small hole in the skull only. The vertical coordinates were calculated as follows: Dorsal to Ventral -4 (Paxinos and Watson, 2007) and a Hamilton syringe containing 10 µL of CHO or 7PA2 CM was lowered to this position **(Figure (11))**.

***Figure (11) Intrahippocampal surgery.***
***The photograph shows the test animal mounted onto the stereotaxic frame with a Hamilton syringe inserted into position ready for administration of media.***



www.manaraa.com

The 10 µl volume was administered into the hippocampus using these coordinates at a rate of 2.5 µl $min^{-1}$. The syringe was allowed to stand for an additional minute after the injection was made, then was removed. The incised skin was then sutured back using coated Vicryl® sutures. The animal was finally given 1 mL of normal saline intraperitonially to prevent dehydration before being allowed to recover from anaesthesia single-housed in a warm incubator controlled at 28-30 °C for 30 minutes. All rats were then housed single-caged overnight in the original ventilated double decker GR1800 cages under normal conditions then returned to their home cage together the next morning until behavioural studies.

### 3.2.6. NOR

#### 3.2.6.1. Apparatus

The test arena used for the novel object recognition (NOR) test was a 52 $cm^3$ open-top cube made of PVC. The floor of the box was white and marked with a 3x3 grid with black lines. The four walls were black. The test objects used in this study were inverted black cement-filled flowerpots, white plastic bottles containing water, brown glass bottles containing water, red Coca-Cola cans and grey Diet Coke cans **(Figure (12))**. All objects were previously validated by other lab members to ensure there is no smell, colour or shape bias for any of these objects.

#### 3.2.6.2. Test procedure

The NOR test consisted of four parts: habituation, acquisition, inter-trial interval and retention.

Habituation: One day prior to the test, animals were introduced to the arena to be habituated. They were placed in their original home groups of five without any objects for 20 minutes. This was previously found by former lab members to help reduce the anxiety and unfamiliarity with the arena during the testing.

Acquisition phase: Animals were placed in the arena with two identical objects for three minutes and allowed to freely explore. The objects were placed on the crossing lines of the grid pattern so that they are equidistant from the perimeter walls of the arena. These objects are denoted L for left object and R for right.

Inter-trial interval (ITI): Animals were removed for an inter-trial interval (ITI) of one hour and returned to their home cage. The length of the ITI was chosen to be one hour as this assesses



www.manaraa.com

hippocampal involvement in recognition memory (Grayson *et al.*, 2015). The box and objects were then thoroughly cleaned with 70% (v/v) ethanol to preclude any olfactory bias.

Retention phase: A replica of the initial (familiar, F) object used was placed on one side of the grid and a new (novel, N) object was placed on the other. The position of the new object in the arena was randomised and counterbalanced between groups to avoid a spatial bias. Animals were finally placed back in the box and allowed to explore the familiar and novel objects for a further three minutes.

The time spent interacting with each object was recorded. Interaction is defined as actively scratching, sniffing, licking, chewing or touching an object. Scoring of object interaction was performed blind to treatment groups.

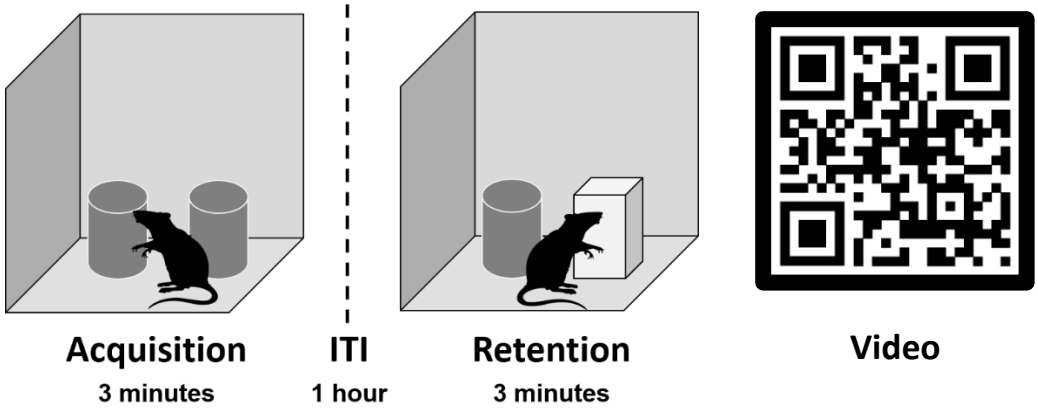


***Figure (12) The novel object recognition (NOR) test.***
***The NOR test consists of two phases separated by an inter-trial interval (ITI). In the acquisition phase, animals were given three minutes to explore two identical objects. In the retention phase, animals were allowed another three minutes to explore two different objects; one was identical to the objects from the acquisition phase and one was an entirely new object. Scan the Quick Response (QR) code to view a sample of the NOR test performed for this project.***

The average time spent at each object (L and R for acquisition and F and N for retention) was calculated for each treatment group. The discrimination index (DI) at retention was used to express the group's ability to differentiate between the novel and familiar objects and was calculated by dividing the difference in time spent at N and F by the total exploration time at retention.

$$DI = \frac{N - F}{N + F}$$



www.manaraa.com

### 3.2.7. Y-maze

#### 3.2.7.1. Apparatus

The test arena used for the Y-maze was an eight-armed radial arm maze with three arms open: arms A, B and C. The three arms were separated by approximately 120$^{o}$ angles. Each arm was 60 cm in length and 10 cm wide. The walls of the arms were made from black PVC and reached 29.5 cm up. The floor of the arena was made from white PVC with no additional markings, patterns or grids. The arena was surrounded by a black curtain that served to minimise distractions and reduce stress.

#### 3.2.7.2. Test procedure

The Y-maze procedure used in this study is based on Dellu's protocol (Dellu *et al.*, 1992). The test animal was placed at the end of one arm and a timer was immediately started. The rat was left to explore the arms freely. Following a one-minute habituation period the sequence of arm entries was recorded live throughout the following five minutes and the percentage of spontaneous alternations was calculated. A spontaneous arm alternation is defined as three unique arm entries in sequence.

The arm where the test was started was randomised and counterbalanced between and within groups to eliminate orientational or spatial bias. After five minutes the animal was removed and returned to the home cage. The test arena was thoroughly cleaned with 70% (v/v) ethanol solution before testing the next rat to eliminate any olfactory bias. Animals were tested 8 days after surgery, n=10 per group.

### 3.2.8. Post-mortem analysis

#### 3.2.8.1. Brain dissection

Upon completion of behavioural experiments, animals were culled by asphyxiation using carbon dioxide and death was confirmed by cervical dislocation. After separating the head from the body, the skin and scalp were cut away to reveal the skull. The skull was cracked open using hull forceps and a pair of scissors, and the brain was immediately harvested from beneath the skull using a scoop to gently free it from the cranial cavity. The brain was snap frozen in isopentane then stored at -80 $^{o}$C until use.

In reference to visually identified brain landmarks, the site of Aβo injection (left dorsal hippocampus) was retrieved from frozen brains following dissection. The rat brain atlas was



www.manaraa.com

used as a guide to identify brain regions (Paxinos and Watson, 2007). Dissected brain sections were placed in Eppendorf tubes and stored in -20 °C until further analysis.

### 3.2.8.2. Tissue preparation

Tissue was homogenised on ice in a 10-fold volume (mg:µL) of homogenisation buffer containing 10 mM Trizma base (Sigma-Aldrich), 320 µM sucrose (Sigma-Aldrich), 2 mM EDTA (Sigma-Aldrich), and protease- and phosphatase- inhibitor cocktails (Sigma-Aldrich) buffered to a pH of 7.4. Phenylmethylsulfonyl fluoride (PMSF) and sodium orthovanadate were added to the solution at a 1% (v/v) concentration.

Tissue was ground until a homogenous cloudy solution was yielded. The homogenate was then centrifuged at 800 x g at 4 °C for 15 minutes. The pellet (P1) was discarded, and the supernatant (S1) was centrifuged again at 12,000 x g at 4 °C for 20 minutes. The pellet (P2) was discarded and the supernatant (S2) was stored at -20 °C until protein testing. See **Figure (13)** below.

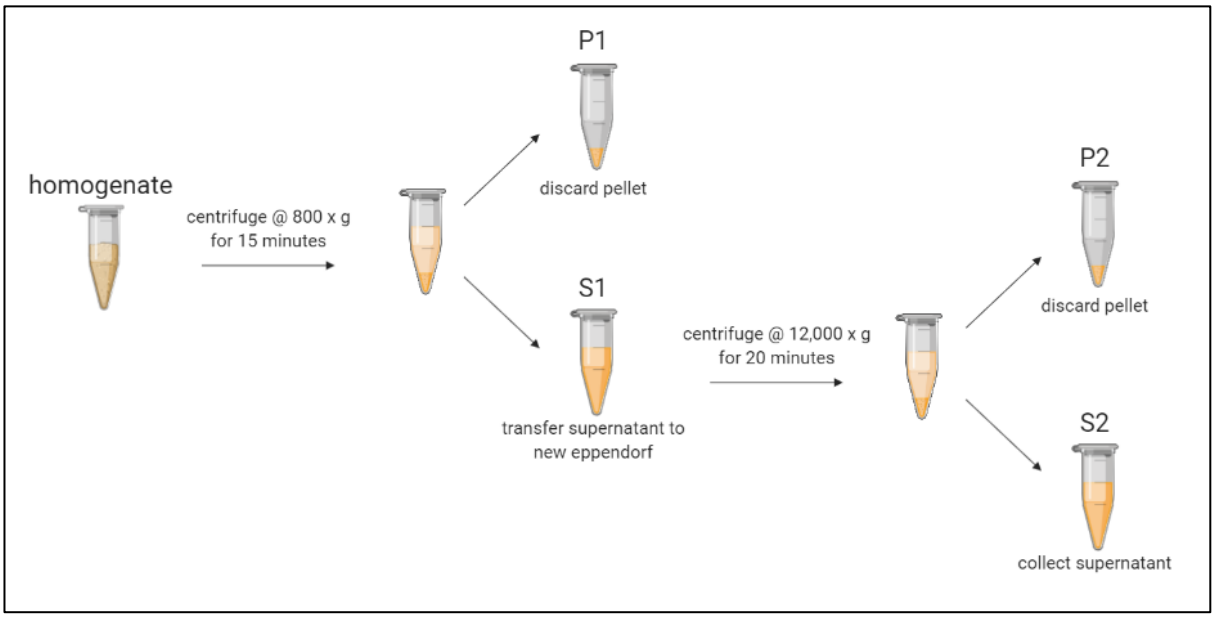


***Figure (13) Brain tissue preparation for protein analysis***
***Homogenised tissue was spun in a cold centrifuge for 15 minutes at 800 x g. The supernatant was transferred to a fresh centrifuge tube and spun again for 20 minutes at 12000 x g in a cold centrifuge. The second supernatant is collected for analysis.***

***Created with Biorender.com***



www.manaraa.com

#### 3.2.8.3. Protein assay

After homogenising the brain tissue and collecting the supernatant S2, a Bradford assay was performed to ascertain the levels of total protein in each sample. Samples were diluted 1 in 5 in Wes sample diluent 1X (ProteinSimple). Known solutions of BSA standards (Bio-Rad) were prepared in concentrations of 1, 0.75, 0.5, 0.2 and 0.1 mg/mL diluted in Wes sample diluent 1X (ProteinSimple). A blank control of sample diluent 1X alone was also prepared as a 0 mg/mL standard. 10 µL of each standard and sample were pipetted in triplicate in a 96-well plate. 200 µL of dye reagent 1X (Bio-Rad) was added to each well. The plate was left to incubate at room temperature for 5 minutes with gentle agitation. The absorbance of the plate was then measured at 595 nm using a BioTek plate reader interfaced with Gen5 reader software. A standard curve was generated from the BSA standards and used to determine protein concentrations of the samples.

#### 3.2.8.4. Protein analysis: capillary electrophoresis immunoblotting

Simple Western analyses were performed using the Wes platform (Harris, 2015), according to the manufacturer's protocol (ProteinSimple). In brief, homogenates of harvested brain tissue from 7PA2 and CHO CM treated animals was diluted using the Bradford assay data to an approximate concentration of 0.1 mg/mL in sample buffer and added to a master mix containing dithiothreitol and fluorescent molecular weight marker. The samples were then heat denatured at 95 °C for 5 minutes. The samples, primary antibodies, HRP-conjugated secondary antibodies, blocking reagent, and chemiluminescent substrate were dispensed into a 384-well plate. After plate loading, the separation electrophoresis and immunodetection steps took place in the capillary system and were fully automated. The plate was pre-loaded with sample and stacking matrices (ProteinSimple). Simple Western analysis was carried out at room temperature and instrument default settings were used. Primary antibodies used were rabbit anti-SNAP-25 (Abcam), mouse anti-PSD-95 (Abcam), rabbit anti-PV (Source Bioscience) and mouse anti-β-actin (Sigma) as listed in **Table (6)** below. All antibodies were optimised prior to use and diluted to final concentrations in antibody diluent (ProteinSimple). Data were analysed using Compass software (ProteinSimple v3.1). Protein densitometry was calculated for each protein of interest and associated loading controls. Data for proteins of interest were then normalised to levels of β-actin and expressed as percentage of control.



www.manaraa.com

***Table (6) Antibodies used for Wes analysis of prepared brain tissue homogenates.***

| Primary antibody | Primary dilution | Secondary antibody | Secondary dilution |
|---|---|---|---|
| SNAP-25 | 1:100 | Anti-rabbit | 1:1000 |
| PSD-95 | 1:200 | Anti-mouse | 1:1000 |
| PV | 1:50 | Anti-rabbit | 1:1000 |
| β-actin | 1:200 | Anti-mouse | 1:1000 |

### 3.2.8.5. Statistical analysis

Data were analysed by a two tailed student's t-test for pairwise comparisons. In data subsets where experimental repeats were normalised to an arbitrary control value (such as 100) a one-sample t-test was performed to compare the control value and column average. All data are presented as the mean ± standard error of the mean unless stated otherwise. Statistical tests were performed in Prism (Version 8.2.1, Graphpad). Graphs were generated using Prism (Version 8.2.1, Graphpad). The table below summarises the statistical analyses used for the data presented in this section.

***Table (7) Statistical tests used for data analysis.***

| Experiment | Measured parameters | Statistical test |
|---|---|---|
| NOR | Difference between L and R exploration time at acquisition | Student t-test |
| | Difference between N and F exploration time at retention | |
| | Difference between total exploration times between treatment groups | |
| | Difference between discrimination indices between treatment groups | |
| Y-maze | Difference between percentage spontaneous alternations | Student t-test |
| Protein analysis | Differences between protein levels between treatment groups | Student t-test |



www.manaraa.com

## 3.3. Results

### 3.3.1. Aβo from 7PA2 cells induce a significant cognitive deficit assessed using the NOR test 7 and 14 days after injection

The NOR task was used to measure progressive changes in recognition memory following IHC injection of Aβo from 7PA2 cells.

**Day 1 summary**

- CHO (control) and 7PA2 (Aβo) animals explored L and R objects equally in the acquisition phase
- CHO and 7PA2 animals spent longer exploring N than F in the retention phase
- There was no significant difference in DI between the CHO and 7PA2 groups
- There was no significant difference in total exploration time between the CHO and 7PA2 groups at acquisition nor retention

**Acquisition**

In the acquisition phase of the task animals in the CHO group explored left (19.76 s ±1.77) and right (21.29 s ±2.7) objects equally ($p>0.05$). Animals treated with Aβo from 7PA2 cells also explored left (19.57 s ±1.88) and right (19.47 s ±1.55) objects equally ($p>0.05$). Therefore, no preference for left or right object was observed in either group.

**Retention**

In the retention phase, animals from both treatment groups were able to significantly distinguish between the novel and the familiar objects. In the CHO group, animals spent 19.96 s ±1.77 interacting with the novel object and 10.45 s ±0.64 on the familiar object ($p<0.001$) – roughly twice as long on novel. Animals receiving Aβo from 7PA2 cells spent 18.57 s ±1.53 on the novel object and 11.58 s ±2.09 on the familiar object ($p<0.01$) **(Figure (14A))**.

**DI**

The DI at retention for the CHO group at Day 1 was 0.3 ±0.03, whereas the DI for the 7PA2 group at the same time point was 0.27 ±0.06. There was no significant difference between the DIs for both groups at retention on Day 1 ($p>0.05$) **(Figure (14E))**.



www.manaraa.com

**Day 4 summary**

- CHO and 7PA2 animals explored L and R objects equally in the acquisition phase
- CHO and 7PA2 animals spent longer exploring N than F in the retention phase
- There was no significant difference in DI between the CHO and 7PA2 groups
- There was no significant difference in total exploration time between the CHO and 7PA2 groups at acquisition nor retention

**Acquisition**

As shown in **Figure (14B)**, on Day 4, animals in both groups explored the objects on the left and right equally during the acquisition phase. Rats in the CHO group spent 20.07 s ±2.22 on the left object and 19.9 s ±1.68 on the right object ($p>0.05$). Animals treated with Aβo from 7PA2 cells also explored left (17.16 s ±1.79) and right (17.97 s ±1.31) objects equally ($p>0.05$). Therefore, no preference for left or right object was observed in either group.

**Retention**

In the retention phase, animals from both treatment groups were able to distinguish between the novel and the familiar objects with significance. In the CHO group, animals spent 21.96 s ±2.7 interacting with the novel object and 12.72 s ±1.97 on the familiar object ($p<0.01$). Animals receiving Aβo from 7PA2 cells spent 15.14 s ±1.32 on the novel object and 11.55 s ±1.36 on the familiar object ($p<0.05$).

**DI**

The DI at retention for the CHO group at Day 4 was 0.27 ±0.05, whereas the DI for the 7PA2 group at the same time point was 0.14 ±0.05 **(Figure (14E))**. Even though there was a lower DI for the 7PA2 group, this difference was not significant ($p>0.05$).



www.manaraa.com

**Day 7 summary**

- CHO and 7PA2 animals explored L and R objects equally in the acquisition phase
- CHO animals spent longer exploring N than F in the retention phase
- 7PA2 animals explored N and F objects equally in the retention phase
- There was a significantly higher DI in the CHO group compared to the 7PA2 group
- There was no significant difference in total exploration time between the CHO and 7PA2 groups at acquisition nor retention

**Acquisition**

Seven days post-surgery as shown in **Figure (14C)**, animals in both groups explored the objects on the left and right equally during the acquisition phase. CHO animals explored the left object for 18.23 s ±1.36 and explored the right object for 19.32 s ±1.22 ($p>0.05$). There was no difference in the time animals treated with Aβo from 7PA2 cells explored left (17.57 s ±1.39) and right (16.32 s ±1.28) objects ($p>0.05$). Therefore, no preference for the left or right object was observed in either group.

**Retention**

Discrimination between novel and familiar objects in the retention phase was observed significantly in the CHO group but not in the group treated with Aβo from 7PA2 cells. In the CHO group, animals spent 10.88 s ±0.74 investigating the familiar object whereas they spent 20.6 s ±0.99 interacting with the novel object ($p<0.001$). Animals receiving Aβo from 7PA2 cells spent 18.55 s ±1.8 on the novel object and 14.81 s ±1.17 on the familiar object ($p>0.05$).

**DI**

**Figure (14E)** shows that at day 7, the DI at retention for the CHO group was 0.31 ±0.03, whereas the DI for the 7PA2 group at the same time point was 0.1 ±0.05. The DI for the CHO group was significantly higher than that of the 7PA2 group ($p<0.01$).



www.manaraa.com

**Day 14 summary**

- CHO and 7PA2 animals explored L and R objects equally in the acquisition phase
- CHO animals spent longer exploring N than F in the retention phase
- 7PA2 animals explored N and F objects equally in the retention phase
- There was a significantly higher DI in the CHO group compared to the 7PA2 group
- There was no significant difference in total exploration time between the CHO and 7PA2 groups at acquisition nor retention

**Acquisition**

Two weeks after surgery, animals in both groups explored left and right objects equally during the acquisition phase. The time spent at left object was 25.41 s ±1.84 and at right was 20.09 s ±1.66 for animals treated with CHO CM, whereas animals treated with Aβo from 7PA2 cells spent 23.59 s ±3.7 on the left object and 21.24 s ±2.14 on the right object (CHO $p>0.05$; 7PA2 $p>0.05$) as shown in **Figure (14D)**. Animals did not exhibit a preference towards either side in the acquisition phase.

**Retention**

In the retention phase, animals in the CHO group explored the novel object for a significantly longer time (24.84 s ±2.74) than they explored the familiar (13.45 s ±1.62) as highlighted in **Figure (14D)** ($p<0.01$). However, animals from the 7PA2 group explored the novel (24.86 s ±2.44) and familiar (20.18 s ±1.45) objects for a similar amount of time during the retention phase of the trial (7PA2 $p>0.05$).

**DI**

At day 14, the DI at retention for the CHO group was 0.29 ±0.05, whereas the DI for the 7PA2 group at the same time point was 0.09 ± 0.08 **(Figure (14E))**. The DI for the CHO group was significantly higher than that of the 7PA2 group ($p<0.05$).



www.manaraa.com

**Total exploration**

The total time animals spent exploring the objects during both phases at each time point was not statistically different between the two groups. The tables below show the total exploration times for this study at acquisition and retention.

***Table (8) Total exploration times during the NOR task.***
***(A) the acquisition and (B) the retention phases of the NOR time course study.***

**(A)**

| Day | Total exploration time (s) | | Student t-test p value |
|---|---|---|---|
| | CHO | 7PA2 | |
| 1 | 41.05 | 39.04 | 0.7 |
| 4 | 39.97 | 35.12 | 0.1 |
| 7 | 37.55 | 33.89 | 0.1 |
| 14 | 45.5 | 44.84 | 0.9 |

**(B)**

| Day | Total exploration time (s) | | Student t-test p value |
|---|---|---|---|
| | CHO | 7PA2 | |
| 1 | 30.41 | 30.15 | 0.9 |
| 4 | 34.68 | 26.69 | 0.1 |
| 7 | 31.48 | 33.36 | 0.3 |
| 14 | 38.29 | 45.05 | 0.1 |



www.manaraa.com

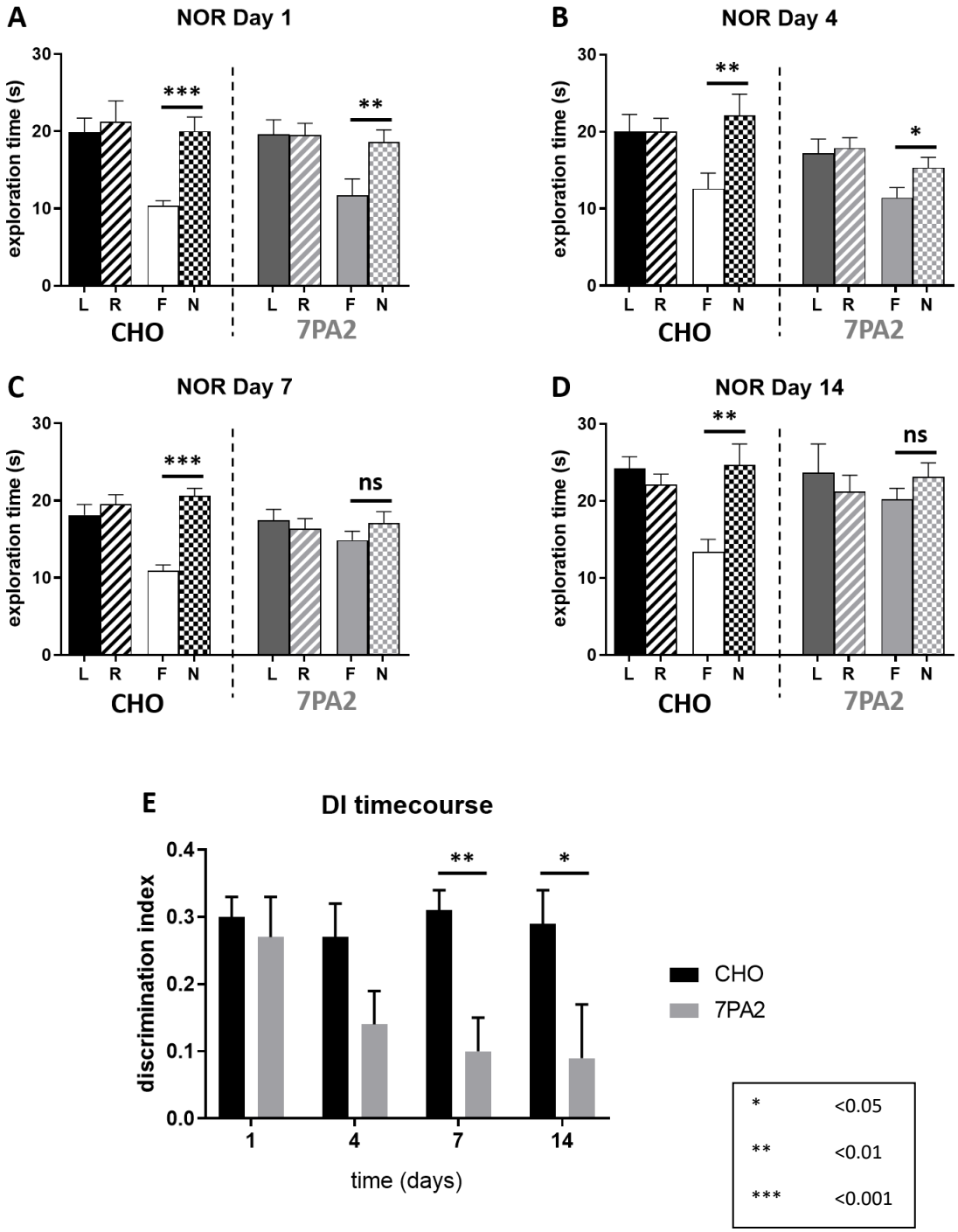


***Figure (14) Novel Object Recognition.***
***Aβo from 7PA2 cells induce a gradual impairment in recognition memory in the NOR test. Data presented as mean ±SEM.***

***(A) and (B) One and four days after surgery, animals from both groups could discriminate between the N and F objects during retention.***

***(C) and (D) Animals in the CHO treatment group successfully discriminated between N and F objects whereas animals receiving Aβo from 7PA2 cells were not.***

***(E) While the DI for CHO animals remained relatively consistent across the four timepoints tested, the DI for 7PA2 animals progressively fell starting at Day 4, becoming significantly different from the CHO group DI at Day 7 and persisted through to Day 14.***

***(Abbreviations: L=left, R=right, F=familiar, N=novel, DI=discrimination index).***



www.manaraa.com

In summary, injecting Aβo from 7PA2 cells intrahippocampally elicited an impairment in recognition memory in the rat starting four days following administration as assessed using the NOR paradigm. This impairment was gradual and progressive, becoming significantly relevant after one week, persisting through to two weeks.

### 3.3.2. Aβo from 7PA2 cells induce a significant cognitive deficit assessed using the Y-maze 8 days after injection

The Y-maze was used on Day 8 to assess changes in working memory following IHC injection of CHO CM and 7PA2 CM in the rat. Following a one-minute habituation, spontaneous alternations were calculated over the five-minute period rats were allowed to explore the maze.

As shown in **Figure (15A)** below, the percentage spontaneous alternations in rats treated with CHO CM was 81.5 ±3.8% whereas spontaneous alternations in animals injected with Aβo from 7PA2 cells was significantly lower at 64.7 ±3.4% ($p<0.01$). On average, no difference was seen in the total number of arm entries between the two groups (average approximately 11 entries per group), $p>0.05$, indicating that changes in alternation behaviour were not due to generalised exploratory, locomotor or motivational effects **Figure (15B)**.

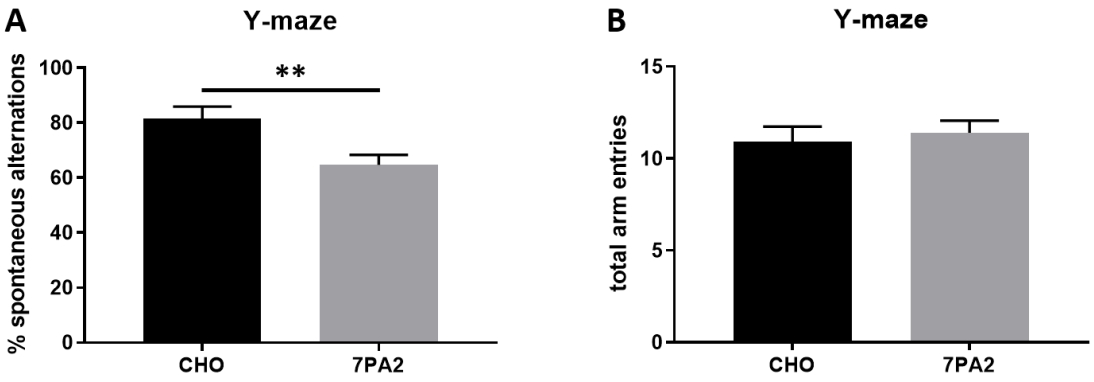


***Figure (15) Y-maze.***
***Aβo from 7PA2 cells induced a deficit in working memory in the Y-maze. (A) Spontaneous alternations in the 7PA2 CM treated group (64.7%) were significantly lower than alternations in the CHO group (81.5%), p=0.004. (B) Total arm entries did not significantly differ between the CHO CM (10.9±0.8) and 7PA2 CM (11.4±0.6) treated animals p=0.6. Data presented as mean ±SEM.***

| | |
|---|---|
| * | <0.05 |
| ** | <0.01 |
| *** | <0.001 |



www.manaraa.com

### 3.3.3. Aβo from 7PA2 cells induced changes in synaptic markers

Relative levels of pre-synaptic marker SNAP-25 determined by chemiluminescence intensity in the Simple Western analysis in the left dorsal hippocampus were compared between CHO and 7PA2 CM treated animals 7 and 14 days after surgery. As illustrated in **Figure (16)** below, levels of SNAP-25 in 7PA2 animals were significantly elevated by 53% on Day 7 ($p<0.001$) and 42% on Day 14 ($p<0.001$).

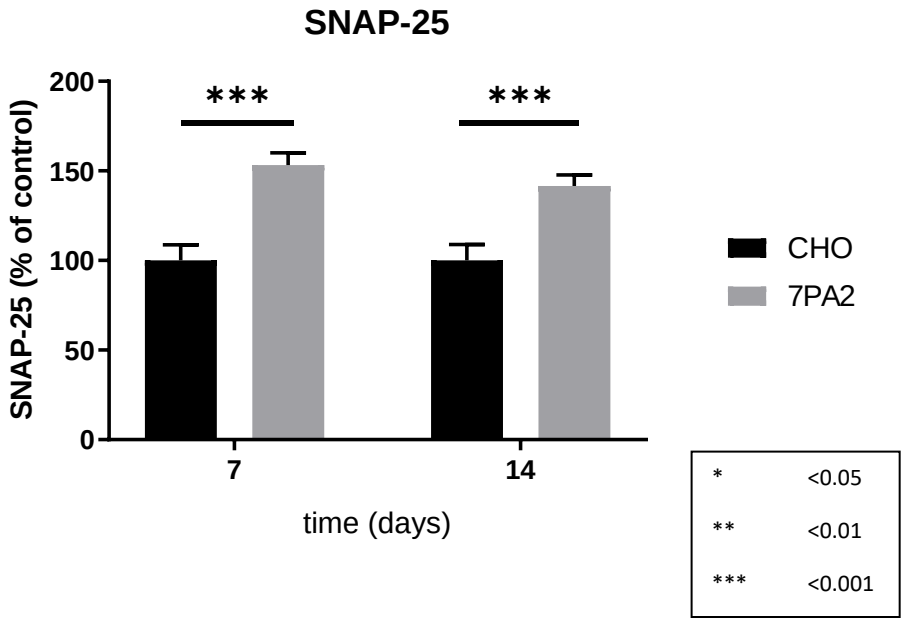


***Figure (16) SNAP-25.***
***Aβo from 7PA2 CM caused an increase in levels of SNAP-25 on Day 7 and Day 14 following surgery. The 7PA2 CM treated group had a 53.27% increase in SNAP-25 compared with CHO controls on Day 4 (p=0.0001) and a 41.65% increase on Day 14 (p=0.0006).***



www.manaraa.com

Relative levels of post-synaptic marker PSD-95 were measured in the left dorsal hippocampus using Simple Western on Day 4 and Day 14. Animals receiving IHC injections of 7PA2 CM had approximately 30% lower PSD-95 intensity than CHO animals at both time points **(Figure (17))**.

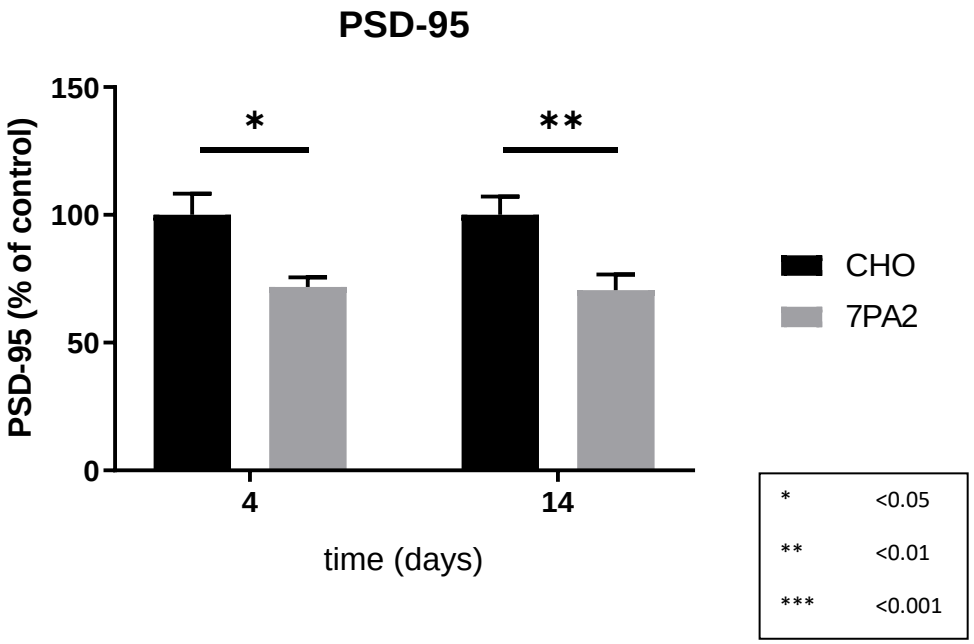


***Figure (17) PSD-95.***
***Aβo from 7PA2 CM caused a significant reduction in levels of PSD-95 4 and 14 days after surgery. Levels of PSD-95 in the 7PA2 CM treated group were 71.78% of controls on Day 4 (p=0.01) and 70.56% of controls on Day 14 (p=0.004).***

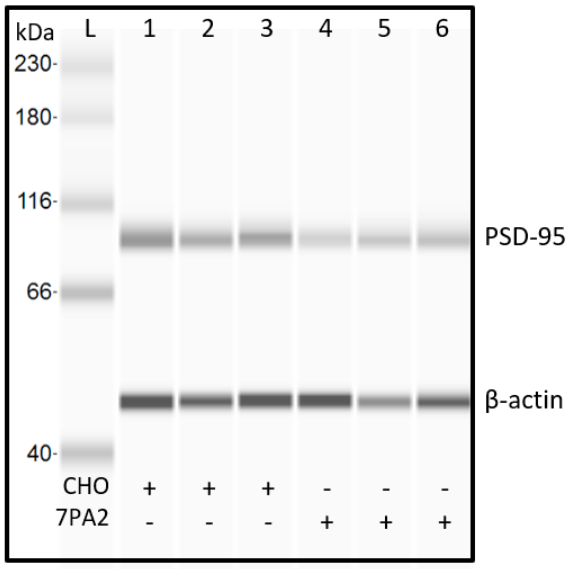


***Figure (18) PSD-95 antibody binding.***
***Representative Wes-generated image of antibody densitometry. Degree of antibody binding is proportional to band intensity. L = ladder, 1–3 = brains from CHO group on Day 4, 4–6 = brains from 7PA2 group on Day 4.***



www.manaraa.com

### 3.3.4. Aβo from 7PA2 cells induced deficits in parvalbumin

Relative levels of GABAergic interneuronal marker PV determined by Simple Western analysis in the left dorsal hippocampus were compared between CHO and 7PA2 CM treated animals 4 days after surgery. PV levels in animals injected with 7PA2 CM were found to be reduced by 40% than CHO animals, although this difference was not statistically significant ($p>0.05$).

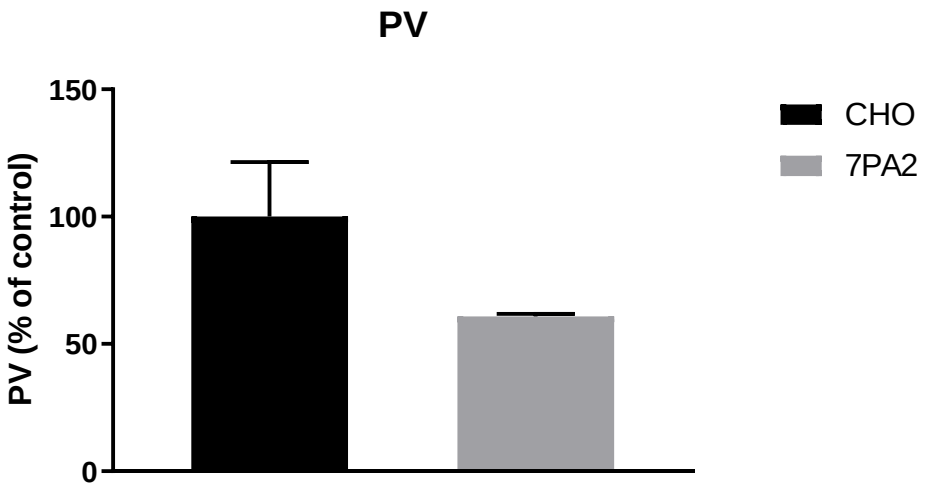


***Figure (19) Parvalbumin.***
***Aβo from 7PA2 CM caused a reduction in levels of PV 4 days after surgery. PV levels in 7PA2 animals were 60.86% of those in controls on Day 4 (p=0.05).***



www.manaraa.com

### 3.3.5. Animal weights unaffected by Aβo from 7PA2 cells

Animals used in this study showed healthy trends of weight gain before the start of experimentations **(Figure (20A))**. After surgery, animals continued to gain weight or remained stable with no overall weight loss observed **(Figure (20B))**. Animals receiving Aβo did not show any differences in weight in comparison with CHO controls (p>0.05).

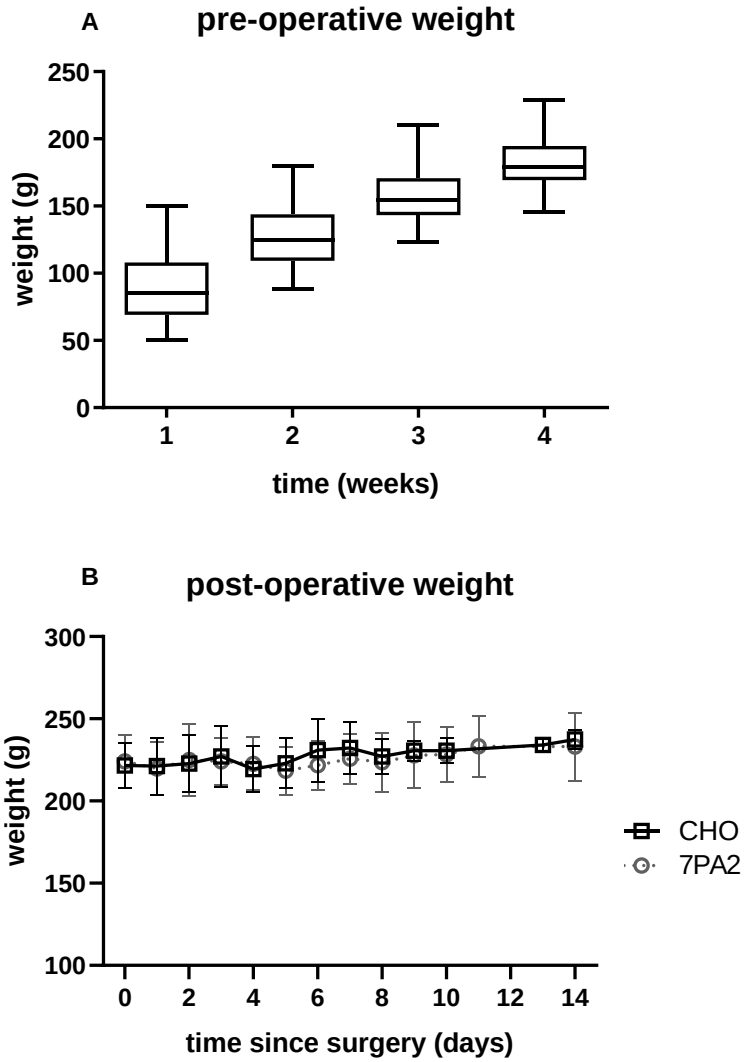


***Figure (20) Animal weights.***
***(A) Animals gained weight steadily over time as they were housed before surgery. Values plotted are mean plus minimum and maximum weights. (B) No adverse effect on weight was seen due to surgical procedures or due to the IHC administration of Aβo up to 14 days after surgery. Values plotted are mean ± standard deviation. An unpaired student t-test analysing differences in CHO and 7PA2 group weights showed no significant differences (p=0.2).***



www.manaraa.com

## 3.4. Discussion

The present study sought to evaluate the effects of IHC administration of Aβo from 7PA2 CM on recognition memory, working memory and pathological markers. As part of this, it was of interest to investigate the time of onset and persistence of changes in cognition and to understand the associated underlying pathology at those time points.

The findings from this study are summarised below:

- All experimental animals were able to perform the NOR task successfully one day after surgery suggesting no adverse effect due to anaesthetic on either group.
- No significant differences between groups in total exploration in the NOR task were observed suggesting no unintended locomotor effects were caused by Aβo.
- In the NOR task, animals treated with CHO CM could always identify the novel object, so using CHO CM is a suitable control.
- Aβo from 7PA2 CM induced a cognitive deficit starting from Day 4, becoming significantly relevant on Day 7 and persisting to Day 14 post-injection as assessed in the NOR test.
- Spontaneous alternations in the Y-maze were reduced in the 7PA2 CM treated animals eight days after surgery.
- Levels of synaptic marker SNAP-25 were increased in the 7PA2 group.
- Levels of synaptic marker PSD-95 were reduced in the 7PA2 group.
- Levels of PV were reduced in the 7PA2 group but not significantly.

### 3.4.1. Object recognition time course

Animals in this study were assigned to CHO or 7PA2 groups randomly. Each animal received 10 µL of CM from either CHO or 7PA2 cell culture. Recognition memory was assessed using the NOR test after 1, 4, 7 and 14 days of receiving the respective IHC injection. On Days 1 and 4, both treatment groups were able to distinguish between the novel and familiar objects. The extent of discrimination between N and F was less pronounced on Day 4, but it was still significantly different. After one week, animals treated with CHO CM were able to differentiate between N and F whereas those in the 7PA2 group were not, and this effect



www.manaraa.com

continued through to two weeks. The gradual onset of this deficit in recognition memory suggests that Aβo may exhibit their toxic effects slowly and progressively.

As alluded to earlier, the NOR test is a useful tool in assessing recognition memory in preclinical models of relevance to AD and has been validated in this laboratory. Grayson's review highlights that testing NOR is suitable for assessing memory deficits caused by Aβ (Grayson *et al.*, 2015). Utilising rats' innate preference to exploring new environments and their inquisitive nature lends itself well to understanding the effects of Aβ on cognitive function. A poor performance in the NOR task likely suggests an interference with recognition memory caused by the agent of interest, which is in this case Aβo from 7PA2 CM. As the total exploration data presented in this study confirms no effect of Aβo on locomotor activity at any of the time points tested, it can be concluded that the inability of rats to distinguish between the novel and familiar objects was down to a cognitive impairment and not a motivational defect (Yamada *et al.*, 1999; Grayson *et al.*, 2015). Observed general husbandry behaviours in addition to post-operative monitoring of weight confirm that Aβo have no effect on the general functioning of the rats tested.

Findings from this study are consistent with previous studies performed within this laboratory where colleagues observed a cognitive deficit following administration of synthetic Aβo in rats (Daniels *et al.*, 2016; Watremez *et al.*, 2018). The cognitive deficit seen in these studies was assessed by NOR as in the present study. Aβo have been shown in other reports to induce a memory dysfunction in NOR. In one study, male Sprague-Dawley rats received ICV injections of Aβ and were assessed using the NOR test. Rats treated with Aβ showed a profound deficit in recognition memory (Nag, Tang and Yee, 2001). In another study, acute ICV injection of Aβo in C57BI/6 mice caused a dysfunction in recognition memory when assessed using the NOR task (Balducci *et al.*, 2010). In this study, Balducci reports that deficits in memory are seen as quickly as one day after mice received the oligomer injection. Balducci also noted that monomers and fibrils of amyloid did not illicit the same effect (Balducci *et al.*, 2010). This provides support for the toxicity of Aβo.

Dissecting the results from the NOR time course study, it is noted that recognition memory does not seem to be affected by Aβo on Day 1. To provide an explanation, it could be suggested that the onset of action of Aβo toxicity is progressive rather than immediate. As time advances and Aβo are given more chance to exert their effect, recognition memory is slightly altered on Day 4, though not significantly. Aβo then continue to cause damage and the deficit in recognition memory is therefore more marked on Day 7. The damage caused is



www.manaraa.com

not reversed by Day 14 as the deficit is still present and is significant. Unpublished work performed by members of this laboratory group has shown that Aβo-induced cognitive deficits are persistent up to 50 days after ICV administration (Jackson, unpublished). Examining the pathology underpinning these changes in cognition may improve our understanding of the mechanisms involved in this progressively worsening effect.

The primary differences in previously published work utilising oligomeric Aβ and the data presented in this thesis pertain to the source and range of amyloid species used, and the site of injection chosen. With regards to the origin of the Aβo, peptides administered in these animals are a host of naturally secreted human Aβ fragments arising from APP processing. They contain A11-positive prefibrillar oligomers in the same conformation they have been found within patient CSF and brain homogenates (Walsh *et al.*, 2002; Kayed *et al.*, 2003; Glabe, 2008). The synthetic oligomers used by Watremez *et al.* have been reported as OC-positive fibrillar oligomers of the $A\beta_{1-42}$ peptide only (Rushworth *et al.*, 2013; Watremez *et al.*, 2018) and so may be limited in their potential to mirror the effects of human Aβo. As for the site of administration, the hippocampus was chosen as it is one of the first structures affected by amyloid deposition and neurodegeneration in patients (Braak and Braak, 1995). In addition, since hippocampal-dependent memory retention is also severely affected in AD patients, assessing the effects of Aβ directly in the hippocampus is of particular interest. This is also why in this study, hippocampal involvement tasks such as the NOR and Y-maze tests were used to examine cognitive function (Ennaceur and Delacour, 1988; Dellu *et al.*, 1992; Yoon *et al.*, 2008; Grayson *et al.*, 2015).

Interestingly, reports of anaesthetic effects on memory function in animals and humans have linked isoflurane with Alzheimer's-like pathology and behaviour (Jiang and Jiang, 2015). However, the data presented in the section above proves contrary to those reports. All animals tested from both groups were able to perform well on the NOR task the day immediately following surgery. Animals from the CHO group consistently discriminated successfully between novel and familiar objects throughout the two weeks of testing, again indicating no effect of isoflurane on recognition memory. A recent clinical study revealed no effect of isoflurane on Aβ levels in the CSF from human subjects (Berger *et al.*, 2016), complimenting findings presented in this present study. Despite this, compelling *in vitro* data suggests that isoflurane promotes Aβ oligomerisation and induces apoptosis when incubated with cells for a six-hour period (Jiang and Jiang, 2015). Animals in this present study were exposed to isoflurane for approximately 15-20 minutes on average and no more than 30



www.manaraa.com

minutes in extreme cases. Therefore, it is unlikely that isoflurane had any effect on the natural behaviour and memory of the animals used in this experiment.

Overall, this part of the study revealed a trend of worsening decline in memory function over time as a result of IHC injection of Aβo from 7PA2 CM.

### 3.4.2. Y-maze

Eight days following administration of 7PA2 CM, animals underwent working memory testing in the Y-maze arena. The data obtained showed a significantly robust reduction in spontaneous alternations in the 7PA2 group as compared with the CHO group. This disruption in working memory has also been seen in other studies. One study notes that after repeated daily IHC injections of Aβ for six days, an impairment in memory assessed by the Y-maze is seen in mice (Brouillette *et al.*, 2012). An earlier study reported a cognitive deficit assessed using the Y-maze in Wistar rats receiving a continuous ICV infusion of Aβ (Yamada *et al.*, 1999). In Pillot's lab, mice receiving an ICV injection of synthetic Aβo were also assessed using the Y-maze. In this study, Aβo adversely affected performance in the Y-maze and in other tests of learning and memory (Youssef *et al.*, 2008).

Using the Y-maze as an additional analysis of memory function in this present study consolidates the findings from the NOR data. As discussed previously, like NOR, the Y-maze also relies on natural rodent behaviour and does not subject animals to unnecessary distress caused by food or water restriction and requires no prior training. Animals in the control CHO group were able to successfully make spontaneous alternations over 80% of the time, which provides a good baseline control with which to compare the performance of the 7PA2 group.

This part of the study was performed for a single time point and displayed a loss of working memory function as a result of IHC injection of Aβo from 7PA2 CM. Expanding this study further by examining the effects on more time points – especially earlier time points – would be interesting to help clarify whether both working and recognition memory have a progressive onset and a lasting effect following Aβo exposure.

### 3.4.3. Synaptic impairment

To complement the findings from the behavioural studies, brains were collected and prepared for neurochemical analysis. Hippocampal structures were of particular interest since that was the site of administration. Additionally, as mentioned before, completion of working memory tasks such as the Y-maze requires hippocampal input (Yoon *et al.*, 2008).



www.manaraa.com

Therefore, studying pathological markers in the dorsal hippocampus seemed a logical next step.

Synaptic markers were investigated in this study to attempt to understand the molecular mechanisms of the Aβo-mediated cognitive dysfunction observed in the rat. The present study examined levels of SNAP-25 and PSD-95 after IHC administration of Aβo. The data presented above demonstrates a significant rise in SNAP-25 levels on Days 7 and 14 in 7PA2 animals when compared with CHO controls. In normal physiology, SNAP-25 plays an important role in mediating synaptic communication via aiding synaptic vesicle fusion (Hodel, 1998; Brinkmalm *et al.*, 2014). Furthermore, evidence suggests a role for SNAP-25 in mediating hippocampal synaptic plasticity by interacting with glutamate receptors. Synaptic plasticity is considered the basis of learning and memory and can deteriorate in AD as a result of Aβo toxicity (Selkoe, 2002; Shankar *et al.*, 2008; Selkoe and Hardy, 2016; Hussain *et al.*, 2019). Long-term potentiation (LTP) is an electrophysiological correlate of synaptic plasticity in which synapses become stronger with frequent activation and, in the hippocampus, this process relies on an increase in postsynaptic glutamate (NMDA) receptor expression (Hussain *et al.*, 2019). In the presence of Aβo, studies have reported a reduction in LTP as evaluated using electrophysiology (Selkoe, 2002; Shankar *et al.*, 2008; O'Hare *et al.*, 2013; Selkoe and Hardy, 2016). A reduction in LTP would normally be expected to accompany a reduction in SNAP-25. However, the present study saw a rise in SNAP-25 levels. This increase may be due to decreased inhibition from PV interneurons. The reduction in PV expression observed in this study as a result of Aβo treatment indicates a reduced activity of these inhibitory neurons. The resulting disinhibition of glutamatergic neurons could cause an upregulation of synaptic communication and subsequently an upregulation of related proteins, such as SNAP-25. Therefore, the observed PV reduction could explain the elevated SNAP-25 levels reported here and supports associated findings by colleagues within this laboratory which found a spike in LTP after IHC administration of Aβo from 7PA2 cells in the rat (Sun, in preparation).

Deranged levels of SNAP-25 (both increased and decreased) have been reported in the literature and associated with synaptic degeneration in AD in several human studies. A study examined levels of SNAP-25 in the CSF and examined their relationship with clinical dementia scores. Increasing levels of SNAP-25 were found in AD compared with controls but levels alone did not correlate with deteriorating cognition, whereas increased SNAP-25:Aβ ratios did (Zhang *et al.*, 2018). Another study exploring levels of synaptic marker SNAP-25 in AD patients analysed brain tissue homogenates and CSF and noted that SNAP-25 levels were



www.manaraa.com

significantly lower in AD brains than controls, but significantly elevated in CSF in AD patients, particularly in the earlier stages of disease development. Moreover, rising CSF levels of SNAP-25 correlated significantly with severity of cognitive impairment independent of age (Brinkmalm *et al.*, 2014). Findings from the present study indicate an elevated level of SNAP-25 obtained from tissue homogenates and can also be correlated with worsening recognition memory as assessed by the NOR task and the Y-maze.

Assessment of synaptic markers in the human frontal cortex saw a 25% reduction in presynaptic marker, synaptophysin, in patients with mild, early stage AD, but didn't see as profound nor as early a reduction in marker of synaptic activity, synaptotagmin. This could suggest that, despite the overall synaptic loss, compensatory mechanisms are in place allowing the upregulation of other molecules, such as synaptotagmin. This could provide support for the finding in this present study concerning elevated levels of SNAP-25 (Masliah *et al.*, 2001).

A marked reduction in PSD-95 levels in the dorsal hippocampus on both Days 4 and 14 were also observed. The reduction in PSD-95, a post-synaptic marker, correlates with associated memory deficits observed in the same animals, suggesting a possible association between synaptic damage and the onset of cognitive decline. Though earlier time points were not tested (due to insufficient samples), exploring the time of onset of this synaptic dysregulation would be very interesting. Nonetheless, synaptic markers were shown to be reduced in this study, which is a useful indication to the underlying processes potentially mediating the deficit in memory.

Aβo-induced pathological changes in preclinical animal models have been reported widely in the literature. Forny-Germano and team infused synthetic Aβo every three days for up to four weeks in macaques and followed the spread of Aβ in the brain and recorded the associated pathological effects. They observed a pattern of synaptic dysfunction along with other markers such as tau phosphorylation and astrocyte and microglial activation (Forny-Germano *et al.*, 2014). Other studies examined the link between changes in cognition and changes in pathology. The cognitive deficits observed by Watremez and colleagues were associated with an impairment in synaptic function. Levels of SNAP-25 and PSD-95 in the frontal cortex and hippocampus were examined in rats 35 days following acute ICV injection of synthetic Aβo. SNAP-25 levels were unchanged in either brain region, whereas levels of PSD-95 had fallen significantly in the frontal cortex in the Aβo-treated group, but no change was observed in the hippocampus (Watremez *et al.*, 2018). Though these findings are not



www.manaraa.com

entirely aligned with results obtained in the present study, it is important to note that the site of administration might play a role in the location and extent of the synaptic damage caused. Injecting Aβ into the ventricles is useful in assessing the effects of Aβ spread when carried by CSF but injecting into the hippocampus provides an opportunity to assess direct localised effects on tissue.

Robert Koffie and his team investigated Aβo-associated synaptic damage in mice. They observed that plaques were surrounded by a halo of Aβo and that these oligomers caused synaptic loss. Brain sections were stained for PSD-95 and Aβ animals were found to express less PSD-95 than controls. In this study, the reduction in PSD-95 and dendritic spine loss were linked together and it was concluded that PSD-95 is involved in the mechanisms underlying cognitive dysfunction in AD (Koffie *et al.*, 2009). This notion is in line with findings from the present study and is supported by others in the field (Selkoe, 2002).

Observing a deficit in PSD-95, which ordinarily plays a role in synaptic plasticity essential for memory formation (Xu *et al.*, 2008; Koffie *et al.*, 2009), can be linked very well with the decline in memory seen in the NOR task. Appearance of this deficit as early as Day 4 correlates with human data suggesting that synaptic dysregulation occurs early in the development of AD.

In summary, findings from this section of the present study confirm a dysfunction in synaptic activity caused by acute intrahippocampal administration of Aβo from 7PA2 CM. The associated memory dysfunction accompanying the synaptic changes is a useful indication of some of the mechanisms underpinning the sequence of pathological damage occurring in AD as highlighted in the literature (Braak and Braak, 1995; Selkoe, 2002).

### 3.4.4. Parvalbumin dysregulation

The PV protein is found in a subset of fast-spiking inhibitory GABAergic interneurons. Studying changes in PV expression in the hippocampus is of interest when investigating neurodegenerative diseases such as AD (Chen *et al.*, 2018).

In the present study, western analysis of brain tissue four days following IHC administration of 7PA2 CM reveals a trend towards an Aβo-induced reduction in PV expression. Findings from this present study have been mirrored by others in the field. Diminishing levels of PV interneurons in stained brain sections was seen by Watremez and colleagues following ICV administration of synthetic Aβo in rats. These changes were associated with a decline in cognition as assessed by the NOR test (Watremez *et al.*, 2018). In aged transgenic AD mice,



www.manaraa.com

Fatima Zallo and her team investigated PV immunoreactivity in free floating brain sections and also found a fall in PV-positive interneurons in the dorsal hippocampus (Zallo *et al.*, 2018), matching the data observed in the experiment presented here. In both studies cited here, it can be concluded that the presence of Aβ may cause a disruption to the normal expression and function of PV.

A series of published and some unpublished data generated by colleagues in this laboratory have described PV interneuron deficits following ICV injection of Aβo in the rat despite there being a stable total number of neurons in treated and untreated groups (Jackson, unpublished). This suggests that Aβo toxicity targets specific subsets of neurons and is not necessarily responsible for neuronal death directly (Watremez *et al.*, 2018). In fact, reductions in PV interneurons have been reported in a number of preclinical models of cognitive dysfunction. Colleagues have discussed that preclinical models for cognition in relation to schizophrenia, for example, investigated in the lab saw diminishing levels of PV associated with a decline in cognitive function assessed by NOR. This further suggests that PV and GABAergic pathways play an important role in maintaining functioning recognition memory (Jackson, unpublished). In an APP-expressing transgenic mouse model of AD, PV was found to be a mediator of Aβo toxicity. Depletion of PV function resulted in deficits in LTP. This supports the claim that damaged GABAergic interneurons are associated with abnormal activity of neural circuits and therefore lead to a cognitive deterioration in AD (Zhang *et al.*, 2017). To further illustrate the role of dysregulated PV in causing cognitive impairment, a study utilising transgenic APP mice saw a reduction in PV-mediated inhibition of oscillatory rhythms involved in memory formation, suggesting that Aβ had an impact on PV integrity and cognition function as assessed by the Morris water maze (Verret *et al.*, 2012). In human studies, a qualitative analysis investigating PV interneurons revealed a decrease in density in the hippocampus of AD patient brains compared with controls, though this was not significant (Brady and Mufson, 1997).

To summarise, the results presented in this section show a reduction in PV levels in brain homogenates four days after acute administration of Aβo from 7PA2 cells. This data, in line with other reports, suggest a role involving the GABAergic system, where Aβo possibly exert their action by mediating PV disinhibition. These findings, along with the SNAP-25 pattern discussed above and the ongoing electrophysiological analysis aforementioned leads to interesting conclusions around the sequence of synaptic damage and compensatory mechanisms in response to exposure to Aβo.



www.manaraa.com

### 3.4.5. Aβo-induced dysfunction of cognition and pathology

In the literature, 7PA2-derived Aβo have been demonstrated to induce cognitive deficits in rodent models of relevance to AD. Studies have utilised a variety of behavioural assessment tools, including NOR, Y-maze, alternating lever cycle ratio assay, Morris water maze, fear conditioning and others to show the toxic effect of Aβo retrieved from 7PA2 cell culture (Poling *et al.*, 2008; Kittelberger *et al.*, 2012; O'Hare *et al.*, 2013, 2016; Rammes *et al.*, 2015). The analysis of behaviour completed in the present study adds confirmation to the reports in the literature and expands the knowledge base by exploring the earlier changes in cognition exhibited by acute administration of 7PA2 CM in the rat's brain. Coupling these results with the findings exploring pathological markers have enriched our understanding of the potential mechanisms by which Aβo may induce cognitive impairment and have provided insight into the possible therapeutic directions towards which we should aim in order to halt or slow down the worsening cognitive decline experienced by patients with dementia.

Researches investigating deteriorating cognitive function in AD have been interested in studying early changes in synaptic pathophysiology as formation of new memories depends on normally functioning synapses. Synaptic level damage caused by Aβo could explain the worsening memory function in the animals studied in this experiment, and by extrapolation, could also explain why patients with AD suffer from relentlessly progressive memory loss (Small, Mok and Bornstein, 2001; Selkoe, 2002).

In 2002, Dennis Selkoe published a paper calling for research into the earlier stages of disease progression. He asserted that AD is primarily a synaptic dysfunction, and that the earlier we look within human and preclinical studies the better. Selkoe believes that understanding what initiates AD symptomatology and how it occurs is widely proven to lie with synapses, since neuronal loss almost always follows synaptic damage, and not the other way around (Selkoe, 2002). Selkoe, and indeed other prominent scientists in the field of AD, support investigating multi-layered preclinical models that are able to incorporate important elements such as Aβ, tau and ApoE, to enable the correlation of behavioural, biochemical and electrophysiological analyses of this complex disease (Selkoe, 2002; Haass and Selkoe, 2007; Viola and Klein, 2015).

Preclinical AD models, despite their wide variation, have proven that Aβo are implicated in the loss of presynaptic proteins and synaptic dysfunction (Shankar *et al.*, 2008; Brinkmalm *et al.*, 2014). In light of Selkoe's suggestion and given the speed with which cognitive and pathological changes appear in the animal model described in the present study, it is logical



www.manaraa.com

to investigate synaptic changes at earlier time points of disease progression in patients. This understanding can contribute to better insights and could support the evidence that claims Aβo as the first trigger in the sequence of events at a molecular level that lead to cognitive deficits. This would also help guide therapeutic interventions and approaches to treatment, as targeting the right aspect of the pathway at the right time could provide better outcomes for patients.

The study outlined in this chapter has demonstrated that Aβo-mediated synaptotoxicity resulted in a clear, progressive memory impairment reminiscent of that seen in AD. Therefore, IHC administration of Aβo from 7PA2 CM in the rat is a reliable model for investigating the acute effects of Aβo on early cognitive and pathological changes. Moving forward, to investigate longer-lasting, slower onset effects of Aβo, formulating Aβo-producing 7PA2 cells in a three-dimensional bioengineered system will be explored.



www.manaraa.com

## 3.5. Chapter summary and forward link

In this chapter, prefibrillar Aβo from 7PA2 cells induced a progressive cognitive decline associated with synaptic dysregulation. Considering the chronic nature of amyloid accumulation in the AD brain, in the next chapter, Aβo-secreting 7PA2 cells will be formulated in a sustained secretion 3-dimensional cellular system to mirror this chronicity.

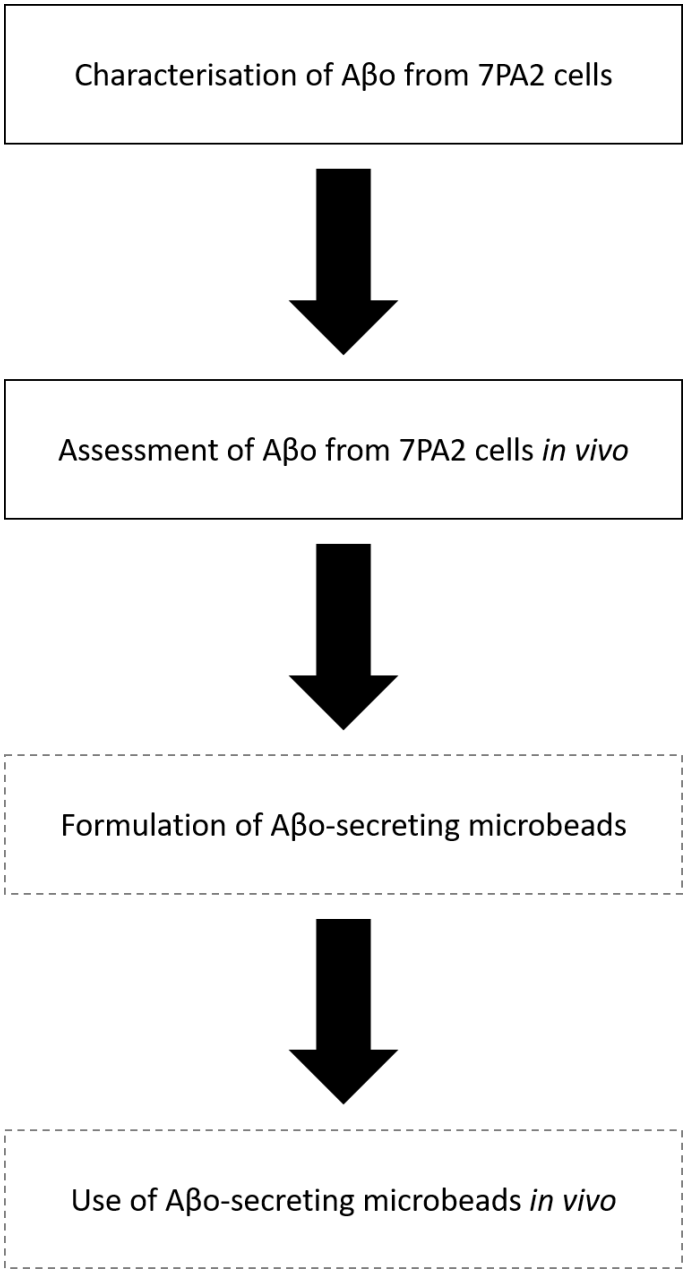




www.manaraa.com

# Chapter 4:

## Fabrication of Aβo-secreting 3D cell culture system



www.manaraa.com

## Overview: Chapter 4

# Fabrication of an Aβo-secreting 3D cell culture system

Hypothesis: 7PA2 cells can be formulated in an alginate hydrogel to allow sustained Aβo secretion

Fabrication parameters were optimised to achieve a uniform size distribution

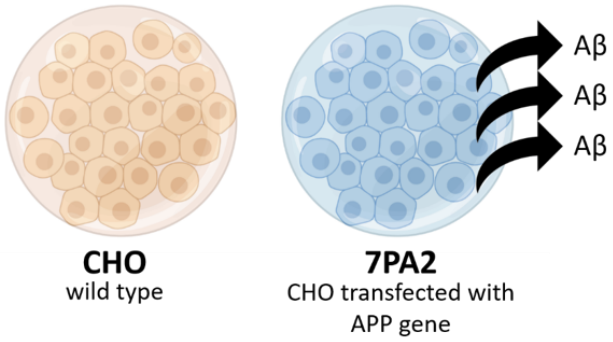


Prefibrillar Aβo were secreted continually from 3D microbeads encapsulating 7PA2 cells

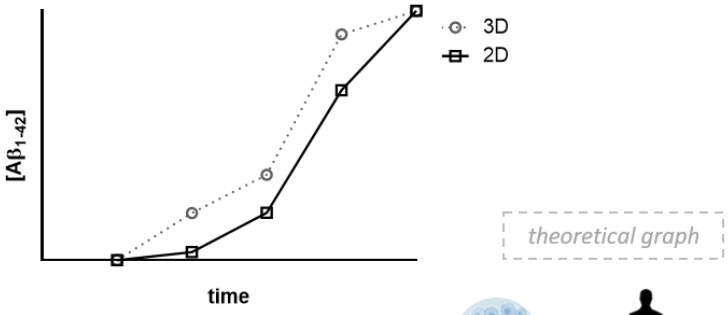


**Why is this important?**
Aβ accumulation in patients with AD is slow and gradual.



www.manaraa.com

# 4.1. Introduction

### 4.1.1. The need for chronic models to study Alzheimer's disease

Modelling aspects of neurodegenerative diseases such as AD in rodents is not without challenges. One of the key characteristics of AD is its slow and progressive onset. Clinical reports for over three decades indicate that increased Aβ production and disturbances in Aβ clearance precede the symptomatic presentation of dementia in patients. As such, Aβ starts to accumulate while individuals are still cognitively normal, and over a period of 20 to 30 years, dysregulation of synaptic function and neurodegeneration occurs (Jack *et al.*, 2010). The graph in **Figure (21)** below is a theoretical representation of the underlying changes in biological markers based on observations made in patients.

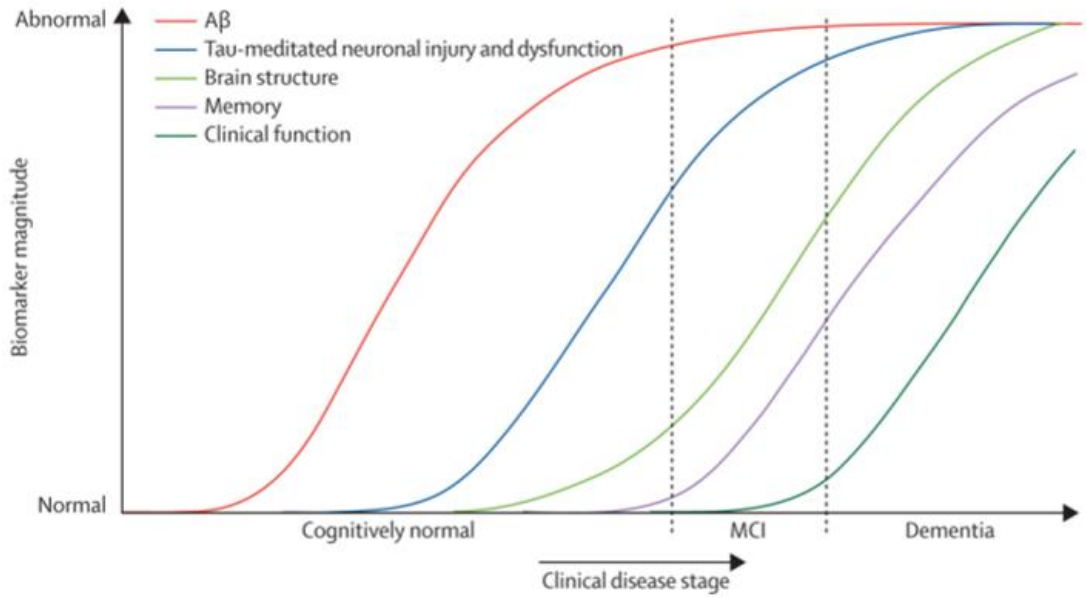


***Figure (21) Dynamic biomarkers of the AD pathological cascade.***
***This theoretical graph expresses how the accumulation of Aϐ (and other markers of relevance to AD) precedes behavioural changes associated with memory and cognition. This plot is reproduced directly from (Jack et al., 2010).***

As outlined in the graph above, it is clear that Aβ build up is a long-term, gradual phenomenon which leads to the relentless loss of neurons and brain atrophy, finally resulting in dementia. In order to attempt to more accurately model aspects of this disease, models must try and replicate the chronicity of the damage caused by Aβ. Dennis Selkoe stressed in a recent report that targeted development of rodent models earlier in disease staging is



www.manaraa.com

critical for progress in the field. In these models, Selkoe advises that investigating synaptic changes as early as possible is more useful in yielding better understanding of disease mechanisms and finding targets for treatment (Selkoe, 2002).

Moving forward, Selkoe also highlights the importance of studying natural assemblies of human Aβ (such as those arising from 7PA2 cells) under physiological conditions. He further elaborates by stating that the highly concentrated synthetic Aβ peptides used in model development in the micromolar range should be substituted with a more subtle nanomolar-scaled concentration, similar to that seen in human brain and CSF. Thus, more realistic models can be developed, and effective therapeutic options can be more seriously explored (Selkoe, 2002).

Animal models described in section 1.4. have reported various strategies to extend the timeline of the models developed. For example, use of osmotic pumps allows the sustained delivery of a finite amount of Aβ over days or weeks, as in Yamada's work (Yamada *et al.*, 1999). Repeated hippocampal and cerebroventricular injections of Aβ *in vivo* have been used to prolong the timelines of Brouillette's and Forny-Germano's models respectively (Brouillette *et al.*, 2012; Forny-Germano *et al.*, 2014). However, with the longest of these timelines only lasting up to five weeks, the effects observed may only be considered acute. Furthermore, repeated invasive injections into cerebral areas could risk model validity and expose animals to inflammation unattributable to the study variables.

Overall, there is an obvious need for the development of a novel experimental preclinical model which can replicate the progressive nature of the disease for a longer time period comparable to human timescales in order to ultimately make progress in therapeutics.

#### 4.1.2. Bioengineered 3D systems for modelling Alzheimer's disease

2-dimensional (2D) cell culture systems are widely used to study and model the effects of Aβ *in vitro* and have provided useful information to assist our understanding of molecular mechanisms associated with AD (Henstridge and Spires-Jones, 2018). Cultured primary neurons from mouse embryos are used in Bate's laboratory, for instance, and cell viability is used to investigate the toxicity of Aβo, whereas synaptophysin is used to assess synaptic activity (Bate and Williams, 2011; McHale-Owen and Bate, 2018; Williams and Bate, 2018). In 2D cell culture models, measurements of cell signalling and cytokine changes in response to varying culture conditions, such as addition of a drug, can be made to provide insight into basic mechanistic pathways (Henstridge and Spires-Jones, 2018).



www.manaraa.com

*In vitro* biological techniques increasing in complexity, including co-culture and tri-culture systems, offer the advantage of studying multiple outputs such as changes in signalling molecules and pathways, and the interactions between different types of cells in addition to testing cell viability in response to external stimuli (Henstridge and Spires-Jones, 2018). Microfluidic technology has also proven useful in modelling aspects of disease. One such model created by Park and colleagues incorporates a 3-dimensional (3D) culture matrix in which APP-expressing human stem cell-derived neurons and astrocytes are grown, resulting in excess Aβ production. Microglia are also included in the matrix at different time points through the microfluidic channels and the behaviour of these three cell types are studied in response to Aβ. Signalling chemokines and cytokines released from one cell type can travel across the gels in the system and interact with other cell types. This model allows control over co-incubation times and allows the manipulation of the system to test variable conditions (Park *et al.*, 2018).

The use of tissue engineering methods to create organoids and more complex and relevant biological *in vitro* systems is another useful way to model health and disease conditions. Geoffrey Potjewyd and colleagues fabricated a novel 3D neurovascular unit model by bioprinting a multicellular physiological environment that attempts to mirror *in vivo* conditions, allowing interactions to occur between different components of the model. They form hydrogels by formulating gelatin, collagen and fibrin to replicate the matrix surrounding the cells to provide cell-adhesion sites (Potjewyd *et al.*, 2018).

Using bioengineered multi-faceted *in vitro* systems such as those listed above are very useful in providing initial comprehension of normal, healthy mechanisms and how they are altered in disease. They also provide a high throughput way in which targets for treatment and drug candidates can be screened quickly and efficiently, often yielding reproducible results (Sun and Tan, 2013; Henstridge and Spires-Jones, 2018). The exhaustive use of *in vitro* models also supports the refinement and reduction objectives of using animals in scientific research, helping preclude the unnecessary sacrifice of experimental animals.

However, whilst these systems are of valuable benefit, they often only focus on one, two or occasionally three types of cells and risk overlooking important systemic contributions and larger-scale pathways in organic physiological *in vivo* conditions. Even though adding layers to *in vitro* systems increases their complexity and improves their translatability, they remain limited in expressing the physiological environment holistically. Furthermore, mimicking the chronic conditions of neurodegenerative diseases is a challenge not easily overcome.



www.manaraa.com

Therefore, using a combination of bioengineered systems and *in vivo* experimentation allows the additional examination of behaviour and pathology, enhancing the validity and translatability of the modelling system. It also allows the extension of timelines supporting the mirroring of disease chronicity.

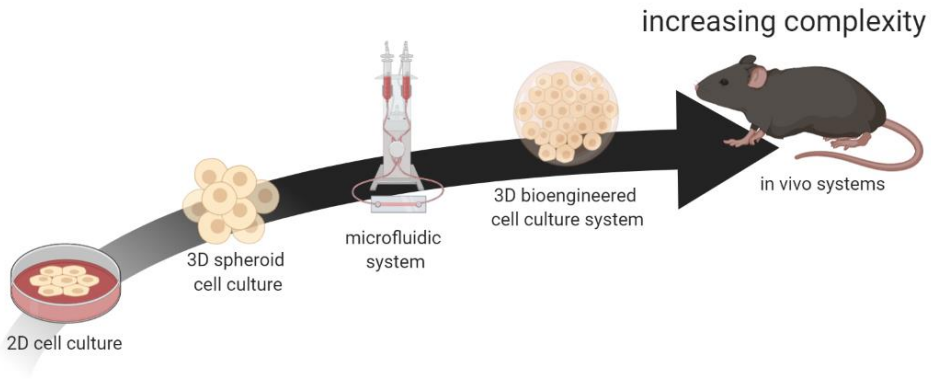


***Figure (22) A schematic illustrating the increasing complexities of in vitro and in vivo systems.***

***Created with Biorender.com***

### 4.1.3. Alginate-based 3D cellular system for modelling Alzheimer's disease

Hydrogels have been successfully used for decades in many biomedical applications. They are useful tools capable of delivering materials, such as drugs, proteins or tissue, to specific sites in the body. Their properties have allowed their utilisation in a wide range of biomedical and pharmaceutical fields, including regenerative medicine, wound healing and sustained drug delivery (Tønnesen and Karlsen, 2002; Tran *et al.*, 2014). In addition, they have been used in basic biological research to develop more translatable in vitro cell culture models (Rios de la Rosa *et al.*, 2018).

One such hydrogel is alginate. Alginate is a naturally occurring polysaccharide extracted from brown algae and is a highly biocompatible polymer. Its properties have enabled its use in immobilising and delivering biomolecules such as DNA, proteins and cells. Alginate can form a hydrogel in a process free of organic solvents, which helps avoid the interference of the gelation process with normal biological functions (Tønnesen and Karlsen, 2002; Sun and Tan, 2013).

Alginate gels provide an appropriate supporting matrix for immobilised cells as the gelation process occurs under mild conditions using reagents that do not impair cell viability or normal cellular processes. Encapsulation of cells in alginate microbeads has been achieved for a number of cell types and applications, such as hepatic cells (Tran *et al.*, 2014) colorectal



www.manaraa.com

cancer cells (Rios de la Rosa *et al.*, 2018) and pancreatic cells (Calafiore and Basta, 2014). One of the main applications of cell encapsulation in alginate is its popular and revolutionary use to encapsulate islets of Langerhans. Encapsulated islet cells are implanted within tissue in diabetic patients to restore pancreatic function, therefore allowing patients to produce insulin physiologically, eliminating the need to use insulin injection therapy (Lim and Sun, 1980; Calafiore and Basta, 2014).

Encapsulated cells are afforded the advantages of protection from mechanical stress and isolation from surrounding tissue, which is beneficial in averting potential rejection or unwanted immune responses after engraftment *in vivo*. At the same time, the properties of fabricated microbead hydrogel systems allow diffusion of soluble components; small molecules and proteins can diffuse across the gel (Tønnesen and Karlsen, 2002; Simó *et al.*, 2017), allowing access to surrounding environments for nutrient exchange and clearance of waste materials. Moreover, alginate hydrogels can be controlled in their stiffness by varying alginate concentration and cross-linking density, which can affect cells in culture. This is essential in maintaining the normal phenotypic behaviour of encapsulated cells *in vitro* and avoids inflammatory effects after implantation *in vivo* (Tirella *et al.*, 2009; Higham *et al.*, 2014; Hoesli *et al.*, 2017; Rios de la Rosa *et al.*, 2018).

In summary, as alginate is readily available, biocompatible and does not inhibit cell viability, it was selected as a suitable biomaterial to fabricate a delivery system for secreted cell products *in vivo*.



www.manaraa.com

#### 4.1.3.1. Alginate gelation

Alginate is a polysaccharide composed of repetitive D-mannuronic acid (M) and L-guluronic acid (G) units **(Figure (23))**. Their content may vary as function of the algae source.

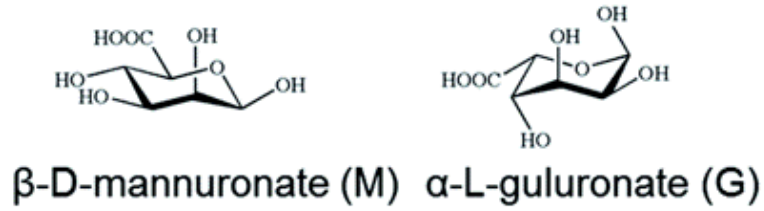


***Figure (23) Chemical structures of alginate monomers.***
***D-mannuronic acid (left) and L-guluronic acid (right). Structures adapted from (Higham et al., 2014)***

Alginate residues typically align in three types of segments: consecutive GG blocks, consecutive MM blocks or alternating GM blocks as illustrated in **Figure (24)** below. The distribution, alignment and ratios of G and M monomers can impact the mechanical properties of the alginate (Higham *et al.*, 2014; Simó *et al.*, 2017).

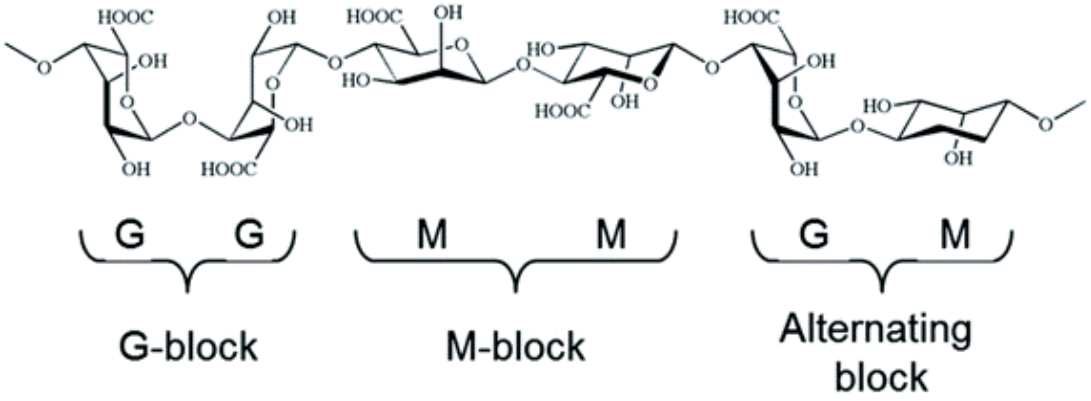


***Figure (24) Assembly of alginate monomers.***
***Alginate residues align either by a GG block (left) where two guluronic acid residues are covalently bonded, an MM block (centre) where two mannuronic acid residues are covalently bonded, or an GM block (right) where a mannuronic acid and guluronic acid residue are covalently bonded. Figure adapted from (Higham et al., 2014)***

In the presence of divalent cations, such as $Ca^{2+}$, aqueous solutions of sodium alginate salt form gels. Gelation occurs via the ionic cross-linking of negatively charged carboxyl groups with positively charged divalent cations driven by G blocks. Chelation of the cations forms tight junctions of alginate creating the shape of the polymer known as the "egg-box" structure, as illustrated in **Figure (25)** below (Sun and Tan, 2013; Higham *et al.*, 2014; Simó *et al.*, 2017).



www.manaraa.com

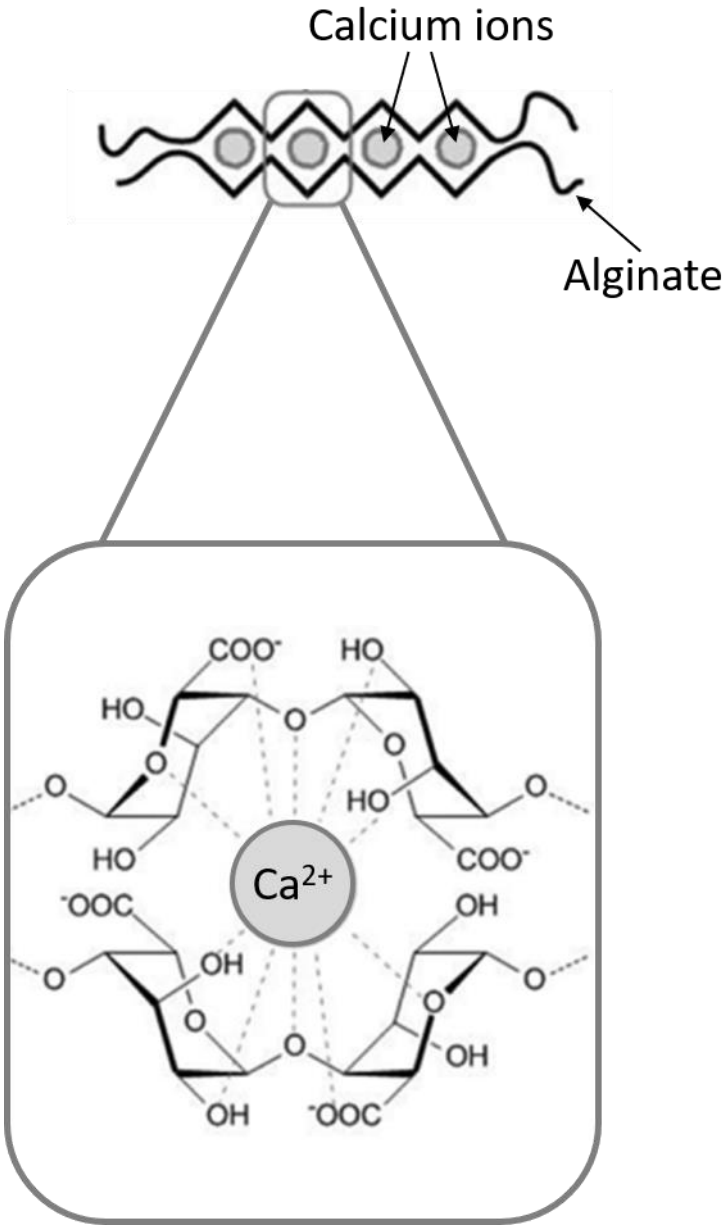


***Figure (25) Formation of alginate gel.***
***Alginate chains chelate calcium ions and ionic bonds form between G monomers and calcium ions forming the "egg-box" shaped structure. Figure modified from (Simó et al., 2017)***

Extruding a stream of aqueous alginate droplets into a $Ca^{2+}$-containing bath (e.g. calcium chloride, $CaCl_2$) causes the diffusion of the divalent ions from the bath into the alginate droplets and promotes the cross-linkage of the alginate. Incorporating cells into the alginate solution facilitates the entrapment of cells in the alginate gel matrix (Tirella *et al.*, 2009; Sun and Tan, 2013; Rios de la Rosa *et al.*, 2018).



www.manaraa.com

There are a few available methods used to fabricate beads using alginate. One of the most common methods uses a laminar jet of cells suspended in an alginate solution that is extruded through a nozzle resulting in a stream of droplets (Marison, 2004). The laminar jet can be disrupted in different ways; in this study, a vibrating head set at a controlled frequency resulting in droplets equal in size was used. Furthermore, an external electric field imparts a temporary partial negative charge on the droplets in the stream and causes the separation of the formed droplets as a consequence of electrostatic repulsion. Upon contact with a solution of $CaCl_2$, the alginate in the droplets quickly form cross-links with $Ca^{2+}$ ions, instantaneously forming a hydrogel and preserving the droplets' spherical shape. Alginate hydrogel microbeads are left to incubate in the gelation bath thereby allowing the consolidation of spherical microbeads containing cells within a homogeneous physical hydrogel matrix (Marison, 2004; Rios de la Rosa *et al.*, 2018; Almari *et al.*, 2019).



www.manaraa.com

### 4.1.4. Aims

So far in this thesis, the relevance of using 7PA2 cells as a source of prefibrillar Aβo like those found in patient CNS has been established. Administering a bolus injection of highly concentrated Aβo from 7PA2 cells has resulted in progressive cognitive impairment associated with synaptic dysregulation. The effects seen in these parts of the study were following an acute administration and were exhibited for a maximum of two weeks.

To establish a more representative chronic *in vivo* animal model that will be of benefit in the research field, formulation of a delivery system allowing the sustained secretion of Aβo will be explored **(Figure (26))**. This will be a bioengineered 3D *in vitro* cellular system encapsulating 7PA2 cells in an alginate gel microbead for engraftment in the rat brain in future studies. In principle, naturally secreted Aβ species will be secreted from microbeads over time in adult animals, more closely mimicking the prolonged accumulation of Aβ seen in patients. This will permit the assessment of the effects of Aβo secreted at physiological levels at different stages and will thus be comparable to AD at different stages of its progression.

The microbeads encapsulating 7PA2 cells will aim to meet the following specifications:

- Microbead diameter of 500 – 600 µm. These dimensions are set to allow adequate oxygen perfusion and exchange of cellular by-products;
- Encapsulation of 100-200 cells per microbead allowing the secretion of Aβo in the nanomolar per millilitre scale.

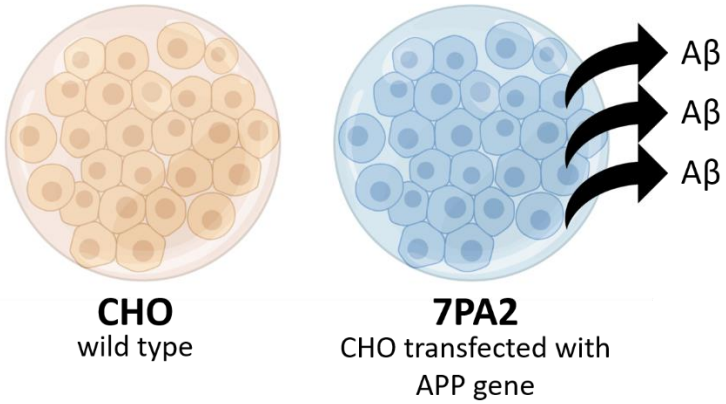


***Figure (26) Alginate microbeads.***
***Diagrammatic representation of proposed formulated alginate microbeads containing CHO and 7PA2 cells. Alginate gel matrix entraps cells within the microbead and allows the exchange of biomolecules across the gel.***

***Created with Biorender.com***



www.manaraa.com

## 4.2. Methods

### 4.2.1. Optimisation of encapsulation protocol

#### 4.2.1.1. Materials

**Table (9)** below lists the materials used in the fabrication of the microbeads.

***Table (9) List of materials used in the fabrication of alginate microbeads. All materials in this list were obtained from Sigma, UK.***

| Material | Catalogue no. |
|---|---|
| Alginic acid sodium salt from brown algae | A0682 |
| Calcium chloride ($CaCl_2$) | C1016 |
| (4-(2-hydroxyethyl)-1-piperazineethanesulfonic acid (HEPES) | H4024 |
| Phosphate-buffered saline (PBS) | D1408 |
| Sodium chloride (NaCl) | 433209 |
| Trisodium citrate dihydrate ($Na_3C_6H_5O_7$) | W302600-K |
| Trypsin-EDTA 0.25% solution | T4049 |

The alginate used in this study was a low-viscosity alginic acid sodium salt of molecular weight 120,000–190,000 g $mol^{-1}$ and a mannuronic to guluronic ratio of 1.56 M/G.

The optimisation process for the fabrication of microbeads meeting the criteria outlined above took three stages:

**Stage 1:** Fabrication of empty alginate beads using water as a solvent

**Stage 2:** Fabrication of empty alginate beads using solvents supporting cell viability

**Stage 3:** Fabrication of alginate beads encapsulating CHO and 7PA2 cells



www.manaraa.com

#### 4.2.1.2. Apparatus and procedure

**Figure (27)** below is a diagrammatic representation of the fabrication apparatus used in the production of alginate microbeads. The Inotech Encapsulator® Research IE-50R machine (serial no. 05.002.01-2005) allows the tuning of fabrication parameters in order to control microbead size depending on the intended use.

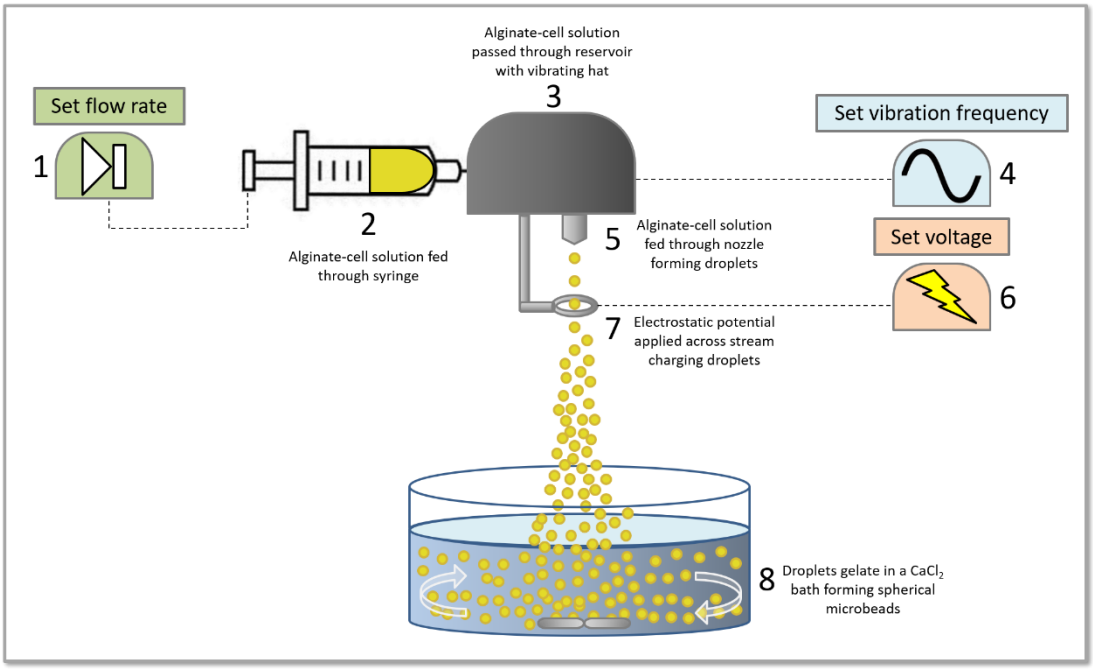


***Figure (27) A schematic representation of the encapsulation system.***
***(1) Pump speed is set to control the flow rate. (2) Alginate solution in a syringe is pushed through the feeder. (3) The vibrating hat vibrates at a frequency set by a waveform generator (4) to disrupt the stream at equal intervals. (5) The solution is fed through a nozzle. (6) The voltage is set by a voltage generator. (7) An electrostatic potential (voltage) is applied across an electrode. (8) Calcium chloride bath allows physical gelation of alginate by $Ca^{2+}$-driven cross-linking.***

The concept of the encapsulation process used here is described by Ian Marison and is based on nozzle extrusion with vibration technology (Marison, 2004). The parameters that were adjusted are outlined in **Figure (27)**. The internal diameter of the nozzle used has a substantial impact on the size of the droplets. A nozzle of 300 µm diameter was chosen to fabricate microbeads meeting the size specifications outlined above. Further parameters, namely extrusion speed, vibration frequency and voltage, were optimised to achieve a consistent bead size and size distribution. **Table (10)** overleaf briefly summarises the impact of changing different parameters on microbead size fabricated using this system.



www.manaraa.com

***Table (10) The influence of fabrication parameters on microbead size.***

| Parameter | Nozzle size ↑ | Vibration frequency ↑ | Flow rate ↑ | Electrode voltage ↑ |
|---|---|---|---|---|
| **Bead size** | ↑↑ | ↓ | ↑ | – |

**Stage 1: Fabrication of empty alginate beads using water as a diluent**

Alginate was hydrated in deionised MilliQ water at concentrations of 2%, 4% and 8% (w/v). The solutions were stirred using a magnetic stirrer at 500 rpm and were heated to 50 $^{o}$C to allow complete alginate hydration. A solution of $CaCl_2$ in deionised MilliQ water was prepared at a concentration of 0.5 M.

Initially, to optimise the fabrication parameters, alginate was gelated without the addition of cells. Alginate solutions were loaded in turn into a 20 mL syringe and attached through a feeder to the encapsulator. The solution was fed through a reservoir at a constant and controlled extrusion speed set at the syringe pump, resulting in a constant alginate flow rate through the nozzle. Pump speed (or alginate flow rate) was tuned in order to optimise the size of the resultant microbeads to conform to the desired size. A frequency was set to control the vibrating hat. Such vibrations homogeneously disrupted the alginate stream, forming equally sized droplets at equal intervals. The frequency of vibrations was also controlled during the optimisation steps to achieve the desired bead size. In this phase, as the alginate solution was extruded through the 300 µm nozzle, the droplets in the stream were formed. To increase the control over the manufacturing process, an additional parameter allows the spreading of the stream or formed beads: the electrostatic field. Values of electrostatic potential were varied until optimised. The electrostatic potential was set by a voltage generator and applied between the electrode and the solution. The applied voltage slightly charged the surface of the droplets, allowing the stream to spread as a result of repelling electrostatic forces avoiding beads coalescence. The voltage was also varied until all the fabrication parameters were optimised. As alginate droplets interact with the gelation bath, $Ca^{2+}$ ions immediately cross-link with the G-block of the alginate chains resulting in the instantaneous formation of spherical microbeads.



www.manaraa.com

Physical gelation of microbeads was allowed to continue for one minute with gentle stirring of the gelling bath to keep microbeads in suspension (100 rpm using a magnetic stirrer), followed by four minutes without agitation. Microbeads were transferred to a vessel containing water to stop the gelation and were processed for imaging.

The fabrication parameters that were varied in **Stage 1** were:

- Electrostatic potential (kV)
- Vibration frequency (Hz)
- Extrusion speed (arbitrary units, a.u.)

Variation of these parameters took an iterative sequence starting with mid-scale values and tuning each variable in turn until the desired size criteria of 500 to 600 µm was achieved.

#### 4.2.1.3. Diameter measurements

Microbeads were imaged using a Leica DMI6000 B inverted microscope at objective magnifications of 2.5×, 10× and 20× interfaced with ImageJ imaging software. Assessment of microbead morphology and diameters was made. Average diameters and standard deviations were calculated to determine microbead uniformity. A minimum of 50 beads from each run were analysed.

**Stage 2: Fabrication of empty alginate beads using diluents supporting cell viability**

The following parameter was then optimised to obtain prime conditions supporting microbead stability and cell viability:

Type of solvent:

- Phosphate-buffered saline (PBS)
- Cell culture media (DMEM-F12)
- HEPES-buffered saline (HBS, 20 mM HEPES and 150 mM NaCl in deionised water)

Each diluent was tested individually. The test diluent was used to make 2% (w/v) alginate solution and 0.5 M $CaCl_2$ solution.

#### 4.2.1.4. Diameter measurements

Microbeads were imaged using a Leica inverted microscope at objective magnifications of 2.5×, 10× and 20× interfaced with ImageJ software. Average diameters and standard deviations were calculated to determine microbead uniformity. Fabricated empty



www.manaraa.com

microbeads were incubated in standard cell culture conditions up to three weeks and diameter readings were taken every day for four days then every week to assess microbead stability. Dramatic changes in diameter or morphology (e.g. 20% diameter reduction over 7 days) are indicative of alginate degradation. A minimum of 50 beads from each run were analysed.

**Stage 3: Fabrication of alginate beads encapsulating CHO and 7PA2 cells**

The protocol was further optimised after the inclusion of cells into the alginate solution as the inclusion of cells altered the viscosity of the solution, requiring re-tuning of fabrication parameters. The procedure in this section is repeated as above but also under sterile conditions. All reagents used in this study were sterile filtered before use and handled under a category 2 cell culture laminar flow cabinet. All equipment was exposed to ultraviolet light for at least 30 minutes prior to the start of experiments.

Fabrication parameters fine-tuned:

- Electrostatic potential (kV)
- Vibration frequency (Hz)
- Extrusion speed (arbitrary)

Variation of these parameters took a similar iterative process using values optimised in **Stage 1** as a starting guide until the stable microbeads with the desired size criteria of 500 to 600 µm were achieved with as little variation as possible.

Results from **Stages 1 & 2** of optimising the encapsulation protocol concluded that an alginate solution at a concentration of 2% (w/v) made in HBS would be used. An alginate-cell suspension containing $1.5 \times 10^6$ cells $mL^{-1}$ was prepared. This cell concentration was calculated to obtain beads containing approximately 100-200 cells each based on a microbead 550 µm in diameter as follows (where V = volume and r = radius):

$$V = \frac{4}{3}\pi r^3$$

The volume of a single microbead is $V = 8.8 \times 10^{-5}$ mL; therefore, the number of cells per microbead at time of encapsulation = $(1.5 \times 10^6) \times (8.8 \times 10^{-5}) \approx$ approximately 130 cells.

CHO and 7PA2 cells at passage 9 were prepared for encapsulation by washing briefly with sterile PBS then detaching from near-confluent flasks using trypsin-EDTA 0.25% solution. Flasks were incubated at 37 °C for 5-10 minutes. Cell detachment was visualised and



www.manaraa.com

confirmed under an inverted microscope. A sample of cleaved cells was isolated for estimation of cell density, and the rest were centrifuged at 1000 rpm for 5 minutes to obtain a cell pellet. The pellet was resuspended in sterile-filtered HBS to double the final desired cell concentration (e.g. for a final concentration of $1.5 \times 10^6$ cells $mL^{-1}$, the cells were resuspended in a volume of HBS to achieve a concentration of $3 \times 10^6$ cells $mL^{-1}$). In a 50 mL centrifuge tube, the cell suspension was mixed in a 1:1 ratio with 4% (w/v) alginate solution to obtain a final suspension containing $1.5 \times 10^6$ cells $mL^{-1}$ in a 2% (w/v) alginate solution.

The alginate-cell suspension was extruded through a 300 µm wide nozzle via the Inotech Encapsulator® Research IE-50R machine **(Figure (27))** as described above and dropped into a 0.5 M $CaCl_2$ in HBS bath. The encapsulation parameters were tuned using a similar iterative process as before using the refined parameters identified in **Stages 1 & 2** as a starting guide. Gelation of beads was allowed for one minute with gentle stirring followed by four minutes without stirring. Microbeads were retrieved from the $CaCl_2$ bath and transferred to a centrifuge tube by washing with DMEM-F12 culture medium. Beads were left to equilibrate for five minutes in DMEM-F12 before being transferred to a sterile flask for incubation and further experiments.

### 4.2.2. Optimised cell encapsulation procedure

The optimised encapsulation protocol developed in this part of the present study was recently published in the Journal of Visualised Experiments (JoVE) (Almari *et al.*, 2019).

***Scan the Quick Response (QR) code to view a video of the optimised encapsulation protocol for this study.***

The optimisation process for **Stage 3** of the protocol concluded that the following fabrication parameters would be used for further studies:

Alginate-cell suspension at a concentration of $1.5 \times 10^6$ cells $mL^{-1}$ made in 2% (w/v) alginate in HBS solution, extruded at an arbitrary pump speed of 900 a.u. (roughly equating to 8.9 mL $min^{-1}$), with a voltage of 1.0 kV and a vibration frequency of 5500 Hz. Encapsulating using these parameters obtained microbeads approximately 550 µm in diameter.



www.manaraa.com

#### 4.2.3. 3D cell culture

Fabricated 3D microbeads containing CHO or 7PA2 cells were incubated in the same standard cell culture conditions as 2D cell culture (section 2.2.1.) for one week. Media was collected at 24-hour intervals up to 96 hours and frozen at -20 $^{o}$C for future analysis.

##### 4.2.3.1. Diameter measurements

Microbeads were imaged as described above. ImageJ software was used to assess microbead morphology and diameters. Average diameters and standard deviations were calculated to determine microbead uniformity. Diameter readings were taken on days 0, 1, 2, 3, 4 and 7 to investigate microbead stability. A minimum of 50 beads from each run were analysed for statistical purposes.

##### 4.2.3.2. Estimations of cell density and cell proliferation

A solution to dissolve alginate hydrogel (termed "dissolution mix") of trisodium citrate in HBS solution buffered with NaOH and HCl to pH 7.4 was made as follows: 100 mM HEPES, 500 mM trisodium citrate dihydrate, in PBS 1×.

Immediately after encapsulation, a sample of microbeads was collected, and the hydrogel was disrupted by adding the dissolution mix. The sample was incubated at room temperature for 10 minutes with gentle agitation. Following dissolution, the cells (now in solution) were stained with trypan blue to assess changes in cell viability as a result of the encapsulation process, in a dye exclusion test using a haemocytometer.

An MTS assay was performed to assess the impact of alginate on 7PA2 cell proliferation up to one week. Cells with and cells without alginate were seeded at a density of 15,000 cells/cm$^2$ (5000 cells per well) in triplicate in a 96-well plate and incubated in standard culture conditions. Estimations of viable cell density were made using the MTS assay (as described in section 2.2.1.2.).

##### 4.2.3.3. Media analysis

ELISA and dot blot analysis was performed on conditioned media from 3D cell cultures of CHO and 7PA2 cells as described in sections 2.2.2.

##### 4.2.3.4. Media analysis

Data were analysed by a two tailed student's t-test for pairwise comparisons. In data subsets where experimental repeats were normalised to an arbitrary control value (e.g. total



www.manaraa.com

concentration at the end of the experiment) a one-sample t test was performed to compare the control value and column average. Data are presented as the mean ± standard deviation for diameter measurements unless stated otherwise. Statistical tests were performed in Prism (Version 8.2.1, Graphpad). Graphs were generated using Prism (Version 8.2.1, Graphpad).



www.manaraa.com

## 4.3. Results

### 4.3.1. Fabrication parameters were optimised to produce spherical alginate microbeads

**Stage 1:** Fabrication of empty alginate beads using water as a diluent

Production of a homogeneous and constant stream through the nozzle of the encapsulator system was only possible with an alginate concentration of 2% (w/v). Higher concentrations of alginate solution were too viscous to run through the aperture of a 300 µm nozzle at room temperature and produce an evenly running stream, which means consistency could not have been guaranteed. Therefore, concentrations of 4% and 8% (w/v) alginate were not investigated further.



www.manaraa.com

#### 4.3.1.1. Varying pump speed

Alginate solution was extruded through the nozzle and dropped into a bath of $CaCl_2$. Using a mid-frequency (2500 Hz) and mid-voltage (1.0 kV) setting as a starting point for this iterative process, the extrusion speed (pump speed) was varied from the minimum speed that successfully gave rise to a stream to the maximum speed available with the system. Variable microbead size distribution was obtained in the first run. **Table (11)** and **Figure (28)** below shows the variation of microbead diameters with varied extrusion speed (pump speed): diameter decreased with pump speed up to 850, then increase in brads size was recorded (as well as size distribution).

***Table (11) Average microbead diameters with variable pump speed (n=50).***

| Pump speed (a.u.) | Average diameter (µm) ± standard deviation |
|---|---|
| 700 | 618.83 ± 28.39 |
| 750 | 592.78 ± 46.31 |
| 800 | 537.40 ± 42.29 |
| 850 | 504.56 ± 25.16 |
| 900 | 518.60 ± 36.91 |
| 950 | 665.94 ± 42.82 |

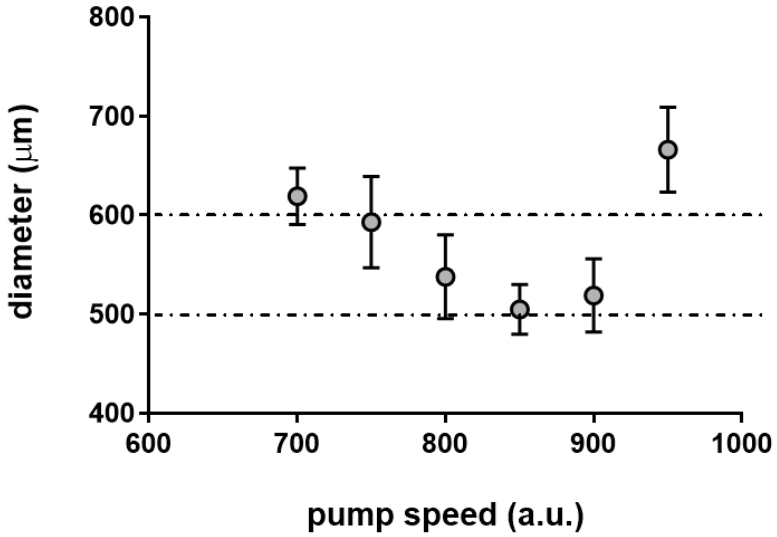


***Figure (28) Changes in average microbead diameters with varying extrusion speed.***
***Parameters: 2% (w/v) alginate in MilliQ water, 2500 Hz frequency, 1.0 kV electrostatic potential. Extrusion speed range: 700-950 a.u.***



www.manaraa.com

Using these settings, the largest microbeads obtained had an average diameter of 666 µm, whilst the smallest were at 505 µm. Standard deviations varied, with the biggest at ± 46 The speed setting of 850 a.u. resulted in microbeads of average diameter 505 µm with a standard deviation of ± 25. This speed setting was therefore used as a grounding setting with which to test subsequent parameters. In the photographs presented in **Figure (29)** below, it is visually clear from image B (pump speed 850 a.u.) that the microbeads were most consistent in morphology and diameter.

Although arbitrary, a pump speed of 850 is roughly equivalent to 10.5 mL $min^{-1}$ of water if a 20 mL syringe is used. Since alginate solution is more viscous, the equivalent flow rate would be smaller.

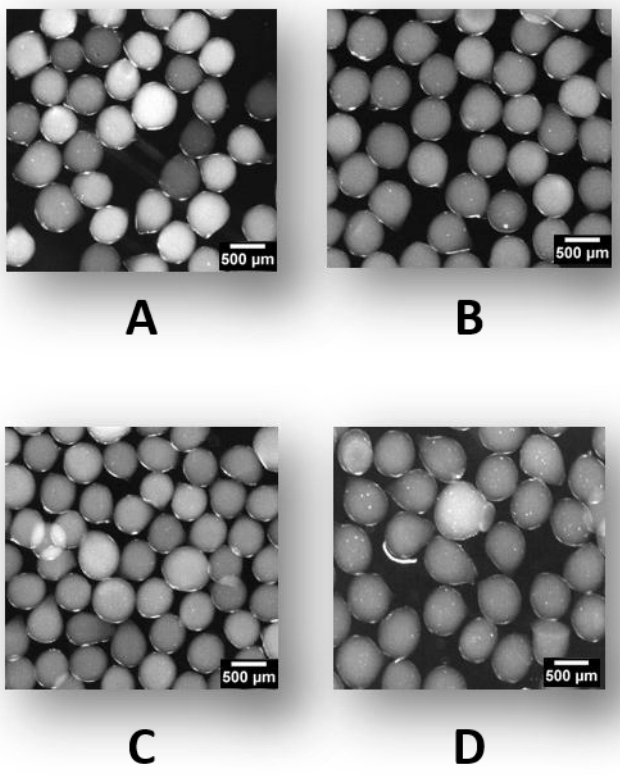


***Figure (29) Fabricated microbeads.***
***Microbeads imaged at 2.5× magnification using a Leica DMI6000 B inverted microscope. All microbeads here were fabricated using a 2% (w/v) alginate solution in MilliQ distilled water, extruded through a 300 µm nozzle at a voltage of 1.0 kV and a frequency of 2500 Hz. Pump speed (a.u.) was varied as follows:***
***A = 800, B = 850, C = 900, D = 950.***



www.manaraa.com

#### 4.3.1.2. Varying voltage

The next part of the iterative process was to vary the electrostatic potential (also known as voltage). The images in **Figure (30)** below show the spread of the droplets in the stream as a result of applying different electrostatic potential values.

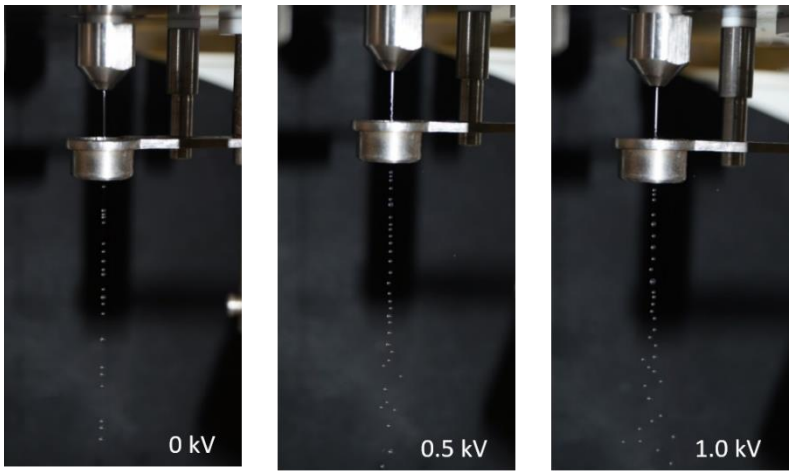


***Figure (30) Stream dispersion.***
***Photographs showing the effect of adjusting the voltage applied across the electrode on stream dispersion.***

***Table (12) Average microbead diameters with variable voltage (n=50).***

| Voltage (kV) | Average diameter (µm) ± standard deviation |
|---|---|
| 0.6 | 574.59 ± 34.66 |
| 1.0 | 586.56 ± 22.02 |
| 1.2 | 577.48 ± 22.60 |
| 1.6 | 583.96 ± 26.85 |

As evident from **Table (12)** above and the graph in **Figure (31)** overleaf, the most consistent microbeads when 2% (w/v) alginate solution was extruded at settings of 500 Hz stream disruption frequency and a pump speed of 850 a.u. were produced with a voltage of 1.0 kV. They were also the largest of the microbeads at an average diameter of 587 µm ± 22. The lowest electrostatic potential gave rise to microbeads with least consistency (diameters 575 µm, standard deviation ± 35), but still more consistent than most of those produced with the settings used in the first part of the process. Hence, an electrostatic potential of 1.0 kV was used as a grounding setting with which to test subsequent parameters. Images A-D in **Figure (32)** overleaf show the effect of voltage on microbead uniformity.



www.manaraa.com

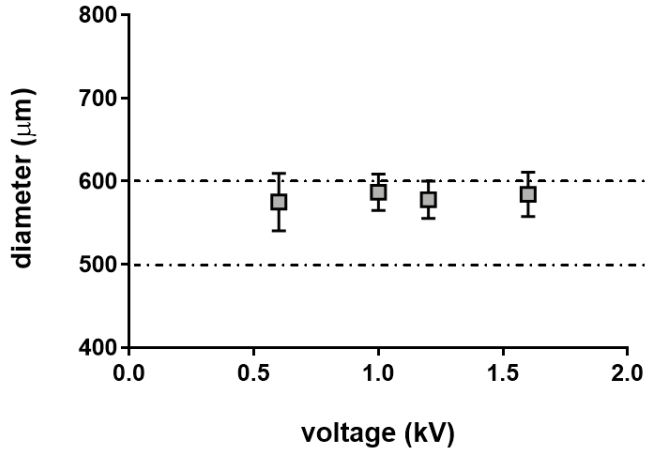


*Figure (31) Changes in average microbead diameters with varying voltage.*
*Parameters: 2% (w/v) alginate in MilliQ water, 500 Hz frequency, 850 a.u. pump speed. Electrostatic potential range: 0.6-1.6 kV.*

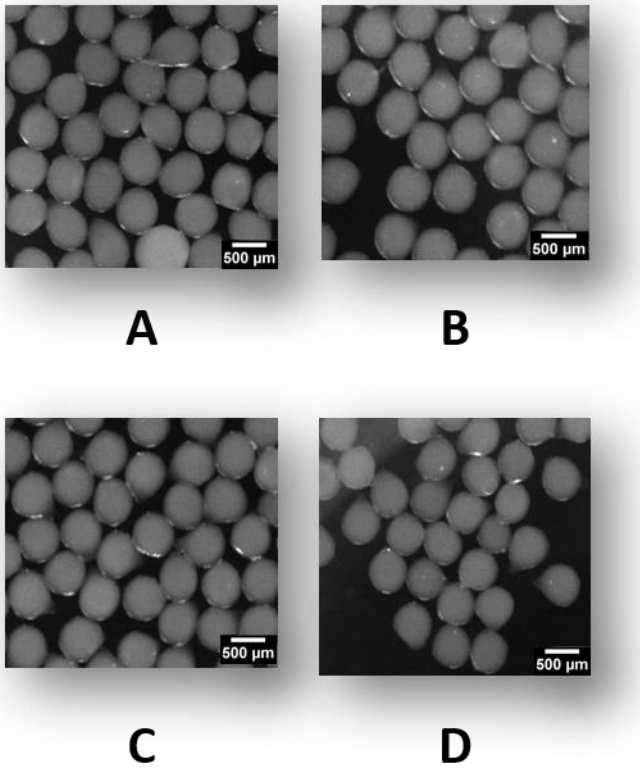


*Figure (32) Fabricated microbeads.*
*Microbeads imaged at 2.5× magnification using a Leica DMI6000 B inverted microscope. All microbeads here were fabricated using a 2% (w/v) alginate solution in MilliQ distilled water, extruded through a 300 μm nozzle at a pump speed of 850 a.u. and a frequency of 500 Hz. Voltage (kV) was varied as follows:*
*A = 0.6, B = 1.0, C = 1.2, D = 1.6.*



www.manaraa.com

#### 4.3.1.3. Varying frequency

Finally, with an alginate concentration of 2% (w/v), an extrusion speed of 850 a.u. and an electrostatic potential of 1.0 kV, the frequency with which the stream was disrupted was changed in the next iteration. The images in **Figure (33)** below show droplets formed at different vibration frequencies.


***Figure (33) Droplet formation.***
***Photographs demonstrating the effect of adjusting the vibrating frequency on droplet size.***

As the frequency of vibrations was varied using the aforementioned grounding settings, there was now very little inconsistency in the diameters of the microbeads produced. Diameters ranged from 586 µm ±26 at a frequency of 1000 Hz and 615 µm ±27 at a frequency of 2500 Hz **(Table (13))**. The smallest standard deviation in microbead diameter was ±18.9 and was seen at a frequency of 1500 Hz, as shown in the graph in **Figure (34)** over the page.



www.manaraa.com

*Table (13) Average microbead diameters with variable frequency (n=50).*

| Frequency (Hz) | Average diameter (µm) ± standard deviation |
|---|---|
| 1000 | 585.97 ± 26.12 |
| 1500 | 593.91 ± 18.86 |
| 2000 | 603.36 ± 28.45 |
| 2500 | 614.93 ± 27.43 |
| 3000 | 610.66 ± 23.26 |
| 3500 | 611.82 ± 24.47 |
| 4000 | 595.11 ± 22.64 |
| 4500 | 598.12± 26.80 |
| 5000 | 593.17 ± 28.10 |

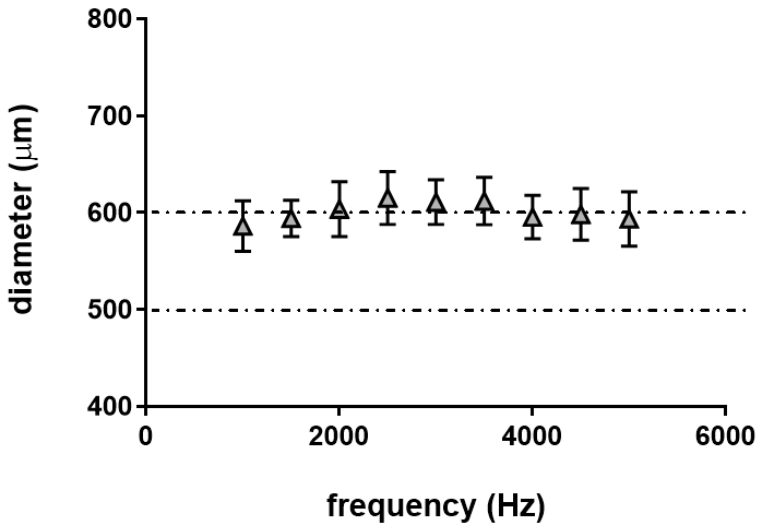


*Figure (34) Changes in average microbead diameters with varying frequency.*
*Parameters: 2% (w/v) alginate in MilliQ water, 1.0 kV voltage and 850 a.u. pump speed. Frequency range: 1000-5000 Hz.*



www.manaraa.com

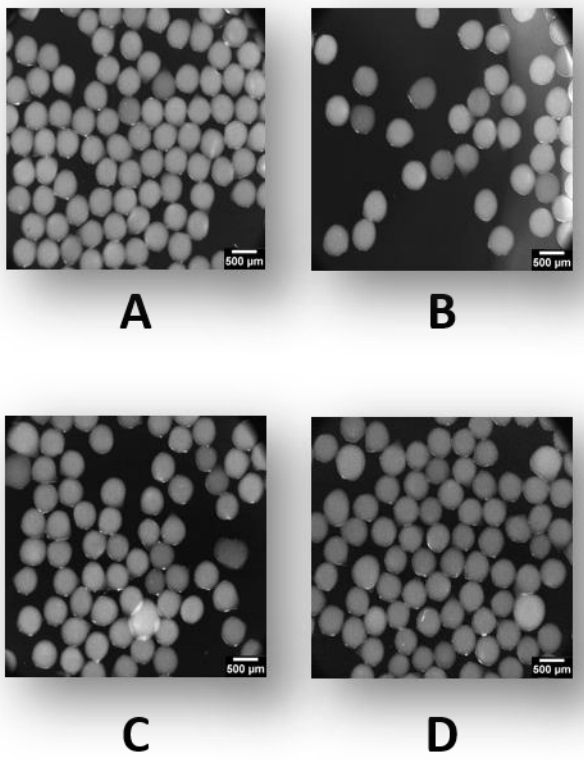


***Figure (35) Fabricated microbeads.***
***Microbeads imaged at 2.5× magnification using a Leica DMI6000 B inverted microscope. All microbeads here were fabricated using a 2% (w/v) alginate solution in MilliQ distilled water, extruded through a 300 µm nozzle at a pump speed of 850 a.u. and a voltage of 1.0 kV. Frequency (Hz) was varied as follows:***
***A = 1000, B = 1500, C = 4000, D = 5000.***

Images A-D in **Figure (35)** above are photographs of microbeads fabricated at the parameters described above. It is difficult to distinguish by the naked eye which frequency produces the most consistent microbeads. Image B where the stream was disrupted at a frequency of 1500 Hz showed the most uniform microbeads experimentally.

To conclude **Stage 1** of the optimisation process, fabrication parameters to be taken forward will be 850 a.u. pump speed, 1.0 kV voltage and 1500 Hz frequency.



www.manaraa.com

### 4.3.2. Choosing the vehicle in which alginate was dissolved

**Stage 2:** Fabrication of empty alginate beads using diluents supporting cell viability

Having successfully and reproducibly fabricated alginate microbeads with little inconsistency in average diameter using distilled water as a solvent, fabrication of microbeads using alginate dissolved in diluents appropriate for cell viability was investigated next.

Alginate salt at a concentration of 2% (w/v) was hydrated in:

- PBS
- DMEM-F12
- HBS

Solutions were extruded via the Inotech Encapsulator® **(Figure (27))** and dropped into a 0.5 M $CaCl_2$ bath using the parameters identified in **Stage 1**.

The images in **Figure (36)** below are representative photographs of microbeads fabricated using the three solvents described above.

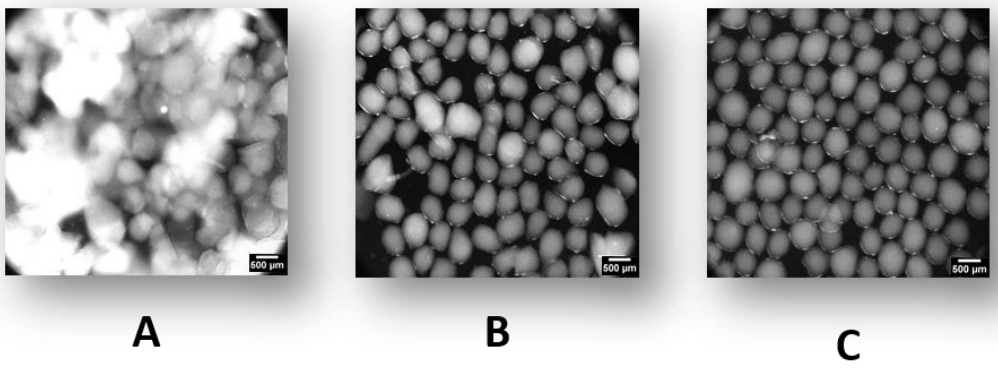


***Figure (36) Fabricated microbeads.***
***Microbeads imaged at 2.5× magnification using a Leica DMI6000 B inverted microscope. All microbeads here were fabricated using a 2% (w/v) alginate solution, extruded through a 300 µm nozzle at a pump speed of 850 a.u., a voltage of 1.0 kV and a frequency of 1500 Hz.***
***(A) Alginate in PBS, (B) Alginate in DMEM-F12, (C) Alginate in HBS***

The results clearly indicate that PBS 1 × **(Figure (36A))** is not a suitable diluent with which to create microbeads. Phosphate ions in the PBS interfere with $Ca^{2+}$ ions in the gelling bath, resulting in the immediate break down of alginate cross-linking. The photograph in A was taken minutes after encapsulation and reveals a non-defined pool of alginate solution and



www.manaraa.com

alginate gel. Consequently, despite PBS providing normo-physiological conditions suitable for cells, it does not provide microbead stability and therefore is not suitable for encapsulation.

When DMEM-F12 was used as a diluent **(Figure (36B))**, better microbeads were fabricated (that is to say, the gelated hydrogel did not break down immediately). However, consistency (as determined by microbead size distribution as detailed above) was difficult to achieve in comparison with alginate in water solution. Additionally, small quantities of $Ca^{2+}$ added to growth media by manufacturers could impact long term microbead stability leading to degradation of cross-linked alginate.

Alginate dissolved in HBS **(Figure (36C))** successfully produced stable and consistent microbeads as measured using microbead size distribution. The optimum fabrication parameters were then further fine-tuned in the next stage to achieve reproducibly uniform microbeads with the incorporation of cells as determined by the lowest achievable size distribution

To conclude **Stage 2** of the optimisation process, **Figure (37)** below shows representative images of beads fabricated using these parameters.

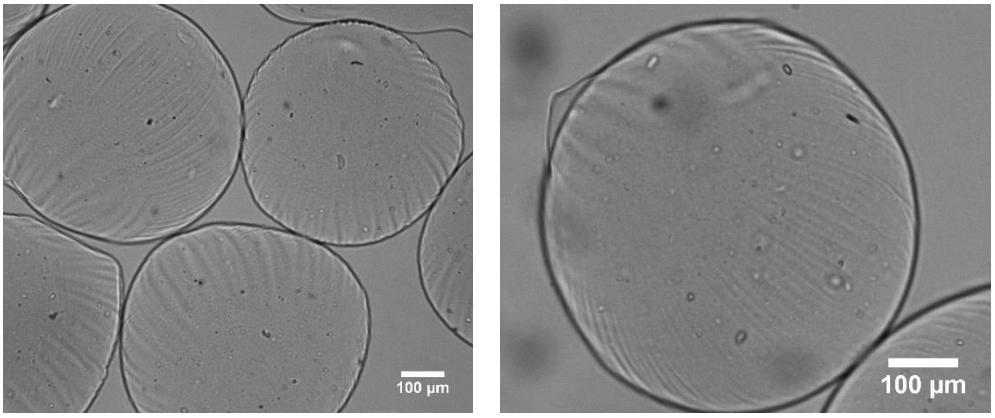


***Figure (37) Fabricated microbeads.***
***Empty alginate microbeads imaged using a Leica DMI6000 B inverted microscope. Fabrication parameters: pump speed of 850 a.u., voltage of 1.0 kV and frequency of 1500 Hz. (A) 10× magnification (B) 20× magnification. Artefacts seen here are due to microbead preparation under non-sterile conditions.***



www.manaraa.com

### 4.3.3. Microbeads were stable for three weeks in cell culture media

Empty alginate microbeads fabricated using the parameters described above were transferred to a cell culture plate and incubated in DMEM-F12 at 37 ºC and standard cell culture conditions for three weeks. No overall changes in microbead diameter were observed over the three-week period, suggesting no alginate degradation **(Figure (38))**.

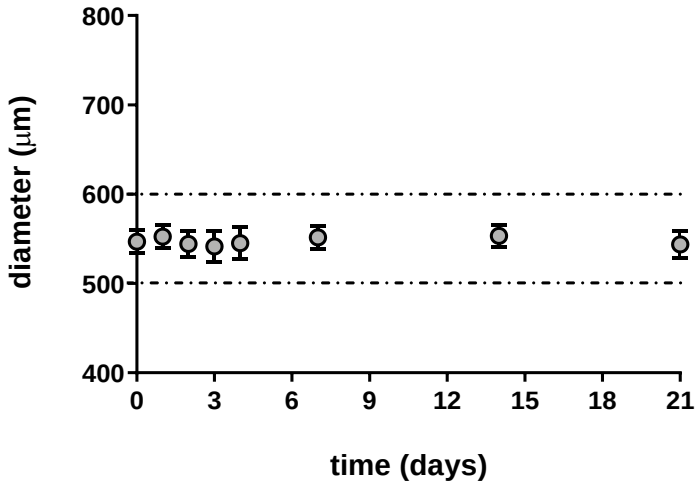


***Figure (38) Fabricated microbead diameters.***
***Graph illustrating the unchanging average microbead diameters of the same population of microbeads over three weeks in normal culture conditions, n=50. Slight variations seen are due to the random sampling process of 50 beads from a population of hundreds of beads.***



www.manaraa.com

### 4.3.4. CHO and 7PA2 cells were successfully encapsulated in alginate microbeads

**Stage 3:** Fabrication of alginate beads encapsulating CHO and 7PA2 cells

The aim of this stage was to determine the final fabrication parameters to be used to generate microbeads 500 – 600 µm in diameter encapsulating CHO or 7PA2 cells.

At this stage, cells were introduced in the 2% (w/v) alginate-HBS solution at a final concentration of $1.5 \times 10^6$ cells $mL^{-1}$. The cell-alginate-HBS solution was extruded through a 300 µm nozzle into a 0.5 M $CaCl_2$ bath also made in HBS. The fabrication parameters were varied until a final set of parameters was identified (see **Figure (40)**). The image in **Figure (39)** below shows an example of evenly distributed cells encapsulated in the alginate gel matrix immediately after the gelation process (Day 0).

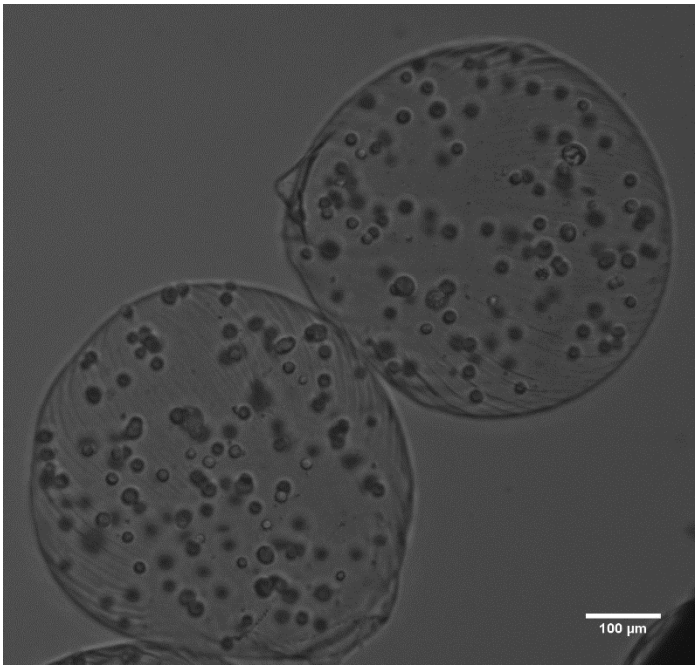


***Figure (39) Fabricated microbeads encapsulating cells.***
***Alginate beads encapsulating 7PA2 cells imaged using a Leica DMI6000 B inverted microscope at 10× magnification. Fabrication parameters: pump speed of 900 a.u., voltage of 1.0 kV and frequency of 5500 Hz.***

As mentioned earlier, parameters from **Stage 1 & 2** were refined further after the addition of cells due to the altered viscosity of the cell-alginate solution. The graphs in **Figure (40)** overleaf illustrate the uniformity achieved in microbead diameter in the final optimisation process.



www.manaraa.com

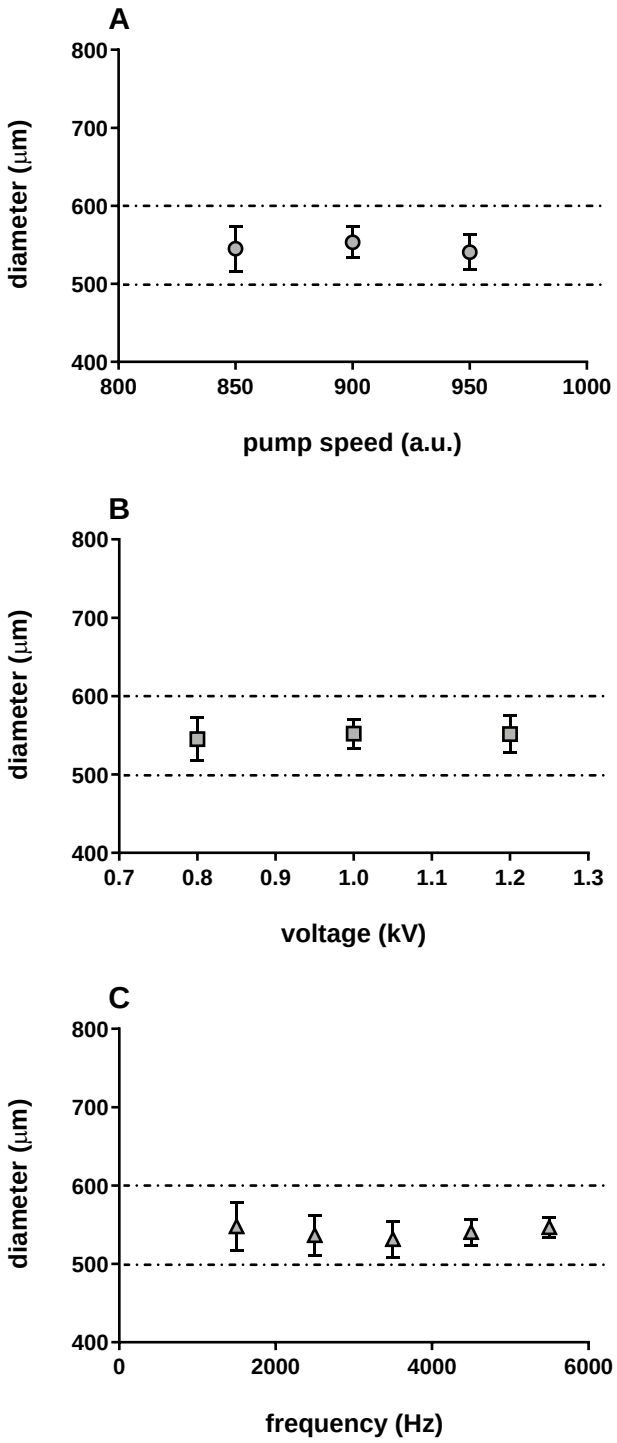


***Figure (40) Changes in microbead diameters with varying fabrication parameters.***
***(A) Changes in average microbead diameters with varying pump speed. Parameters: 2% (w/v) alginate in HBS, 1.0 kV voltage and 1500 Hz frequency. (B) Changes in average microbead diameters with varying voltage. Parameters: 2% (w/v) alginate in HBS, 900 a.u. pump speed and 1500 Hz frequency. (C) Changes in average microbead diameters with varying frequency. Parameters: 2% (w/v) alginate in HBS, 1.0 kV voltage and 900 a.u. pump speed. Optimum parameters to produce the least variable microbeads were 900 a.u. pump speed (A), 1.0 kV voltage (B) and 5500 Hz frequency (C). This yielded microbeads 546.67 µm ±12.69 in diameter.***



www.manaraa.com

Microbeads at an average diameter of 553 µm ± 20 were produced when a pump speed of 900 a.u. was used to extrude the alginate through the encapsulator nozzle **(Figure (40A))**. Since this was the setting that yielded the most uniform size distribution, it was carried forward. At an electrostatic potential of 1.0 kV, microbeads with an average diameter of 552 µm ± 19 were achieved **(Figure (40B))**. Hence, an electrostatic potential of 1.0 kV was used as the final optimised setting. **Figure (40C)** shows that increasing the frequency of vibrations had a substantial impact on microbead size distribution. The highest frequency tested was 5500 Hz and resulted in an average microbead size of 547 µm ± 13 in diameter. Since this was the parameter that achieved beads with least variability in size, this was concluded as the optimised frequency to use in microbead fabrication.

As evident from the graphs in **Figure (40)** above, fine-tuning of fabrication parameters after the inclusion of cells in the alginate solution yielded the most consistent microbeads when 2% (w/v) alginate-cell suspension was extruded at settings of 900 a.u. speed, 1.0 kV voltage and 5500 Hz stream disruption frequency.

To conclude **Stage 3**, further fine-tuning of parameters to obtain a more uniform size distribution of encapsulated microbeads using HBS as a vehicle finally resulted in the formation of spherical microbeads using 900 a.u. pump speed, 1.0 kV voltage and 5500 Hz frequency. With these parameters, an average microbead diameter of 547 µm ±13 was achieved.



www.manaraa.com

### 4.3.5. Alginate does not affect normal cell proliferation

Theoretically, a microbead with a diameter of 550 µm is expected to encapsulate an estimated 130 cells if the system were 100% efficient. To determine the cell numbers within the microbeads immediately after encapsulation, a sample of beads was isolated. The hydrogel was disrupted using the dissolution mix and cells (now in solution) were counted by trypan blue staining and using a haemocytometer chamber. Each bead contained an average of 116 ± 17 cells immediately following encapsulation (n = 5).

The MTS assay was used to assess the viable cells in proliferation and their rate of proliferation of 7PA2 cells with or without alginate. To run this assay, 5,000 7PA2 cells per well were plated in a 96-well plate. The rate of 7PA2 cells proliferation did not change when alginate was present. The graph in **Figure (41)** below is a representation of the cell proliferation rate for 7PA2 cells at passage 9 without alginate and laden with alginate.

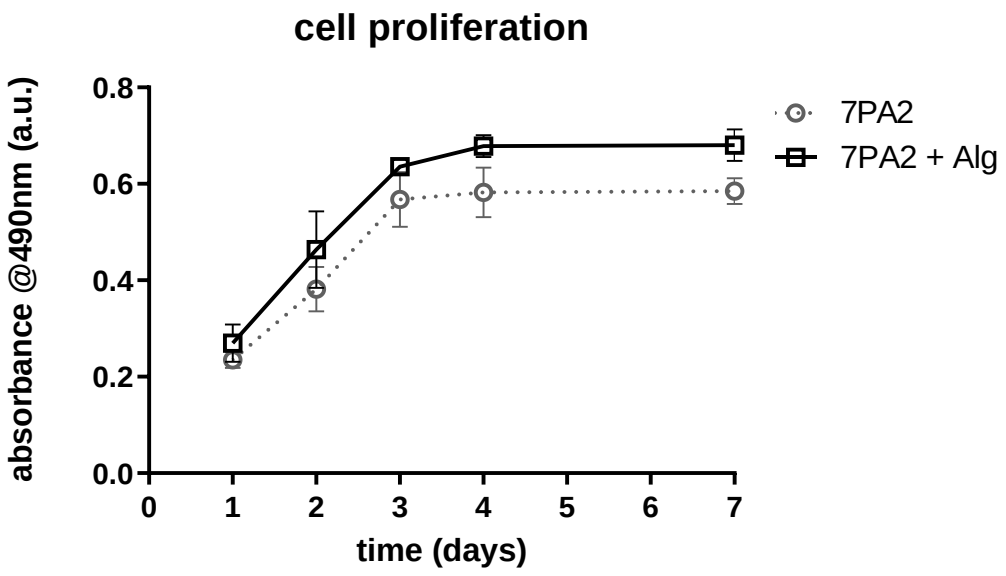


***Figure (41) MTS assay.***
***7PA2 cells seeded with and without alginate show a similar profile of proliferation, p=0.7. The degree of formazan absorption was used to indicate the rate of metabolic activity and proliferation in the MTS assay over a 7-day period.***



www.manaraa.com

### 4.3.6. Microbeads encapsulating cells were stable for one week in cell culture media

Alginate microbeads containing cells fabricated using this protocol were transferred to a cell culture plate and incubated in DMEM-F12 at 37 °C and standard cell culture conditions for one week. No overall changes in microbead diameter were observed over the one-week period, suggesting no alginate degradation and no microbead disruption due to cells growth **(Figure (42))**.

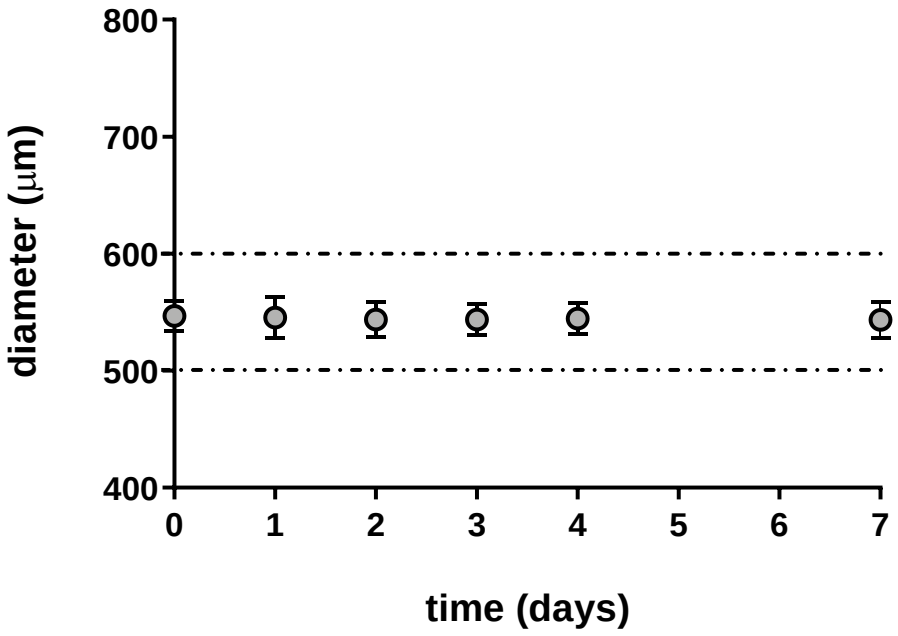


***Figure (42) Microbead diameters.***
***Graph illustrating the unchanging average microbead diameters of the same population of microbeads over one week in normal culture conditions, n=50. Slight variations seen are due to the random sampling process of 50 beads from a population of hundreds of beads. p=0.1.***



www.manaraa.com

### 4.3.7. Aβ1-42 and prefibrillar Aβo were secreted from 7PA2 cells in microbeads

CM from CHO and 7PA2 3D cultures was analysed using ELISA and compared with levels obtained from 2D culture controls. Levels of $A\beta_{1-42}$ detected in 7PA2 3D CM increased with time as cells proliferated in the beads, as illustrated in **Figure (43)**. $A\beta_{1-42}$ was absent in CM from CHO 2D and 3D cell culture, blanks and media controls.

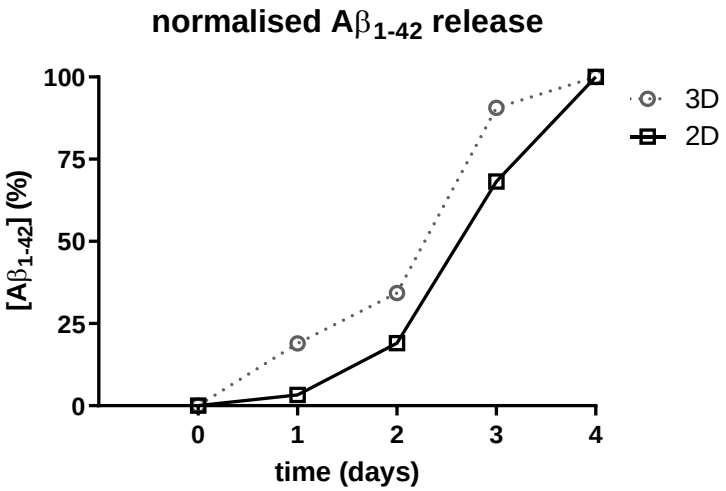


***Figure (43) Aβ$_{1-42}$ secretion.***
***Levels of Aβ$_{1-42}$ normalised against total final concentration at Day 4. The two plots show similar rates of secretion of Aβ$_{1-42}$ over time, regardless of the culturing methods, p=0.7. Secretion of amyloid is not altered by the presence of alginate or the process of encapsulation.***

A student t-test showed that there were no significant differences between the rates of secretion of $A\beta_{1-42}$ detected from either 2D or 3D cultures ($p>0.05$).

7PA2 3D CM was analysed for 6E10, A11 and OC reactivity using dot blot to ascertain the configuration of amyloid species contained in the media. Prefibrillar oligomers were confirmed in the 3D culture **(Figure (44))**. OC reactivity was not seen. No antibody reactivity was seen with CM from CHO 3D cell culture, blanks and media controls.

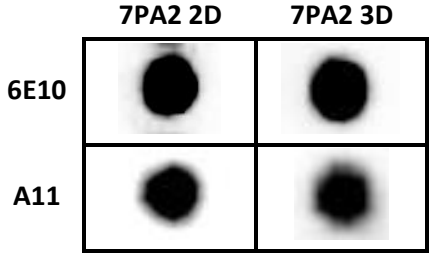


***Figure (44) Dot blot.***
***Representative images of 7PA2 3D CM antibody reactivity. Dot blots show that encapsulated 7PA2 cells secrete Aβ species with a prefibrillar (A11 positive) oligomeric configuration as in 2D culture.***



www.manaraa.com

## 4.4. Discussion

The present study sought to optimise a protocol for the formulation of Aβ-secreting alginate microbeads for use in AD research. As part of this, fabrication parameters were refined to generate microbeads with diameters between 500 to 600 µm containing 100-200 7PA2 cells each. 7PA2 cell secretory function was assessed to confirm the continuous production of prefibrillar Aβo from 3D cultures. The purpose of fabricating this 3D delivery system was for future use in developing longer-scaled *in vivo* models mirroring the chronic nature of Aβ release in AD.

The main findings from this study are summarised below:

- A protocol for the high throughput fabrication of alginate microbeads was successfully developed. Using finely tuned fabrication parameters yields microbeads ~550 µm in diameter with high uniformity.
- Alginate hydrogel microbeads are stable for at least three weeks in standard cell culture conditions.
- Alginate has no adverse effect on cell viability or normal cellular function. 7PA2 cells proliferated at the same rate in the absence and presence of alginate.
- 7PA2 cells in 3D alginate microbead culture continually produce amyloid species. When measured using ELISA, levels of $A\beta_{1-42}$ secreted from proliferating 7PA2 cells encapsulated in alginate increased with time.
- Dot blot analysis of Aβ in 7PA2 3D CM showed immunoreactivity to 6E10 and A11 antibodies. This means prefibrillar Aβo are present in the media.

In this section of the present study, wild type CHO and transfected 7PA2 cells were successfully encapsulated in spherical hydrogel microbeads after optimising fabrication parameters to meet previously defined criteria. Cell encapsulation has been employed as a bioengineered technique for a wide range of applications in the biomedical industry. Cell encapsulation within hydrogels is most commonly used for its simplicity and mild working conditions that support cell survival (Simó *et al.*, 2017). Among the benefits of encapsulating cells is protection from surrounding environments, which is important for avoiding immune reactions when implanting cells *in vivo* (Tønnesen and Karlsen, 2002; Calafiore and Basta,



www.manaraa.com

2014). Additionally, entrapment of cells in a gel matrix allows tight control over cell number and therefore allows control over the rate of delivery of biological products from cells (Rios de la Rosa *et al.*, 2018; Almari *et al.*, 2019).

For this study, alginate was selected as the hydrogel in which to encapsulate CHO and 7PA2 cells. Using alginate solution and the formed hydrogel of choice is advantageous as it is safe as approved by regulatory bodies including the Food and Drug Agency (USA) and the Medicines and Healthcare Product Regulatory Agency (MHRA, UK). It is also biocompatible and stable over time (Sun and Tan, 2013). In the results reported here, alginate microbeads are shown to remain stable for at least three weeks in standard cell culture conditions. The MTS data presented here indicating that alginate does not impair normal cellular proliferation is supported by other studies demonstrating the compatibility of alginate with other cell types (Tran *et al.*, 2014; Rios de la Rosa *et al.*, 2018). In a review by Simo and team, a list of studies using alginate to encapsulate cells also report no modification of normal cellular metabolic activity (Simó *et al.*, 2017). Therefore, it can be concluded that alginate is a suitable hydrogel to use.

The key characteristic of the protocol developed in this study is that it allows control over microbead size. The rationale for creating uniform microbeads is to manufacture Aβ delivery systems with the same release profiles so that they can be used in further studies. For example, one anticipated use of these microbeads is the *in vivo* engraftment in the rat brain to study the effects of sustained Aβ release on behaviour and pathology in relation to AD. It is of interest in this case to administer the same size microbead containing roughly the same number of cells in each experimental animal to ensure comparable experimental factors. This would be the equivalent of injecting the same amount of synthetic Aβ in each animal as reported in previous studies (Forny-Germano *et al.*, 2014; Watremez *et al.*, 2018). There are other methods that can be used to encapsulate cells in an alginate hydrogel. One such example uses a stirring vessel to form alginate gel in an emulsion, which triggers the internal gelation of alginate. However, the drawback from this method is the broad bead size distribution which compromises on the control of cell number and, in effect, rate of release of cellular products (Hoesli *et al.*, 2017).

Assessing the secretion of $A\beta_{1\text{-}42}$ over time by encapsulated 7PA2 cells reveals a continuous production of Aβ. This is a crucial finding as it provides a proof of concept to further enable the development of *in vivo* models investigating chronic timelines utilising encapsulated 7PA2 cells. However, even though ELISA was used to quantify levels of $A\beta_{1\text{-}42}$ from 3D CM, a



www.manaraa.com

potential limitation of this encapsulation technique is the difficulty in the quantification of amyloid secreted over a longer period. Although predictions can be made using the estimations calculated from the ELISA results obtained in this section and section 2.3.3., further characterisation is required to ascertain the full range of amyloid species secreted and the levels at which they are produced.

As 7PA2 3D CM reactivity to A11 and 6E10 was positive in the dot blot analysis, Aβ oligomers ranging between 48 and 135 kDa were detected, which suggests that the permeability of the alginate casing allows for proteins of molecular weight up to at least 135 kDa to pass through its pores. This is valuable as important molecular products of enzymatic APP processing can leave the microbeads and their effects in cell culture models or in *in vivo* systems can be assessed. However, the rate of diffusion of these molecules across the alginate membrane needs further investigation, since controlled release is somewhat dependent on the alginate permeability (Tønnesen and Karlsen, 2002). To have tighter control over molecular release rates from hydrogel beads, other studies have reported manipulating the hydrogel casing by using multi-layered coating using a combination of natural and synthetic polymers, such as chitosan, glutaraldehyde, protamine and polyaminoacids (including poly-L-lysine and polyornithine). While these methods may be useful in improving mechanical properties and controlling diffusion across the alginate membrane, they may further limit the application of the beads as a decreased size-exclusion limit could stop the release of key proteins of interest (Simó *et al.*, 2017).

Some of the clinical applications of alginate-encapsulated cells in spherical beads have been outlined in section 4.1. Among the most prominent uses of alginate microbeads is the encapsulation of islet cells for engraftment in the human pancreas (Lim and Sun, 1980; Omer *et al.*, 2005; Calafiore and Basta, 2014). The microbeads fabricated in this present study were designed for subsequent use in novel *in vivo* model development. To our knowledge, no such attempts at creating a hydrogel-based amyloid-secreting system has been developed. As reported above, 7PA2 cells encapsulated in alginate microbeads exhibited a sustained release of $A\beta_{1-42}$. This property can be used to assess the effects of chronic Aβ secretion in a preclinical model. **Figure (45)** overleaf shows a proposed use of the alginate microbeads to be embedded within the hippocampus of the rat. *Ex vivo* sections are used here for illustration purposes, comparing a millimetre-scaled alginate bead versus a microbead fabricated using this protocol.



www.manaraa.com

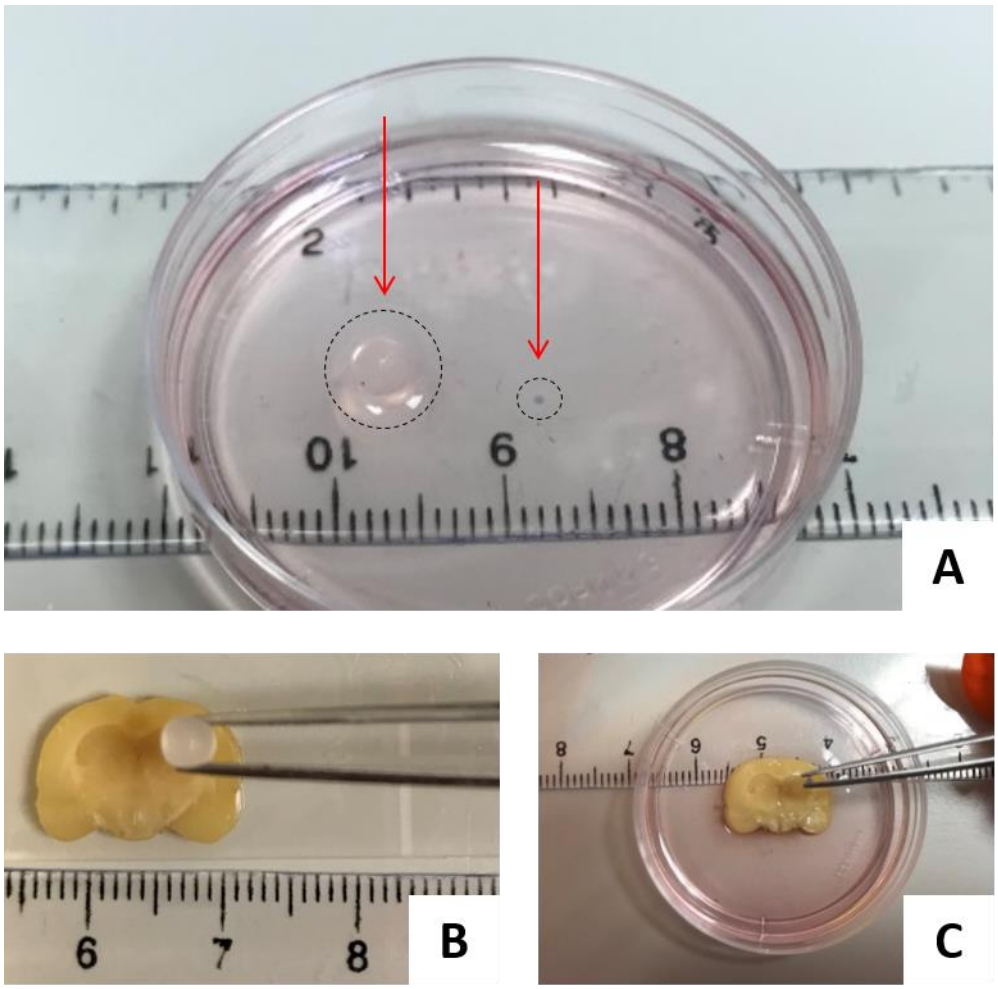


***Figure (45) Using microbeads for relevant preclinical applications.***
***Microbeads for engraftment in the rat brain must be small enough to be embedded without creating a lesion too large to avoid damage to the brain parenchyma and adversely affect normal brain function. Image (A) shows a size comparison between a millimetre-scaled bead and a micrometre-scaled bead side by side. (B) Implanting a millimetre-scaled bead within the brain for in vivo purposes would not work. Image (C) shows a microbead fabricated using this protocol. The size is suitable for insertion within the hippocampus of the rat without having a detrimental effect on normal physiology.***

The images in **Figure (45)** above highlight the importance of controlling the size of the microbead for the intended application. They demonstrate the need for the criteria outlined at the start of this chapter of diameters under 600 µm. Microbeads can be implanted with minimally invasive injection (e.g. using a Hamilton syringe) to better control the location of injected beads within the brain (Almari *et al.*, 2019).

In summary, encapsulating 7PA2 cells gives control over the size of microbeads, number of encapsulated cells and the prediction of Aβ secreted from the microbeads (e.g. concentration, release profile). Controlling the size of the microbeads is essential for two



www.manaraa.com

reasons. First, to permit fine-tuned control over the concentration of released Aβ, and second, to allow implantation in a controlled region of the rat brain. The results obtained here describe the careful tuning of alginate microbeads and highlight potential applications for further studies.

In conclusion, the data presented in this chapter provides evidence that a useful method has been developed for the encapsulation of CHO and 7PA2 cells and has yielded a narrow size distribution of alginate microbeads. 7PA2 cells in a 3D alginate matrix secrete amyloid species, including Aβo in the prefibrillar form. The hydrogel-encapsulated cells can be utilised in subsequent relevant applications, such as *in vivo* hippocampal engraftment, precluding potential immune reactions in the surrounding tissue.



www.manaraa.com

## 4.5. Chapter summary and forward link

In this chapter, Aβo-secreting 7PA2 cells were successfully fabricated using an optimised protocol. The demonstrated sustained secretion from a 3-dimensional cellular system can be used to mirror chronic Aβo accumulation in future *in vivo* studies.

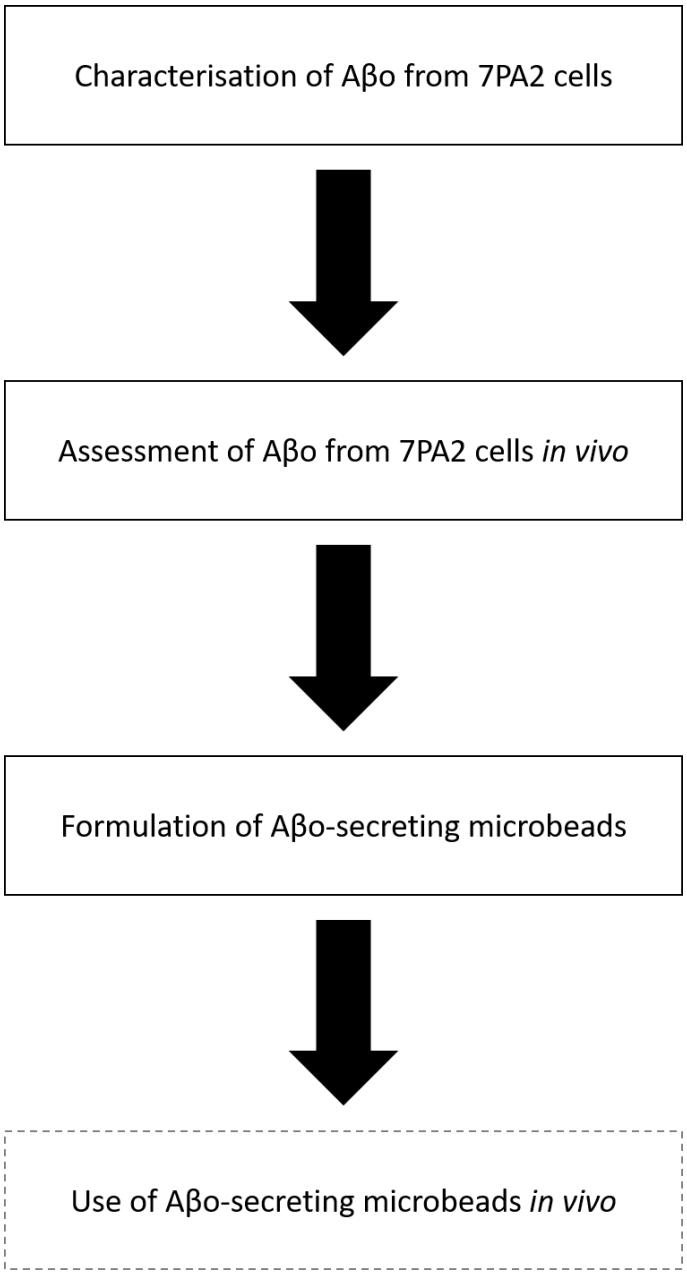




www.manaraa.com

# Chapter 5:
## Conclusions & discussion



www.manaraa.com

## 5.1. Conclusions

- 7PA2 cells are a CHO cell line transfected with human APP. They secrete the $A\beta_{1-42}$ peptide and prefibrillar Aβo in standard 2D cell culture conditions.
- Aβo are detected as early as 24 hours and are stable up to 96 hours in culture.
- Injection of Aβo from 7PA2 cells at a concentration of 100 µM into the hippocampus of wild-type adult rats induces a dysregulation of synaptic markers and a progressive cognitive deficit in object recognition.
- After one week, rats injected with Aβo from 7PA2 cells at a concentration of 100 µM exhibit a cognitive deficit in working memory in the Y-maze.
- Synaptic dysregulation is observed as a result of acute Aβo administration.
- Aβo have no impact on normal rat husbandry, feeding habits or locomotor activity.
- Alginate can be used to successfully generate microbeads encapsulating 7PA2 cells with a narrow size distribution.
- Encapsulated 7PA2 cells are stable in 3D culture for up to at least one week.
- Aβo can be detected in 3D culture of 7PA2 cells
- Encapsulated 7PA2 cells can be used in future studies to model chronic Aβ release in *in vitro* and *in vivo* systems.

## 5.2. Final discussion

Alzheimer's disease (AD) is the most common type of dementia and is characterised by a progressive decline in cognitive function, extensive amyloid plaque deposition and neurofibrillary tangle (NFT) formation. The amyloid-β (Aβ) peptide is thought to be the initiating trigger causing the synaptic damage that leads to the symptoms and neuropathology seen in patients (Selkoe, 2002; Selkoe and Hardy, 2016). The Aβ peptide is a product of the enzymatic cleavage of the amyloid precursor protein (APP) by secretase enzymes and exists in health and disease in isoforms of varying lengths of amino acid residues. The length of Aβ most commonly associated with AD is the $A\beta_{1-42}$ peptide, which is prone to self-aggregate, and has been shown to elicit synaptic damage and cognitive impairment in preclinical models of disease when it has taken on an oligomeric configuration (Walsh and Selkoe, 2007; Freir *et al.*, 2011; Brouillette *et al.*, 2012; Kayed and Lasagna-Reeves, 2012).



www.manaraa.com

There is a vast bank of established preclinical rodent models developed for investigating cognitive and pathological dysregulation related to AD, most of which consist of transgenic mouse models (Cavanaugh, Pippin and Barnard, 2014; Puzzo *et al.*, 2015; Mullane and Williams, 2019). The staggering failure rate of novel compounds identified for AD treatment in bringing about any clinical benefit in phase III clinical trials has cast doubt upon the relevance and translatability of existing preclinical animal models (Drummond and Wisniewski, 2017; Mullane and Williams, 2019). The main limitation of currently available models is their inadequate replication of the progressiveness of the condition. This has formed the rationale behind the design of the present study.

The overall aim of this project was to investigate the possibility of developing a novel preclinical animal model which more representatively mimics the chronic and progressive nature of the disease. This animal model would be of benefit in the research field, as it would provide the opportunity for drug candidates to target different stages of disease progression in order to yield better patient outcomes. The milestone for this project were to establish a source of Aβo of close relevance to human AD (chapter 2), assess the impact of obtained oligomers on behaviour and pathology in a non-chronic *in vivo* study (chapter 3) and finally formulate a sustained delivery system allowing the chronic secretion of Aβo from 3-dimensional (3D) cell culture models for subsequent *in vivo* administration (chapter 4).

Collectively, the results presented in chapters 2 and 3 of this thesis allude to the following conclusions:

- 7PA2 cells are a reliable source of prefibrillar Aβo which are present in standard 2D cell culture as early as 24 hours and are stable for up to at least 96 hours in culture.
- Aβo from 7PA2 cells induce a synaptic imbalance, which likely results in the progressive behavioural deficits observed in an acute-injection animal model.

These key findings form the basis for further exploring the development of a chronic secretion model based on encapsulated 7PA2 cells.

### 5.2.1. Understanding the link between pathology and cognition

In this investigation, a cognitive deficit was observed using two behavioural tasks: the novel object recognition (NOR) test **(Figure (14))** and the Y-maze **(Figure (15))**. In the NOR task, which is considered a test of recognition memory (Ennaceur and Delacour, 1988), rats receiving prefibrillar Aβo from 7PA2 cells exhibited a time-dependent worsening ability to discriminate between novel and familiar objects. One day immediately following



www.manaraa.com

administration, animals did not struggle to identify the novel object (DI = 0.3 for controls and 0.27 for Aβo-treated animals). While this ability remained consistent over two weeks for animals in the control group receiving CHO conditioned media (CM) (DI of 0.27, 0.31 and 0.29 for Day 4, 7 and 14 respectively), animals treated with Aβo from 7PA2 cells had a gradually diminishing DI (0.14, 0.1, 0.09 for Day 4, 7 and 14 respectively, see **Figure (14E)**). To explain this progressive effect, associated neuropathology was assessed. Levels of synaptic marker PSD-95 were significantly reduced starting from Day 4. The fall in cognitive function and synaptic markers could potentially illustrate a causative link between the two. Reports in the literature have demonstrated that Aβo-mediated synaptic damage causes an inhibition of learning and memory as assessed by electrophysiological and behavioural analyses (Selkoe, 2002; Shankar *et al.*, 2007; Balducci *et al.*, 2010; Viola and Klein, 2015).

The progressive element of the cognitive decline observed in this present study could be attributed to the time-dependent synaptic damage caused by Aβo. The hypothesis suggested here would imply that Aβo are starting to cause synaptic damage, but perhaps not enough to cause a disruption of memory-forming pathways on Day 1. This would then progress into more apparent synaptic damage by Day 4, causing a reduction in the DI, but still not enough to completely abolish recognition memory pathways. By Day 7, widespread synaptic damage would have ensued and would, therefore, explain the inability of 7PA2 animals to identify the novel object. This damage would be irreversible and would persist for a long time, e.g. 70 days as seen in Watremez's study (Watremez *et al.*, 2018).

Though there was unfortunately insufficient sample to assess pathological changes on Day 1, it would have been advantageous to see if the changes in synaptic markers were also gradual to provide further validation to the hypothesis here proposed. Similarly, performing the Y-maze task and other behavioural assessments at earlier time points would support this claim further. This could fit in well with the progressive cognitive decline and could help explain the reasons behind the observed behavioural deficits.

To relate the observed rise in pre-synaptic marker, SNAP-25, reported one and two weeks after surgery to the hypothesis described here, it is possible that Aβo initially bind to receptors on post-synaptic terminals and cause a spike in feedforward compensatory mechanisms, thereby boosting the expression of SNAP-25. Such mechanisms have been alluded to in reports in animals and in some human studies (Masliah *et al.*, 2001; Koffie *et al.*, 2009; Brinkmalm *et al.*, 2014; Zhang *et al.*, 2018). The associated parvalbumin deficit noted in the animals tested in this study on Day 4 could provide substantiation to the concept



www.manaraa.com

in which Aβo are implicated in causing a glutamatergic/GABAergic imbalance and thus resulting in a disruption of learning and memory processes (Freir *et al.*, 2011; Zallo *et al.*, 2018). An investigation utilising APP/PSEN1 transgenic mice concluded that Aβ caused a PV dysfunction which, when restored, prevented memory loss and hyperexcitability (Hijazi *et al.*, 2019). The deficit in cognition assessed by the Y-maze, a test of working memory (Dellu *et al.*, 1992), would fit into this hypothesis **(Figure (15))**. An altered inhibitory interneuron function has been reported to affect network connectivity assessed by gamma oscillations in electrophysiology, and cognition assessed by the Morris water maze in transgenic APP mice (Verret *et al.*, 2012). Alterations of working memory in response to Aβo administration has been reported in preclinical rat models of disease, in line with the results obtained here (Poling *et al.*, 2008).

In short, this study identified possible links between synaptic dysregulation and cognitive dysfunction. Further analysis at earlier time points is required to elucidate mechanisms by which these are linked and to ascertain a time of onset for such mechanisms. This information, though valuable, pertains only to acute mechanisms of Aβo toxicity but may provide some insight into mechanisms of chronic toxicity.

### 5.2.2. Utilising Aβo from 7PA2 cells in future model development

Multiple analyses were used to determine the potential for 7PA2 cells to be used in the development of novel preclinical *in vivo* models of relevance to AD. In chapter 2, analysis of the CM obtained from standard 2D 7PA2 cell culture confirmed the presence of prefibrillar oligomeric configurations of Aβ which are known to be synaptotoxic and have been demonstrated to cause cognitive dysfunction in many animal models of AD (Cleary *et al.*, 2005; Poling *et al.*, 2008; O'Hare *et al.*, 2013, 2017; Rammes *et al.*, 2015). These are similar in structure to amyloid found in the brains and CSF of AD sufferers. Therefore, studying them may be useful in recapitulating the amyloidogenic picture seen in AD.

Acute ICV (O'Hare *et al.*, 2013) and IHC (present study) injection of 7PA2 CM causes a cognitive dysfunction. However, as outlined previously, acute injection models are limited in their potential to translate well to the clinical setting since they omit the critical element of time. Therefore, the microbeads fabricated in this study (chapter 4) were designed in the anticipation of their use in adding a progressive time aspect to preclinical *in vivo* models (Almari *et al.*, 2019).



www.manaraa.com

After implantation into the rodent hippocampus, the rate of release of Aβ is expected to be steady and long-term to mirror the graduality of Aβ deposition in disease. The theoretical graph of predicted Aβ release profile is exemplified in **Figure (46)** below.

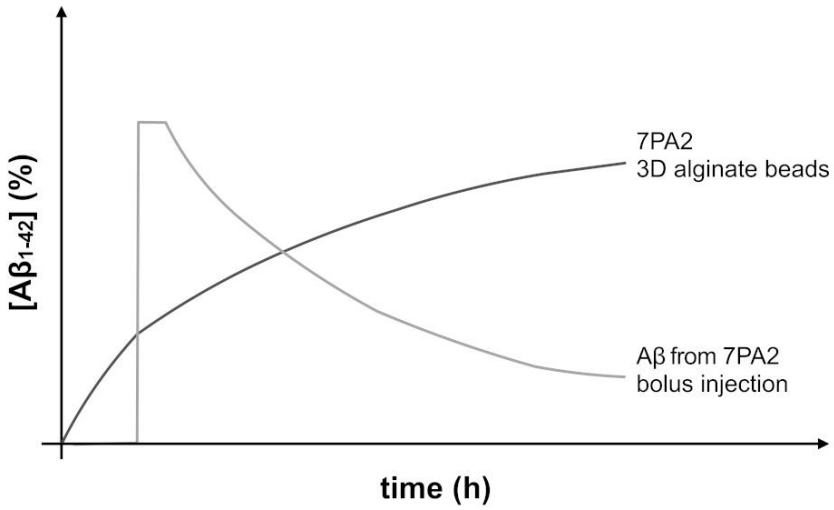


***Figure (46) Predicted Aβ release from encapsulated 7PA2 cells***
***The graph shows a predicted release profile of $Aβ_{1-42}$ from encapsulated 7PA2 cells compared with a bolus injection. The profile of Aβ release from engrafted 7PA2-containing microbeads allows the testing of the effects of chronic and sustained Aβ in an animal model of relevance to AD. Conversely, a bolus injection would create a spike in Aβ levels over a short period of time, followed by a rapid clearance of Aβ from the brain.***

Because microbeads contain live cells, the production of Aβ is expected to continue for as long as the cells remain viable, which is expected to be for weeks-months. This will aid the modelling of the chronicity of Aβ production *in vivo* (Almari *et al.*, 2019).

Among the limitations of this proposed model for future development is that 7PA2 cells are an APP cell line. This means only proteolytic products of APP (which include Aβ) will be secreted. Furthermore, the APP transfected in this cell line is a human FAD mutation which has not shown any tau or NFT pathology in previous studies (tau pathology was not investigated in this study). While these arguments pose important questions and provide valid criticisms, the fabrication of microbeads can be designed to include multiple cell lines. E.g. tau-expressing cells can be mixed with 7PA2 cells and alginate in known ratios to yield a combination bead. Alternatively, 7PA2 microbeads can be implanted within existing transgenic mouse lines expressing tau or other mutations of relevance to AD. This would enable the experimentation of multiple variables and is a suggested way forward in Puzzo's review (Puzzo *et al.*, 2015). In addition, implanting the 7PA2 beads into animals designed to model other risk factors associated with AD, such as obesity, diabetes, ion-deficiency, etc.,



www.manaraa.com

can be considered to investigate the effect of gradual Aβ production on factors of risk and resilience. They can also be used to study multi-faceted protein misfolding diseases, such as the effects of chronic Aβ accumulation on α-synuclein models of Parkinson's disease.

A pertinent question put forward to future model development utilising encapsulated 7PA2 cells is the degree of long-term stability of these beads *in vivo* – will it work? Even though studies in this investigation reported stable microbeads over a three-week period, alginate is known to be degradable in extremely long-term time scales (many months to years). Implanted beads in the rat peritoneum for insulin release were examined after 18 weeks and were found to be stable. Encapsulated cells remained viable over this period (Omer *et al.*, 2005). However, encapsulated islet cells engrafted within diabetic patients often need replacing every so often due to the degradation of the alginate and islet cell death and escape (Calafiore and Basta, 2014). Cell escape is also a risk which may lead to immunological reactions and inflammation. In order to answer these questions, further experimentation and examination of rat hippocampal engraftment conditions is needed. However, to our knowledge, this will be the first attempt to engraft alginate beads within the rat brain for the purpose of model development, and so the prospect is exciting.

To conclude, 7PA2 cells secreting oligomeric Aβ in the prefibrillar configuration have been established to induce a cognitive and synaptic dysregulation. Their encapsulation in alginate microbeads has been successfully achieved. Secretory products of 7PA2 cells can pass through alginate microbead pores and enter the surrounding areas. The potential for the use of encapsulated 7PA2 cells in novel preclinical model development has been outlined and should be pursued in future studies.



www.manaraa.com

# Chapter 6:

## References



www.manaraa.com

Almari, B. *et al.* (2019) 'Fabrication of Amyloid-β-Secreting Alginate Microbeads for Use in Modelling Alzheimer's Disease', *Journal of Visualized Experiments*, (149), p. e59597. doi: 10.3791/59597.

Alzheimer's Association (2016) '2016 Alzheimer's disease facts and figures', *Alzheimer's & Dementia*. Elsevier, 12(4), pp. 459–509. doi: 10.1016/J.JALZ.2016.03.001.

Armstrong, R. A. (2005) *Folia neuropathologica.*, *Folia Neuropathologica*. Termedia. Available at: https://www.termedia.pl/The-molecular-biology-of-senile-plaques-and-neurofibrillary-tangles-in-Alzheimer-8217-s-disease,20,13830,1,1.html (Accessed: 15 August 2019).

Audrain, M. *et al.* (2018) 'βAPP Processing Drives Gradual Tau Pathology in an Age-Dependent Amyloid Rat Model of Alzheimer's Disease', *Cerebral Cortex*. Narnia, 28(11), pp. 3976–3993. doi: 10.1093/cercor/bhx260.

Balducci, C. *et al.* (2010) 'Synthetic amyloid-beta oligomers impair long-term memory independently of cellular prion protein.', *Proceedings of the National Academy of Sciences of the United States of America*. National Academy of Sciences, 107(5), pp. 2295–300. doi: 10.1073/pnas.0911829107.

Bate, C. and Williams, A. (2011) 'Ethanol protects cultured neurons against amyloid-β and α-synuclein-induced synapse damage', *Neuropharmacology*. Pergamon, 61(8), pp. 1406–1412. doi: 10.1016/J.NEUROPHARM.2011.08.030.

Bateman, R. J. *et al.* (2012) 'Clinical and biomarker changes in dominantly inherited Alzheimer's disease.', *The New England journal of medicine*. NIH Public Access, 367(9), pp. 795–804. doi: 10.1056/NEJMoa1202753.

Bentahir, M. *et al.* (2006) 'Presenilin clinical mutations can affect gamma-secretase activity by different mechanisms', *Journal of Neurochemistry*. John Wiley & Sons, Ltd (10.1111), 96(3), pp. 732–742. doi: 10.1111/j.1471-4159.2005.03578.x.

Berger, M. *et al.* (2016) 'The Effect of Propofol Versus Isoflurane Anesthesia on Human Cerebrospinal Fluid Markers of Alzheimer's Disease: Results of a Randomized Trial.', *Journal of Alzheimer's disease : JAD*. NIH Public Access, 52(4), pp. 1299–310. doi: 10.3233/JAD-151190.

Blanco-Silvente, L. *et al.* (2017) 'Discontinuation, Efficacy, and Safety of Cholinesterase Inhibitors for Alzheimer's Disease: a Meta-Analysis and Meta-Regression of 43 Randomized Clinical Trials Enrolling 16 106 Patients.', *The international journal of neuropsychopharmacology*. Oxford University Press, 20(7), pp. 519–528. doi: 10.1093/ijnp/pyx012.

Bolmont, T. *et al.* (2008) 'Dynamics of the Microglial/Amyloid Interaction Indicate a Role in Plaque Maintenance', *The Journal of Neuroscience*. Society for Neuroscience, 28(16), p. 4283. doi: 10.1523/JNEUROSCI.4814-07.2008.

Braak, H. and Braak, E. (1995) 'Staging of alzheimer's disease-related neurofibrillary changes', *Neurobiology of Aging*. doi: 10.1016/0197-4580(95)00021-6.

Brady, D. . and Mufson, E. . (1997) 'Parvalbumin-immunoreactive neurons in the hippocampal formation of Alzheimer's diseased brain', *Neuroscience*. Pergamon, 80(4), pp. 1113–1125. doi: 10.1016/S0306-4522(97)00068-7.

Brinkmalm, A. *et al.* (2014) 'SNAP-25 is a promising novel cerebrospinal fluid biomarker for synapse degeneration in Alzheimer's disease', *Molecular Neurodegeneration*. BioMed Central, 9(1), p. 53. doi: 10.1186/1750-1326-9-53.

Brouillette, J. *et al.* (2012) 'Neurotoxicity and memory deficits induced by soluble low-molecular-weight amyloid-β1-42 oligomers are revealed in vivo by using a novel animal model.', *The Journal of neuroscience : the official journal of the Society for Neuroscience*. Society for Neuroscience, 32(23), pp. 7852–61. doi: 10.1523/JNEUROSCI.5901-11.2012.

Calafiore, R. and Basta, G. (2014) 'Clinical application of microencapsulated islets: Actual prospectives on progress and challenges'. doi: 10.1016/j.addr.2013.09.020.

Do Carmo, S. and Cuello, A. C. (2013) 'Modeling Alzheimer's disease in transgenic rats.', *Molecular neurodegeneration*. BioMed Central, 8, p. 37. doi: 10.1186/1750-1326-8-37.

Casey, D. A., Antimisiaris, D. and O'Brien, J. (2010) 'Drugs for Alzheimer's disease: are they effective?', *P & T : a peer-reviewed journal for formulary management*. MediMedia, USA, 35(4), pp. 208–11. Available at: http://www.ncbi.nlm.nih.gov/pubmed/20498822 (Accessed: 28 September 2019).

Cavanaugh, S. E., Pippin, J. J. and Barnard, N. D. (2014) 'Animal models of Alzheimer disease: historical pitfalls



www.manaraa.com

and a path forward', *ALTEX*, 31(3), pp. 279–302. doi: 10.14573/altex.1310071.

Chasseigneaux, S. and Allinquant, B. (2012) 'Functions of Aβ, sAPPα and sAPPβ : similarities and differences', *Journal of Neurochemistry*. John Wiley & Sons, Ltd (10.1111), 120, pp. 99–108. doi: 10.1111/j.1471-4159.2011.07584.x.

Chen, L. *et al.* (2018) 'Novel Quantitative Analyses of Spontaneous Synaptic Events in Cortical Pyramidal Cells Reveal Subtle Parvalbumin-Expressing Interneuron Dysfunction in a Knock-In Mouse Model of Alzheimer's Disease.', *eNeuro*. Society for Neuroscience, 5(4), p. ENEURO.0059-18.2018. doi: 10.1523/ENEURO.0059-18.2018.

Chromy, B. A. *et al.* (2003) 'Self-Assembly of Aβ 1-42 into Globular Neurotoxins'. doi: 10.1021/bi030029q.

Cleary, J. P. *et al.* (2005) 'Natural oligomers of the amyloid-β protein specifically disrupt cognitive function', *Nature Neuroscience*. Nature Publishing Group, 8(1), pp. 79–84. doi: 10.1038/nn1372.

Cohen, R. M. *et al.* (2013) 'A Transgenic Alzheimer Rat with Plaques, Tau Pathology, Behavioral Impairment, Oligomeric A , and Frank Neuronal Loss', *Journal of Neuroscience*, 33(15), pp. 6245–6256. doi: 10.1523/JNEUROSCI.3672-12.2013.

Daniels, M. J. D. *et al.* (2016) 'Fenamate NSAIDs inhibit the NLRP3 inflammasome and protect against Alzheimer's disease in rodent models.', *Nature communications*. Nature Publishing Group, 7, p. 12504. doi: 10.1038/ncomms12504.

Dawkins, E. and Small, D. H. (2014) 'Insights into the physiological function of the β-amyloid precursor protein: beyond Alzheimer's disease.', *Journal of neurochemistry*. Wiley-Blackwell, 129(5), pp. 756–69. doi: 10.1111/jnc.12675.

Dellu, F. *et al.* (1992) 'A two-trial memory task with automated recording: study in young and aged rats', *Brain Research*, 588(1), pp. 132–139. doi: 10.1016/0006-8993(92)91352-F.

Didic, M. *et al.* (2010) 'Impaired Visual Recognition Memory in Amnestic Mild Cognitive Impairment is Associated with Mesiotemporal Metabolic Changes on Magnetic Resonance Spectroscopic Imaging', *Journal of Alzheimer's Disease*, 22, pp. 1269–1279. doi: 10.3233/JAD-2010-101257.

Drummond, E. and Wisniewski, T. (2017) 'Alzheimer's disease: experimental models and reality', *Acta Neuropathologica*. Springer Berlin Heidelberg, 133(2), pp. 155–175. doi: 10.1007/s00401-016-1662-x.

Duyckaerts, C., Potier, M.-C. and Delatour, B. (2008) 'Alzheimer disease models and human neuropathology: similarities and differences.', *Acta neuropathologica*. Springer, 115(1), pp. 5–38. doi: 10.1007/s00401-007-0312-8.

Edison, P. *et al.* (2008) 'Microglia, amyloid, and cognition in Alzheimer's disease: An [11C](R)PK11195-PET and [11C]PIB-PET study', *Neurobiology of Disease*. Academic Press, 32(3), pp. 412–419. doi: 10.1016/J.NBD.2008.08.001.

Ennaceur, A. and Delacour, J. (1988) 'A new one-trial test for neurobiological studies of memory in rats. 1: Behavioral data', *Behavioural Brain Research*, 31(1), pp. 47–59. doi: 10.1016/0166-4328(88)90157-X.

Forny-Germano, L. *et al.* (2014) 'Alzheimer's Disease-Like Pathology Induced by Amyloid-β Oligomers in Nonhuman Primates', *Journal of Neuroscience*. Society for Neuroscience, 34(41), pp. 13629–13643. doi: 10.1523/JNEUROSCI.1353-14.2014.

Freir, D. B. *et al.* (2011) 'Aβ oligomers inhibit synapse remodelling necessary for memory consolidation.', *Neurobiology of aging*. NIH Public Access, 32(12), pp. 2211–8. doi: 10.1016/j.neurobiolaging.2010.01.001.

Games, D. *et al.* (1995) 'Alzheimer-type neuropathology in transgenic mice overexpressing V717F β-amyloid precursor protein', *Nature*. Nature Publishing Group, 373(6514), pp. 523–527. doi: 10.1038/373523a0.

Glabe, C. G. (2008) 'Structural Classification of Toxic Amyloid Oligomers'. doi: 10.1074/jbc.R800016200.

Goedert, M., Spillantini, M. G. and Crowther, R. A. (1991) *Tau Proteins and Neurofibrillary Degeneration*, *Brain Pathology*. Available at: https://onlinelibrary.wiley.com/doi/pdf/10.1111/j.1750-3639.1991.tb00671.x (Accessed: 25 August 2019).

Gold, M. (2017) 'Phase II clinical trials of anti–amyloid β antibodies: When is enough, enough?', *Alzheimer's & Dementia: Translational Research & Clinical Interventions*. Elsevier, 3(3), pp. 402–409. doi: 10.1016/j.trci.2017.04.005.



www.manaraa.com

Götz, J. *et al.* (2001) 'Formation of Neurofibrillary Tangles in P301L Tau Transgenic Mice Induced by Aβ42 Fibrils', *Science*, 293(5534), pp. 1491 LP – 1495. doi: 10.1126/science.1062097.

Grayson, B. *et al.* (2015) 'Assessment of disease-related cognitive impairments using the novel object recognition (NOR) task in rodents', *Behavioural Brain Research*, 285, pp. 176–193. doi: 10.1016/j.bbr.2014.10.025.

Grueninger, F. *et al.* (2010) 'Phosphorylation of Tau at S422 is enhanced by Aβ in TauPS2APP triple transgenic mice', *Neurobiology of Disease*. Academic Press, 37(2), pp. 294–306. doi: 10.1016/J.NBD.2009.09.004.

Guerreiro, R. and Bras, J. (2015) 'The age factor in Alzheimer's disease.', *Genome medicine*. BioMed Central, 7, p. 106. doi: 10.1186/s13073-015-0232-5.

Haass, C. and Selkoe, D. J. (2007) 'Soluble protein oligomers in neurodegeneration: lessons from the Alzheimer's amyloid β-peptide', *Nature Reviews Molecular Cell Biology*. Nature Publishing Group, 8(2), pp. 101–112. doi: 10.1038/nrm2101.

Hansen, R. A. *et al.* (2008) 'Efficacy and safety of donepezil, galantamine, and rivastigmine for the treatment of Alzheimer's disease: a systematic review and meta-analysis.', *Clinical interventions in aging*. Dove Press, 3(2), pp. 211–25. Available at: http://www.ncbi.nlm.nih.gov/pubmed/18686744 (Accessed: 26 September 2019).

Hardy, J. A. and Higgins, G. A. (1992) 'Alzheimer's disease: the amyloid cascade hypothesis.', *Science (New York, N.Y.)*. American Association for the Advancement of Science, 256(5054), pp. 184–5. doi: 10.1126/SCIENCE.1566067.

Hardy, J. and Selkoe, D. J. (2002) 'The amyloid hypothesis of Alzheimer's disease: progress and problems on the road to therapeutics.', *Science (New York, N.Y.)*. American Association for the Advancement of Science, 297(5580), pp. 353–6. doi: 10.1126/science.1072994.

Harris, V. M. (2015) 'Protein Detection by Simple Western™ Analysis', in. Humana Press, New York, NY, pp. 465–468. doi: 10.1007/978-1-4939-2694-7_47.

Hashimoto, S. *et al.* (2019) 'Tau binding protein CAPON induces tau aggregation and neurodegeneration.', *Nature communications*. Nature Publishing Group, 10(1), p. 2394. doi: 10.1038/s41467-019-10278-x.

Henstridge, C. M. and Spires-Jones, T. L. (2018) 'Modeling Alzheimer's disease brains in vitro', *Nature Neuroscience*. Nature Publishing Group, 21(7), pp. 899–900. doi: 10.1038/s41593-018-0177-2.

Higham, A. K. *et al.* (2014) 'Photo-activated ionic gelation of alginate hydrogel: real-time rheological monitoring of the two-step crosslinking mechanism', *Soft Matter*. The Royal Society of Chemistry, 10(27), pp. 4990–5002. doi: 10.1039/C4SM00411F.

Hijazi, S. *et al.* (2019) 'Early restoration of parvalbumin interneuron activity prevents memory loss and network hyperexcitability in a mouse model of Alzheimer's disease', *Molecular Psychiatry*. Nature Publishing Group, pp. 1–19. doi: 10.1038/s41380-019-0483-4.

Hodel, A. (1998) 'SNAP-25', *The International Journal of Biochemistry & Cell Biology*. Pergamon, 30(10), pp. 1069–1073. doi: 10.1016/S1357-2725(98)00079-X.

Hoesli, C. A. *et al.* (2017) 'Mammalian Cell Encapsulation in Alginate Beads Using a Simple Stirred Vessel', (124). doi: 10.3791/55280.

Holland, A. J. and Oliver, C. (1995) 'Down's syndrome and the links with Alzheimer's disease.', *Journal of Neurology, Neurosurgery, and Psychiatry*. BMJ Publishing Group, 59(2), p. 111. doi: 10.1136/JNNP.59.2.111.

Hussain, S. *et al.* (2019) 'A possible postsynaptic role for SNAP-25 in hippocampal synapses', *Brain Structure and Function*. Springer Berlin Heidelberg, 224(2), pp. 521–532. doi: 10.1007/s00429-018-1782-2.

Jack, C. R. *et al.* (2010) 'Hypothetical model of dynamic biomarkers of the Alzheimer's pathological cascade.', *The Lancet. Neurology*. NIH Public Access, 9(1), pp. 119–28. doi: 10.1016/S1474-4422(09)70299-6.

Jarosz-Griffiths, H. H. *et al.* (2016) 'Amyloid-β Receptors: The Good, the Bad, and the Prion Protein', *The Journal of Biological Chemistry*. American Society for Biochemistry and Molecular Biology, 291(7), p. 3174. doi: 10.1074/JBC.R115.702704.

Jiang, J. and Jiang, H. (2015) 'Effect of the inhaled anesthetics isoflurane, sevoflurane and desflurane on the neuropathogenesis of Alzheimer's disease (review).', *Molecular medicine reports*. Spandidos Publications, 12(1), pp. 3–12. doi: 10.3892/mmr.2015.3424.



www.manaraa.com

Karran, E. and De Strooper, B. (2016) 'The amyloid cascade hypothesis: are we poised for success or failure?', *Journal of Neurochemistry*, 139, pp. 237–252. doi: 10.1111/jnc.13632.

Kayed, R. *et al.* (2003) 'Common Structure of Soluble Amyloid Oligomers Implies Common Mechanism of Pathogenesis', *Science*, 300(5618), pp. 486 LP – 489. doi: 10.1126/science.1079469.

Kayed, R. *et al.* (2007) 'Fibril specific, conformation dependent antibodies recognize a generic epitope common to amyloid fibrils and fibrillar oligomers that is absent in prefibrillar oligomers', *Molecular Neurodegeneration*. BioMed Central, 2, p. 18. doi: 10.1186/1750-1326-2-18.

Kayed, R. and Lasagna-Reeves, C. A. (2012) 'Molecular Mechanisms of Amyloid Oligomers Toxicity', *Journal of Alzheimer's Disease*. Edited by G. Perry et al. IOS Press, 33(s1), pp. S67–S78. doi: 10.3233/JAD-2012-129001.

Kittelberger, K. A. *et al.* (2012) 'Natural Amyloid-Beta Oligomers Acutely Impair the Formation of a Contextual Fear Memory in Mice', *PLoS ONE*. Edited by S. T. Ferreira. Public Library of Science, 7(1), p. e29940. doi: 10.1371/journal.pone.0029940.

Koffie, R. M. *et al.* (2009) *Oligomeric amyloid associates with postsynaptic densities and correlates with excitatory synapse loss near senile plaques*, *PNAS March*. Available at: https://www.ncbi.nlm.nih.gov/pmc/articles/PMC2656196/pdf/zpq4012.pdf (Accessed: 1 September 2019).

Koseoglu, E. (2019) 'New treatment modalities in Alzheimer's disease.', *World journal of clinical cases*. Baishideng Publishing Group Inc, 7(14), pp. 1764–1774. doi: 10.12998/wjcc.v7.i14.1764.

Leon, W. C. *et al.* (2010) 'A Novel Transgenic Rat Model with a Full Alzheimer's-Like Amyloid Pathology Displays Pre-Plaque Intracellular Amyloid-β-Associated Cognitive Impairment', *Journal of Alzheimer's Disease*. IOS Press, 20(1), pp. 113–126. doi: 10.3233/JAD-2010-1349.

Lim, F. and Sun, A. M. (1980) 'Microencapsulated islets as bioartificial endocrine pancreas.', *Science (New York, N.Y.)*. American Association for the Advancement of Science, 210(4472), pp. 908–10. doi: 10.1126/SCIENCE.6776628.

Liu-Seifert, H. *et al.* (2015) 'Cognitive Impairment Precedes and Predicts Functional Impairment in Mild Alzheimer's Disease.', *Journal of Alzheimer's disease : JAD*. IOS Press, 47(1), pp. 205–14. doi: 10.3233/JAD-142508.

Liu, L. *et al.* (2008) 'A transgenic rat that develops Alzheimer's disease-like amyloid pathology, deficits in synaptic plasticity and cognitive impairment', *Neurobiology of Disease*. Academic Press, 31(1), pp. 46–57. doi: 10.1016/J.NBD.2008.03.005.

Marison, I. W. (2004) 'Fundamentals of Cell Immobilisation Biotechnology', 8A(January 2004). doi: 10.1007/978-94-017-1638-3.

Martins, I. V. A. *et al.* (2017) 'Mitochondrial Abnormalities and Synaptic Loss Underlie Memory Deficits Seen in Mouse Models of Obesity and Alzheimer's Disease.', *Journal of Alzheimer's disease : JAD*. IOS Press, 55(3), pp. 915–932. doi: 10.3233/JAD-160640.

Masliah, E. *et al.* (2001) *Altered expression of synaptic proteins occurs early during progression of Alzheimer's disease*. Available at: http://n.neurology.org/content/neurology/56/1/127.full.pdf (Accessed: 20 December 2018).

McGeer, P. L. and McGeer, E. G. (2002) 'Local Neuroinflammation and the Progression of Alzheimer's Disease', *Journal of Neurovirology*. Springer-Verlag, 8(6), pp. 529–538. doi: 10.1080/13550280290100969.

McHale-Owen, H. and Bate, C. (2018) 'Cholesterol ester hydrolase inhibitors reduce the production of synaptotoxic amyloid-β oligomers', *Biochimica et Biophysica Acta (BBA) - Molecular Basis of Disease*. Elsevier, 1864(3), pp. 649–659. doi: 10.1016/J.BBADIS.2017.12.017.

McLean, C. A. *et al.* (1999) 'Soluble pool of Aβ amyloid as a determinant of severity of neurodegeneration in Alzheimer's disease', *Annals of Neurology*. John Wiley & Sons, Ltd, 46(6), pp. 860–866. doi: 10.1002/1531-8249(199912)46:6<860::AID-ANA8>3.0.CO;2-M.

Meyer-Luehmann, M. *et al.* (2008) 'Rapid appearance and local toxicity of amyloid-β plaques in a mouse model of Alzheimer's disease', *Nature*. Nature Publishing Group, 451(7179), pp. 720–724. doi: 10.1038/nature06616.

Mitchell, S. J. *et al.* (2015) 'Animal Models of Aging Research: Implications for Human Aging and Age-Related Diseases', *Annual Review of Animal Biosciences*. Annual Reviews, 3(1), pp. 283–303. doi: 10.1146/annurev-animal-022114-110829.



www.manaraa.com

Mullane, K. and Williams, M. (2019) 'Preclinical Models of Alzheimer's Disease: Relevance and Translational Validity', *Current Protocols in Pharmacology*. John Wiley & Sons, Ltd, 84(1), p. e57. doi: 10.1002/cpph.57.

Nag, S., Tang, F. and Yee, B. K. (2001) 'Chronic intracerebroventricular exposure to β-amyloid(1-40) impairs object recognition but does not affect spontaneous locomotor activity or sensorimotor gating in the rat', *Experimental Brain Research*, 136(1), pp. 93–100. doi: 10.1007/s002210000561.

Näslund, J. *et al.* (2000) 'Correlation Between Elevated Levels of Amyloid β-Peptide in the Brain and Cognitive Decline', *JAMA*. American Medical Association, 283(12), p. 1571. doi: 10.1001/jama.283.12.1571.

Necula, M. *et al.* (2007) 'Small molecule inhibitors of aggregation indicate that amyloid beta oligomerization and fibrillization pathways are independent and distinct.', *The Journal of biological chemistry*. American Society for Biochemistry and Molecular Biology, 282(14), pp. 10311–24. doi: 10.1074/jbc.M608207200.

Nolan, W., McHale-Owen, H. and Bate, C. (2017) 'Sialylated glycosylphosphatidylinositols suppress the production of toxic amyloid-β oligomers.', *The Biochemical journal*. Portland Press Limited, 474(17), pp. 3045–3058. doi: 10.1042/BCJ20170239.

O'Hare, E. *et al.* (2013) 'Orally bioavailable small molecule drug protects memory in Alzheimer's disease models', *Neurobiology of Aging*, 34(4), pp. 1116–1125. doi: 10.1016/j.neurobiolaging.2012.10.016.

O'Hare, E. *et al.* (2016) 'Lack of support for bexarotene as a treatment for Alzheimer's disease', *Neuropharmacology*. Pergamon, 100, pp. 124–130. doi: 10.1016/J.NEUROPHARM.2015.04.020.

O'Hare, E. *et al.* (2017) 'A preclinical screen to evaluate pharmacotherapies for the treatment of agitation in dementia.', *Behavioural pharmacology*, 28(2 and 3-Spec Issue), pp. 199–206. doi: 10.1097/FBP.0000000000000298.

Oakley, H. *et al.* (2006) 'Neurobiology of Disease Intraneuronal-Amyloid Aggregates, Neurodegeneration, and Neuron Loss in Transgenic Mice with Five Familial Alzheimer's Disease Mutations: Potential Factors in Amyloid Plaque Formation'. doi: 10.1523/JNEUROSCI.1202-06.2006.

Oddo, S. *et al.* (2003) *Triple-Transgenic Model of Alzheimer's Disease with Plaques and Tangles: Intracellular A and Synaptic Dysfunction*, *Neuron*. Available at: https://ac.els-cdn.com/S0896627303004343/1-s2.0-S0896627303004343-main.pdf?_tid=0c7c1789-95ab-47cc-ac71-2c0ed8f7ae89&acdnat=1544723338_32a2a059c5ba79bc2e1a27d1841848da (Accessed: 13 December 2018).

Omer, A. *et al.* (2005) 'Long-term Normoglycemia in Rats Receiving Transplants with Encapsulated Islets', *Transplantation*. Transplantation, 79(1), pp. 52–58. doi: 10.1097/01.tp.0000149340.37865.46.

Park, J. *et al.* (2018) 'A 3D human triculture system modeling neurodegeneration and neuroinflammation in Alzheimer's disease', *Nature Neuroscience*. Nature Publishing Group, 21(7), pp. 941–951. doi: 10.1038/s41593-018-0175-4.

Paxinos, G. and Watson, C. (2007) *The rat brain in stereotaxic coordinates*. Elsevier. Available at: https://books.google.co.uk/books?hl=en&lr=&id=0prYfdDbh58C&oi=fnd&pg=PP1&ots=-8iuBVVFCl&sig=4RrPlg7uG7Bz7adYZYTqijrQEsY&redir_esc=y#v=onepage&q&f=false (Accessed: 27 August 2019).

Pike, C. J. *et al.* (1991) 'In vitro aging of ß-amyloid protein causes peptide aggregation and neurotoxicity', *Brain Research*. Elsevier, 563(1–2), pp. 311–314. doi: 10.1016/0006-8993(91)91553-D.

Podlisny, M. B. *et al.* (1995) 'Aggregation of secreted amyloid beta-protein into sodium dodecyl sulfate-stable oligomers in cell culture.', *The Journal of biological chemistry*. American Society for Biochemistry and Molecular Biology, 270(16), pp. 9564–70. doi: 10.1074/JBC.270.16.9564.

Podlisny, M. B. *et al.* (1998) 'Oligomerization of Endogenous and Synthetic Amyloid β-Protein at Nanomolar Levels in Cell Culture and Stabilization of Monomer by Congo Red†'. American Chemical Society. doi: 10.1021/BI972029U.

Poling, A. *et al.* (2008) 'Oligomers of the amyloid-beta protein disrupt working memory: confirmation with two behavioral procedures.', *Behavioural brain research*. NIH Public Access, 193(2), pp. 230–4. doi: 10.1016/j.bbr.2008.06.001.

Portelius, E. *et al.* (2013) 'Mass spectrometric characterization of amyloid-β species in the 7PA2 cell model of Alzheimer's disease.', *Journal of Alzheimer's disease : JAD*. Department of Psychiatry and Neurochemistry, Institute of Neuroscience and Physiology, the Sahlgrenska Academy at the University of Gothenburg, Mölndal, Sweden. erik.portelius@neuro.gu.se, 33(1), pp. 85–93. doi: http://dx.doi.org/10.3233/JAD-2012-120994.



www.manaraa.com

Potjewyd, G. *et al.* (2018) 'Tissue Engineering 3D Neurovascular Units: A Biomaterials and Bioprinting Perspective', *Trends in Biotechnology*, 36(4), pp. 457–472. doi: 10.1016/j.tibtech.2018.01.003.

Prince, M. *et al.* (2014) *Dementia UK: Second Edition - Overview*. Alzheimer's Society. Available at: https://kclpure.kcl.ac.uk/portal/en/publications/dementia-uk-second-edition--overview(22d426a1-c0aa-4b3f-8fcb-1db4a3f4c4d7)/export.html (Accessed: 14 June 2019).

Prince, M. *et al.* (2015) *World Alzheimer Report 2015 The Global Impact of Dementia An analysis of prevalence, incidence, cost and trends*. Available at: www.alz.co.uk/worldreport2015corrections (Accessed: 14 June 2019).

Puzzo, D. *et al.* (2015) 'Rodent models for Alzheimer's disease drug discovery.', *Expert opinion on drug discovery*. NIH Public Access, 10(7), pp. 703–11. doi: 10.1517/17460441.2015.1041913.

Rammes, G. *et al.* (2015) 'MRZ-99030 – A novel modulator of Aβ aggregation: II – Reversal of Aβ oligomer-induced deficits in long-term potentiation (LTP) and cognitive performance in rats and mice', *Neuropharmacology*. Pergamon, 92, pp. 170–182. doi: 10.1016/J.NEUROPHARM.2014.12.037.

Reitz, C. and Mayeux, R. (2014) 'Alzheimer disease: Epidemiology, diagnostic criteria, risk factors and biomarkers', *Biochemical Pharmacology*. Elsevier, 88(4), pp. 640–651. doi: 10.1016/J.BCP.2013.12.024.

Rios de la Rosa, J. M. *et al.* (2018) 'Colorectal tumor 3D *in vitro* models: advantages of biofabrication for the recapitulation of early stages of tumour development', *Biomedical Physics & Engineering Express*. IOP Publishing, 4(4), p. 045010. doi: 10.1088/2057-1976/aac1c9.

Rossor, M. N. *et al.* (1984) 'Neurochemical characteristics of early and late onset types of Alzheimer's disease.', *BMJ*. British Medical Journal Publishing Group, 288(6422), pp. 961–964. doi: 10.1136/bmj.288.6422.961.

Rushworth, J. V *et al.* (2013) 'Prion protein-mediated toxicity of amyloid-β oligomers requires lipid rafts and the transmembrane LRP1.', *The Journal of biological chemistry*. American Society for Biochemistry and Molecular Biology, 288(13), pp. 8935–51. doi: 10.1074/jbc.M112.400358.

Salloway, S. *et al.* (2014) 'Two phase 3 trials of bapineuzumab in mild-to-moderate Alzheimer's disease.', *The New England journal of medicine*. NIH Public Access, 370(4), pp. 322–33. doi: 10.1056/NEJMoa1304839.

Selkoe, D. J. (2002) 'Alzheimer's disease is a synaptic failure.', *Science (New York, N.Y.)*. American Association for the Advancement of Science, 298(5594), pp. 789–91. doi: 10.1126/science.1074069.

Selkoe, D. J. (2019) 'Alzheimer disease and aducanumab: adjusting our approach', *Nature Reviews Neurology*. Nature Publishing Group, 15(7), pp. 365–366. doi: 10.1038/s41582-019-0205-1.

Selkoe, D. J. and Hardy, J. (2016) 'The amyloid hypothesis of Alzheimer's disease at 25 years', *EMBO Molecular Medicine*, 8(6). doi: 10.15252/emmm.201606210.

Sevigny, J. *et al.* (2016) 'The antibody aducanumab reduces Aβ plaques in Alzheimer's disease', *Nature*. Nature Publishing Group, 537(7618), pp. 50–56. doi: 10.1038/nature19323.

Shankar, G. M. *et al.* (2007) 'Natural Oligomers of the Alzheimer Amyloid-Protein Induce Reversible Synapse Loss by Modulating an NMDA-Type Glutamate Receptor-Dependent Signaling Pathway'. doi: 10.1523/JNEUROSCI.4970-06.2007.

Shankar, G. M. *et al.* (2008) 'Amyloid-beta protein dimers isolated directly from Alzheimer's brains impair synaptic plasticity and memory.', *Nature medicine*. NIH Public Access, 14(8), pp. 837–42. doi: 10.1038/nm1782.

Simó, G. *et al.* (2017) 'Research progress in coating techniques of alginate gel polymer for cell encapsulation', *Carbohydrate Polymers*. Elsevier, 170, pp. 1–14. doi: 10.1016/J.CARBPOL.2017.04.013.

Small, D. H., Mok, S. S. and Bornstein, J. C. (2001) 'Alzheimer's disease and Aβ toxicity: from top to bottom', *Nature Reviews Neuroscience*. Nature Publishing Group, 2(8), pp. 595–598. doi: 10.1038/35086072.

Spangenberg, E. *et al.* (2019) 'Sustained microglial depletion with CSF1R inhibitor impairs parenchymal plaque development in an Alzheimer's disease model', *Nature Communications*. Nature Publishing Group, 10(1), p. 3758. doi: 10.1038/s41467-019-11674-z.

Stelzma, R. A., Schnitzlein, H. N. and Murtagh, F. R. (1995) 'An English Translation of Alzheimer's 1907 Paper, "Uber eine eigenartige der Hiranliung der Hirnrinde"', *Clinical Anatomy*, 8, pp. 429–472. Available at: http://info-centre.jenage.de/assets/pdfs/library/stelzmann_et_al_alzheimer_CLIN_ANAT_1995.pdf (Accessed: 14 June 2019).



www.manaraa.com

De Strooper, B. (2014) 'Lessons from a failed γ-secretase Alzheimer trial.', *Cell*. Elsevier, 159(4), pp. 721–6. doi: 10.1016/j.cell.2014.10.016.

De Strooper, B. and König, G. (2001) 'An inflammatory drug prospect', *Nature*. Nature Publishing Group, 414(6860), pp. 159–160. doi: 10.1038/35102656.

Sturchler-Pierrat, C. *et al.* (1997) 'Two amyloid precursor protein transgenic mouse models with Alzheimer disease-like pathology.', *Proceedings of the National Academy of Sciences of the United States of America*. National Academy of Sciences, 94(24), pp. 13287–92. doi: 10.1073/pnas.94.24.13287.

Sun, J. and Tan, H. (2013) 'Alginate-Based Biomaterials for Regenerative Medicine Applications', *Materials*. Multidisciplinary Digital Publishing Institute, 6(4), pp. 1285–1309. doi: 10.3390/ma6041285.

Swerdlow, R. H., Burns, J. M. and Khan, S. M. (2014) 'The Alzheimer's disease mitochondrial cascade hypothesis: Progress and perspectives', *Biochimica et Biophysica Acta (BBA) - Molecular Basis of Disease*. Elsevier, 1842(8), pp. 1219–1231. doi: 10.1016/J.BBADIS.2013.09.010.

Swerdlow, R. H. and Khan, S. M. (2004) 'A "mitochondrial cascade hypothesis" for sporadic Alzheimer's disease', *Medical Hypotheses*, 63(1), pp. 8–20. doi: 10.1016/j.mehy.2003.12.045.

Tamaoka, A. *et al.* (1998) 'Amyloid-β-protein isoforms in brain of subjects with PS1-linked, βAPP-linked and sporadic Alzheimer disease', *Molecular Brain Research*. Elsevier, 56(1–2), pp. 178–185. doi: 10.1016/S0169-328X(98)00044-8.

Tapiola, T. *et al.* (2009) 'Cerebrospinal Fluid β-Amyloid 42 and Tau Proteins as Biomarkers of Alzheimer-Type Pathologic Changes in the Brain', *Archives of Neurology*. American Medical Association, 66(3), pp. 382–389. doi: 10.1001/archneurol.2008.596.

Terry, R. D. *et al.* (1991) 'Physical basis of cognitive alterations in alzheimer's disease: Synapse loss is the major correlate of cognitive impairment', *Annals of Neurology*. John Wiley & Sons, Ltd, 30(4), pp. 572–580. doi: 10.1002/ana.410300410.

Tesson, L. *et al.* (2005) 'Transgenic Modifications of the Rat Genome', *Transgenic Research*. Kluwer Academic Publishers, 14(5), pp. 531–546. doi: 10.1007/s11248-005-5077-z.

Tirella, A. *et al.* (2009) 'A phase diagram for microfabrication of geometrically controlled hydrogel scaffolds', *Biofabrication*. IOP Publishing, 1(4), p. 045002. doi: 10.1088/1758-5082/1/4/045002.

Toda, T. *et al.* (2011) 'Presenilin-2 Mutation Causes Early Amyloid Accumulation and Memory Impairment in a Transgenic Mouse Model of Alzheimer's Disease', *Journal of Biomedicine and Biotechnology*. Hindawi Limited, 2011, pp. 1–12. doi: 10.1155/2011/617974.

Tomiyama, T. *et al.* (2010) 'A mouse model of amyloid beta oligomers: their contribution to synaptic alteration, abnormal tau phosphorylation, glial activation, and neuronal loss in vivo.', *The Journal of neuroscience : the official journal of the Society for Neuroscience*. Society for Neuroscience, 30(14), pp. 4845–56. doi: 10.1523/JNEUROSCI.5825-09.2010.

Tønnesen, H. H. and Karlsen, J. (2002) 'Alginate in drug delivery systems', *Drug Development and Industrial Pharmacy*, 28(6), pp. 621–630. doi: 10.1081/DDC-120003853.

Tran, N. M. *et al.* (2014) 'Alginate hydrogel protects encapsulated hepatic HuH-7 cells against hepatitis C virus and other viral infections', *PLoS ONE*, 9(10), pp. 16–17. doi: 10.1371/journal.pone.0109969.

Urbanc, B. *et al.* (2002) 'Neurotoxic effects of thioflavin S-positive amyloid deposits in transgenic mice and Alzheimer's disease.', *Proceedings of the National Academy of Sciences of the United States of America*. National Academy of Sciences, 99(22), pp. 13990–5. doi: 10.1073/pnas.222433299.

Verret, L. *et al.* (2012) 'Inhibitory Interneuron Deficit Links Altered Network Activity and Cognitive Dysfunction in Alzheimer Model', *Cell*. Cell Press, 149(3), pp. 708–721. doi: 10.1016/J.CELL.2012.02.046.

Viola, K. L. and Klein, W. L. (2015) 'Amyloid β oligomers in Alzheimer's disease pathogenesis, treatment, and diagnosis', *Acta Neuropathologica*, 129(2), pp. 183–206. doi: 10.1007/s00401-015-1386-3.

Vlad, S. C. *et al.* (2008) 'Protective effects of NSAIDs on the development of Alzheimer disease', *Neurology*. NIH Public Access, 70(19), p. 1672. doi: 10.1212/01.WNL.0000311269.57716.63.

Walsh, D. M. *et al.* (2000) 'The Oligomerization of Amyloid β-Protein Begins Intracellularly in Cells Derived from Human Brain†'. American Chemical Society. doi: 10.1021/BI001048S.



www.manaraa.com

Walsh, D. M. *et al.* (2002) 'Naturally secreted oligomers of amyloid beta protein potently inhibit hippocampal long-term potentiation in vivo', *Nature*. London: Nature Publishing Group, 416(6880), pp. 535–539. doi: http://dx.doi.org/10.1038/416535a.

Walsh, D. M. and Selkoe, D. J. (2007) 'Aβ Oligomers - a decade of discovery', *Journal of Neurochemistry*. John Wiley & Sons, Ltd (10.1111), 101(5), pp. 1172–1184. doi: 10.1111/j.1471-4159.2006.04426.x.

Watremez, W. *et al.* (2018) 'Stabilized Low-n Amyloid-β Oligomers Induce Robust Novel Object Recognition Deficits Associated with Inflammatory, Synaptic, and GABAergic Dysfunction in the Rat', *Journal of Alzheimer's Disease*, 62(1), pp. 213–226. doi: 10.3233/JAD-170489.

Welander, H. *et al.* (2009) 'Aβ43 is more frequent than Aβ40 in amyloid plaque cores from Alzheimer disease brains', *Journal of Neurochemistry*. John Wiley & Sons, Ltd (10.1111), 110(2), pp. 697–706. doi: 10.1111/j.1471-4159.2009.06170.x.

Welzel, A. T. *et al.* (2014) 'Secreted amyloid β-proteins in a cell culture model include N-terminally extended peptides that impair synaptic plasticity', *Biochemistry*, pp. 3908–3921. doi: 10.1021/bi5003053.

Williams, R. S. B. and Bate, C. (2018) 'Valproic acid and its congener propylisopropylacetic acid reduced the amount of soluble amyloid-β oligomers released from 7PA2 cells', *Neuropharmacology*. Pergamon, 128, pp. 54–62. doi: 10.1016/J.NEUROPHARM.2017.09.031.

Wyss-Coray, T. and Mucke, L. (2002) 'Inflammation in Neurodegenerative Disease—A Double-Edged Sword', *Neuron*. Cell Press, 35(3), pp. 419–432. doi: 10.1016/S0896-6273(02)00794-8.

Wyss-Coray, T. and Rogers, J. (2012) 'Inflammation in Alzheimer disease-a brief review of the basic science and clinical literature.', *Cold Spring Harbor perspectives in medicine*. Cold Spring Harbor Laboratory Press, 2(1), p. a006346. doi: 10.1101/cshperspect.a006346.

Xu, W. *et al.* (2008) 'Molecular Dissociation of the Role of PSD-95 in Regulating Synaptic Strength and LTD', *Neuron*, 57(2), pp. 248–262. doi: 10.1016/j.neuron.2007.11.027.

Yamada, K. *et al.* (1999) 'Improvement by nefiracetam of beta-amyloid-(1-42)-induced learning and memory impairments in rats.', *British journal of pharmacology*. Wiley-Blackwell, 126(1), pp. 235–44. doi: 10.1038/sj.bjp.0702309.

Yankner, B. A. and Lu, T. (2009) 'Amyloid beta-protein toxicity and the pathogenesis of Alzheimer disease.', *The Journal of biological chemistry*. American Society for Biochemistry and Molecular Biology, 284(8), pp. 4755–9. doi: 10.1074/jbc.R800018200.

Yankner, B., Duffy, L. and Kirschner, D. (1990) 'Neurotrophic and neurotoxic effects of amyloid beta protein: reversal by tachykinin neuropeptides', *Science*, 250(4978), pp. 279–282. doi: 10.1126/science.2218531.

Yoon, T. *et al.* (2008) 'Prefrontal cortex and hippocampus subserve different components of working memory in rats.', *Learning & memory (Cold Spring Harbor, N.Y.)*. Cold Spring Harbor Laboratory Press, 15(3), pp. 97–105. doi: 10.1101/lm.850808.

Youssef, I. *et al.* (2008) 'N-truncated amyloid-β oligomers induce learning impairment and neuronal apoptosis', *Neurobiology of Aging*. Elsevier, 29(9), pp. 1319–1333. doi: 10.1016/J.NEUROBIOLAGING.2007.03.005.

Zallo, F. *et al.* (2018) 'Loss of calretinin and parvalbumin positive interneurones in the hippocampal CA1 of aged Alzheimer's disease mice', *Neuroscience Letters*. Elsevier, 681, pp. 19–25. doi: 10.1016/J.NEULET.2018.05.027.

Zhang, H. *et al.* (2017) 'Ablating ErbB4 in PV neurons attenuates synaptic and cognitive deficits in an animal model of Alzheimer's disease', *Neurobiology of Disease*. Academic Press, 106, pp. 171–180. doi: 10.1016/J.NBD.2017.07.001.

Zhang, H. *et al.* (2018) 'Cerebrospinal fluid synaptosomal-associated protein 25 is a key player in synaptic degeneration in mild cognitive impairment and Alzheimer's disease.', *Alzheimer's research & therapy*. BioMed Central, 10(1), p. 80. doi: 10.1186/s13195-018-0407-6.



www.manaraa.com